Università di Genova

DIMI DIPARTIMENTO DI MEDICINA INTERNA E SPECIALITÀ MEDICHE

DOCTOR OF PHILOSOPHY IN
HEMATO-ONCOLOGY AND CLINICAL-TRANSLATIONAL INTERNAL MEDICINE
(XXXVI)

PATHOPHYSIOLOGY AND CLINIC OF RENAL, CARDIOVASCULAR AND HYPERTENSION DISEASES

Role of the long non-coding RNA DSCR9 in pulmonary artery endothelial cells

Supervisor
Professor Pietro Ameri

Ph.D. Candidate
Nadia Bernardi

Contents

Abstract

Pulmonary arterial hypertension (PAH) is a rare and life-threatening disease. PAH has a multifactorial aetiology and several genetic alterations have been implicated in its development, of which mutations in bone morphogenic protein receptor 2 (BMPR2) are the most prevalent ones. A defective nitric oxide (NO) production in PAH patients' pulmonary endothelium is considered one of the main drivers of PAH pathology, leading either to a loss of pulmonary vascular homeostasis or pulmonary vascular remodelling. Despite several studies investigating this alteration, the molecular factors leading to NO deficiency in PAH are still only partially known.

To better understand the mechanism causing NO deficiency in PAH, commercial primary human Pulmonary Artery Endothelial Cells (hPAEC) were incubated for 24 hours at atmospheric or 40 mmHg-higher pressure in a dedicated chamber. NO production was evaluated using diamino-fluorescein diacetate-FM. Cell viability and proliferation were assessed with MTS assay, flow cytometry, cell cycle analysis and scratch assay, while endothelial nitric oxide synthase (eNOS) phosphorylation and abundance were evaluated by western blot. Changes in the RNA profile were explored with next-generation sequencing (NGS) and differentially expressed genes (DEGs) analysed with ShinyGO vo.6.1. DEGs were considered significant when displaying a p.value < 0.05 and falling within the 90^{th} centile. Following transcriptomic data validation, key DEGs were analysed with RT-PCR, also in primary hPAEC of PAH patients (PAH-hPAEC) and control (control-hPAEC), and endothelial cells (ECs) derived from induced pluripotent stem cells (iPSC-EC) from patients with a PAH-causing mutation in BMPR2. Finally, the effects of lentiviral DSCR9 overexpression were assessed in primary hPAEC.

Exposure to high pressure resulted in a decrease in NO production in commercial hPAEC, not due to a decrease in cell viability or proliferation. Furthermore, NO deficiency was not reverted by the addition of exogenous L-Arginine. Despite an increase in total eNOS expression, there was a decrease in phosphorylated eNOS under high-pressure conditions, as revealed by Western Blot. Among 11,486 DEGs, the long non-coding RNA Down Syndrome Critical Region 9 (DSCR9) was the most upregulated upon incubation of commercial hPAEC at high pressure, and *in silico* analysis revealed its possible involvement in the eNOS pathway. DSCR9 was enriched in Gene Expression Omnibus microarray datasets from patients with PAH (GSE90943, GSE151971, GSE117261) and RT-qPCR confirmed its upregulation. DSCR9 upregulation was also confirmed in PAH-hPAECs and in BMPR2-mutated iPSC-ECs. Furthermore, overexpression of DSCR9 in PAH-hPAEC recreated the imbalance in the eNOS pathway observed in commercial hPAEC exposed to high pressure, with increased total, but decreased phosphorylated protein levels. These results suggest that DSCR9 is involved in PAH pathobiology by modulating eNOS and NO synthesis.

Introduction

Pulmonary arterial hypertension

Pulmonary arterial hypertension (PAH), specifically group 1, is a rare and devastating disease associated with a poor prognosis. Moreover, the scarcity of effective treatment leads to a fatal outcome due to right heart failure[1]. PAH has an incidence of 2,0-7,6 cases per million individuals and a prevalence of 10,6-26 million of individuals[2]. Notwithstanding, PAH is mainly observable in the female population with a predominance reported as a ratio between women and men ranging between 2:1 and 4:1. However, the outcomes are worse in males than females[3].

The hemodynamic classification of PH, which is based on parameters measured during right heart characterization, is outlined in the 6th World Pulmonary Symposium. The Pulmonary Symposium divides PH into three different categories, namely pre-capillary, isolated post-capillary, and combined pre- and post-capillary. PAH condition falls under the pre-capillary pulmonary hypertension. PAH is characterised by a mean pulmonary arterial pressure (mPAP) > 20 mmHg, a pulmonary vascular resistance (PVR) ≥ 2WU, and pulmonary capillary wall pressure (PCWP) ≤ 15mmHG. Post-Capillary PH are characterised by mPAP > 20 mmHg, PVR < 2WU, and PCWR > 15mmHg. Combined pre- and postcapillary are defined by mPAP > 20mmHg, PVR ≥ 2WU, and PCW > 15mmHG.
In 2022, the ESC/ERS PH guidelines introduced a new definition for exercise PH, as a part of the hemodynamic definition of PH. Specifically, exercise PH is defined as an mPAP at rest less than or equal to or equal to 20 mmHg, but with an mPAP/Cardiac Output slope > 3mmHg·min·L^{-1} during exercise [4].

The pathobiology of PAH is heterogeneous with a multifactorial onset, and sometimes, it may be due to genetic predisposition.
PAH corresponds to group 1 of Pulmonary Hypertension (PH) according to the current classification reported by the European Society of Cardiology in 2022[4]. In turn, PAH can be divided into five different subtypes, namely idiopathic PAH (IPAH), heritable or familial PAH (HPAH), drug-induced and toxin-induced PAH, associated PAH (APAH), and persistent PAH (PPAH). Other PH groups comprise PH due to left heart disease (group 2), lung disease or hypoxia (group 3), artery obstruction (group 4), unclear and/or multifactorial mechanisms (group 5)[3].
The most common type of PAH is idiopathic PAH (IPAH) for which risk factors and familial history are difficult to identify. On the contrary, HPAH is characterised by genetic alterations. From 60 to 70% of patients with HPAH have a germline mutation including missense mutation,

nonsense mutation, frameshift alteration or mistake in the RNA splicing, in the gene encoding for the Bone Morphogenetic Protein Receptor 2 (BMPR2). These alterations are responsible for the loss-of-function in the transforming growth factor β (TGF β/BMP) receptor superfamily. Additionally, it has been reported that from 10% up to 25% of patients with IPAH have the same mutation [5–7]. Mutations in the BMPR2 gene reinforce the antiproliferative and apoptotic effects causing defects in the downstream signalling. As a result of these mutations, there is an imbalance in the proliferative and antiproliferative effects enhanced by TGF β and BMPR2, respectively, leading to cell proliferation in the pulmonary vasculature's arterioles[8,9].

Other studies have shown how HPAH may be due to mutation in other genes including genes encoding for the activin receptor-like kinase 1 (ALK1) [5,10–12], caveolin 1 (CAV1)[13], more rarely in endoglin (ENG) [10–12], Potassium channel subfamily K member 3 (KCNK3)[5] and mothers against decapentaplegic homologue 9 (SMAD9)[5,14,15]. Of these, ALK1, ENG and SMAD9 belong to the TGFβ superfamily. Studies reported that ALK1 and SMAD9 missense mutations in HPAH are responsible for the loss of maintenance in the pulmonary vasculature and TGFβ pathway signalling reduction, respectively[12,16] **.** The heterozygous mutation reported in ENG genes need more investigation[12].

Frameshift mutations in the CAV-1 gene give rise to a disruption in a crucial site responsible for anchoring caveolae (structures particularly rich in surface receptors) to the plasma membrane. This results in an impairment of the cell signalling[13]. Simultaneously, mutations observed in the KCNK3 gene cause alterations in the ion channel function, triggering excessive proliferation and vascular remodelling[5]. Although the mutations in BMPR2 and other genes may play a role in the PAH pathogenesis, these mutations alone are not sufficient to determine PAH onset. Notably, almost 25% of patients with PAH lack a genetic predisposition[5], suggesting the presence of other underlying causes. For instance, the aetiology of APAH may be attributed to specific risk factors such as autoimmune disease like systemic sclerosis, or exposure to infectious disease exposure like HIV, the new COVID-19 and *Schistosoma species*[3]. Notably, Covid-19 has been linked with pulmonary vasculopathy, evident in the increase in the vascular wall thickness, secondary to vascular injury phenotype[3]. Furthermore, *Schistosoma species* infection has been highlighted to be involved in PAH development due to worm eggs translocation from the portal circulation to the pulmonary circulation, by triggering the immune system response culminating in vasculopathy and fibrosis[3]. Beyond infectious disease, systemic sclerosis patients may develop PAH secondary to interstitial lung disease.

PH group	Types	Subgroup	Description	Hemodynamic definition
Group 1	Idiopathic PAH (IPAH)	**1.1**	Risk factors and familial history is difficult to highlight, including idiopathic or sporadic cases. Patients can be divided into non responders and acute responders at vasoreactivity testing	**<u>Pre-capillary:</u>** mPAP > 20mmHg PAWP ≤ 15mmHG PVR ≥ 2WU
	Heritable PAH (HPAH)	**1.2**	HPAH secondary to gene mutations (BMPR2, ACVRL1, ALK1,ENG, SMAD1, 4, KCN3, CAV1)	
	Drug- and toxin- induced PAH	**1.3**	induced by drugs or toxins exposure	
	Associated PAH (APAH) with portal hypertension	**1.4**	PAH associated with connective tissue diseases, infectious diseases (e.g. HIV, Covid-19), Schistosomiasis, Congenital Heart Disease,	
	Persistent PAH (pPAH) and PVOD	**1.5**	Typically observed in the newborn	

Table 1I. General overview of the clinical and hemodynamic definition only for pulmonary hypertension (PH) group 1. The five pulmonary arterial hypertension (PAH) subtypes are summarised in the table according to the 6th World Annual Symposium in Dana Point, CA, USA, in 2008. In this classification are reported the idiopathic PAH, heritable PAH, drug and toxin-induced PAH, PAH related to infectious disease, and persistent PAH in the newborn as well as Pulmonary Veno-Occlusive Disease (PVOD).

Histological modification in pulmonary arterial hypertension

PAH is characterised by the remodelling of pulmonary arterioles consequently to endothelial cells dysfunction, smooth muscle and fibroblast proliferation. The five PAH groups share several features related to pathophysiological and histological modifications, as well as to prognosis[17]. Even though the underlying causes differ from one condition to another, all the different PAHs are characterised by an excessive vasoconstriction and an abnormal vascular remodelling affecting all vessels layer.

In PAH, histological modifications of pulmonary medium- and small-size arterial vessels [3] have been reported in PAH patients[18]. When considering these alterations, it is crucial to note that all the three layers (intima, media, adventitia comprising of pulmonary artery endothelial cells (PAEC), pulmonary artery smooth muscle cells (PASMC) and fibroblast, respectively) of the artery wall are involved, classifying this condition as vasculopathy with dyscoagulopathy and in situ thrombus formation[17,19]. Changes in the intimal layer are the results of several phenomena, including altered cross talk among cell types present in the vascular wall. In detail, the thickening of the intima is (in part) due to excessive PAEC proliferation and overproduction of secondary paracrine mediators (fibroblast growth factor, serotonin, angiotensin II, some vasoactive peptides like nitric oxide (NO), prostaglandin I2 (PGI2) endothelin-1 (ET-1) and cytokines including interleukin-1 (IL-1), IL-6, and chemokines) involved in vascular remodelling. PAEC over proliferation results in the formation of plexiform lesions which are the main histological modifications observed in long lasting PAH [20]. A study conducted by Stacher demonstrated an increase of about 20% in the thickness of the media layer due to PASMCs proliferation. In this study, the augmentation in the media thickness was related to an increase in mPAP and PVR[21]. Nevertheless, PASMs proliferation is a characteristic sign of the earliest stages of PAH. Indeed, a recent study Wang suggested that the senescence process is induced by the hypoxic environment, leading to an hypoxia-induced PASMC proliferation. In this scenario, senescence PASMCs release the IL-6 paracrine factors, responsible for accelerating the senescence process on other PASMs by activating the mTOR/S6K1 signalling[22].

While the modification and the potential role of intima and media layers in PAH vascular remodelling has been described quite extensively, the role of adventitial layer is still controversial. To date, two different hypotheses exist regarding the role that the adventitial layer may have in PAH development. The “inside-out” and the “outside-in” hypotheses [23]. The “inside-out” hypothesis suggests that the endothelial cells hyperproliferation and external factors release can cause intima fibrosis, PASMC proliferation and migration as well as the neointima formation. On the contrary, the “outside-in” hypothesis suggests that the different kinds of cells present in the adventitial layer may contribute to the vascular remodelling, even

though the observable structural changes in the adventitial are modest and have a minor impact on pulmonary vascular resistance[21]. Following the modifications in the three monolayers, vasoconstriction occurs, leading to an increase in the pulmonary vascular resistance. Consequently, the right ventricle is subjected to an increase in the volume- and pressure-overload culminating in a compensatory right heart hypertrophy. This adaptation, over time, can progress to right heart failure[3].

At the molecular level, the observable modifications in the vascular vessels may be the result of epigenetic modifications, alteration in the DNA repair process, and metabolic imbalances, extracellular matrix remodelling, endothelial to mesenchymal transition, inflammation and accumulation of immune system cells accumulation[19].

Molecular pathways involved in the pathogenesis of pulmonary arterial hypertension

Currently, three different pathways play a pivotal role in PAH development and progression. Nevertheless, It is well-established that alterations in these pathways are responsible for the pulmonary vascular remodelling observed in PAH patients. These pathways mediate the activities of endothelin 1 (ET-1), prostacyclin (PGI2) the nitric oxide (NO)[24].

Role of endothelin-1 in pulmonary artery hypertension

ET-1 is a key player in vascular homeostasis and significantly contributes to PAH pathogenesis by inducing dysfunction in smooth muscle cells, endothelial cells, and fibroblast. ET-1 is a 21-amino acid vasoconstrictor peptide that is mainly produced by endothelial cells, and released into the bloodstream[25], with 80% of its secretion occurring in a polarised way. For this reason, the ET-1 can exert its function towards the vessel's wall and tissue, impacting smooth muscle cells and fibroblast. Whereas, only the 20% of ET-1 produced reaches the bloodstream circulation, influencing the endothelial cells response [24,26].

Considering the action mechanism, the ET-1 can interact via two receptors: ET_A and ET_B , both located on smooth muscle cells and fibroblast. In contrast, ET_B is present only on endothelial cells[24]. The final impact depends on the cell type that is involved, including proliferation, vasodilatation, vasoconstriction, and fibrosis[24,27].

ET-1 promotes vasoconstriction, proliferation, and fibrosis via binding ET_A and ET_B receptors located on fibroblast and smooth muscle cells. Stimulation of endothelial cells, on the other hand, typically induces mild vasodilation through NO and prostacyclin molecules. However, ET-1 promotes vasoconstriction due to the releasing of the thromboxane A2[25].

Prostacyclin (PGI_2) and nitric oxide pathways alteration in pulmonary artery hypertension

Vasoconstriction is one of the main driver of the pathogenesis of PAH along with cell proliferation and fibrosis. Indeed, unlike in healthy individuals, in PAH patients, it is possible to observe a defect in the production of effector vasodilators acting on smooth muscle cells[24]. The lack in vasodilator effectors production concerns both prostacyclin and NO.

Prostacyclin pathway

The increased pulmonary vascular resistance observed in PAH, is in part due to an imbalance in the prostacyclin production and release by endothelial cells into the pulmonary bloodstream[28–30]. Prostacyclin, a crucial signalling molecule, is synthesised from arachidonic acid in a multistep process involving the prostacyclin synthase and cyclooxygenase (COX) enzymes[28,31]. Prostacyclin belongs to the prostanoid family that includes both prostaglandins (PGD_2, PGE_2, PGI_2 (prostacyclin) and PGF_{2a}) and thromboxane ($TX_{\alpha 2}$). Once produced in the pulmonary vascular endothelium, PGI_2 has a short lifetime. For this reason, generally, PGI_2 elicits its biological function locally by binding the prostacyclin IP receptor, and leading to the activation of the cell surface G-protein-coupled prostanoid receptors culminating in the increase of cyclic adenosine monophosphate (cAMP) and the protein kinase A activation. As a main consequence, the activation of this pathway is responsible for both the relaxation and an anti-proliferative effect in smooth muscle cells. On the contrary, Acting on endothelial cells, it is responsible for the vasodilatation effect. Through this mechanism, PGI_2 can counteract the vasoconstrictive effect of thromboxane ($TX_{\alpha 2}$) and ET-1, normally active in PAH. There exists, in individuals with PAH, an observable imbalance between the vasoactive (NO and PGI_2) and vasoconstrictor (ET-1 and $TX_{\alpha 2}$) effectors[28,32] .

Nitric oxide: a versatile cardiovascular messenger

NO serves as an autocrine and paracrine signalling factor, primarily functioning as a vital endogenous vasodilator. Its multifaceted role include modulating the blood flow by relaxing the vascular tone, mitigation of thrombosis, regulating inflammation and immune system, and control the neural activity by influencing the microcirculation within the cerebral vessels[33].

Chemically, NO is composed of an unpaired electron on the nitrogen atom ($NO^{\bullet}$), thus possesses free radical features. Despite being a radical, NO exhibits low chemical reactivity towards various biomolecules, making it a crucial player in numerous biological processes. This unique property ensures NO's biological versatility and selectivity on specific molecules[34].

In a physiological scenario within the blood vessels, endothelial cells produce and release NO consequently to the shear stress induced by the laminar and turbulent blood flood circulation experienced on their surface. Although shear stress is the primary actor for NO release, other molecules such as[35] vascular endothelial growth factor (VEGF), oestrogen, insulin, angiopoietin, acetylcholine, bradykinin B2 receptor, thrombin and ATP can induce NO release by affecting the intracellular calcium level[36]. NO produced and released by eNOS exerts various functions including the regulation of the blood pressure and vascular tone, inhibition of smooth muscle cells proliferation, prevention of platelet aggregation and leukocyte adhesion. Conversely, inhibiting NO leads to increased vascular resistance, a critical feature of endothelial dysfunction observed in PAH.

Once NO is produced, it cannot be stored inside the cell and diffuses across the cell membranes to exert its functions. Given NO reactive nature, its production requires strict regulation of both biosynthesis and local availability, involving modifications on the NOS enzymes including at transcriptional, translational and posttranslational levels, as well as subcellular localisation[36]. These modifications, including eNOS post-transcriptional modification (myristoylation and acetylation), protein-protein interactions, phosphorylation and eNOS subcellular localisation determine eNOS localisation on the plasma membrane caveolae and lipid rafts [37]. This, in turn, affects eNOS activity, influencing its ability to produce NO, partially dependent on substrate and co-factors availability. Upon activation, eNOS relocates from its original site to other subcellular compartments to exert its function.

Nitric Oxide synthase isoforms: a structural perspective

Three different isoforms of the nitric oxide synthase (NOS) have been identified: neuronal NOS (nNOS, or NOS1), inducible NOS (iNOS, or NOS2) and endothelial NOS (eNOS, NOS3). These isoforms are encoded by different chromosomes, chromosome 12, chromosome 17 and chromosome 7, respectively, and are expressed in different cell types. Specifically, nNOS was pointed out in neuronal and skeletal muscle; iNOS was initially isolated from macrophages and later found in the cardiovascular system, and eNOS is present in the endothelial cells, cardiac myocytes, and blood platelets. The regulation of these isoforms differs in terms of their interaction with calmodulin and intracellular calcium level. Calmodulin binds nNOS and eNOS in presence of high intracellular calcium levels, influencing the activity of these isoforms and resulting in a transient NO production. In contrast, calmodulin remains bound on iNOS even under basal intracellular calcium levels. Consequently, iNOS is responsible for the continuous release of NO. suggesting a distinct regulatory mechanism compared to eNOS and nNOS. Despite this difference, all NOS enzymes utilise the same cofactors in their catalytic

processes. This share utilisation of cofactors underscores the fundamental similarities in the function of these isoforms[38]. **Table 2I** summarises the main information about NOS enzymes.

When focusing on the structure of eNOS, it is composed of two monomers, each with a molecular weight of 140KDa. One monomer houses the reductase domain (COOH-terminal domain or C-domain), while the other one accommodates the oxidative domain (NH2-terminal domain or N-terminal domain). Within the C-terminal domain, several crucial cofactors are located, including nicotinamide adenine-dinucleotide phosphate (NADPH), flavin adenine dinucleotide (FAD), and flavin mononucleotide (FMN). Additionally, within the FMN domain, there is an insert of approximately 40-50 amino acids. This insert plays a pivotal role in destabilising the binding of calmodulin from the binding domain when intracellular calcium level decreases [36,37].This mechanism underscores the intricate regulation of eNOS activity, highlighting the structural elements responsible for modulating its function in response to changes in the cellular environment. Additionally, these cofactors are essential for the proper functioning of eNOS. In the N-terminal domain, an heme group, the (6R)5,6,7,8-tetrahydro-L-biopterin (BH_4) and the site for the L-Arginine amino acid are accommodated. The two monomers are connected via a calmodulin-binding structure. NO production occurs in presence of oxygen and the L-arginine amino acid. Notably, all the three different isoforms are inactive on D-arginine amino acid. Upon the elevation of intracellular calcium level, calmodulin binds the appropriate site, facilitating the electron transfer from the cofactor (NADPH) in the C-domain to the N-terminal domain, with the support of FAD and FMN [33]. Subsequently, the heme group is reduced, and upon binding the oxygen , it determines the formation of an oxyferrus-complex. Following this, electrons from the NADPH complex initiate the reduction of this oxy-ferrous complex. This reaction is facilitated by the BH_4 cofactor that is used as electron donors to reduce the oxyferrus-complex, which then can dissociate in ferric heme and superoxide. Importantly, the BH_4 cofactor is essential for the formation of NO. This is achieved by preventing the generation of the superoxide anion via the reduction of superoxide during the reaction, in a process known as eNOS uncoupling.

The generation of the superoxide anion can result from either the heme group and the flavin in the oxygenase domain and reductase domain, respectively, or direct heme inhibitors and accumulation of eNOS inhibitors inside the cell[39]. Generally, eNOS uncoupling is involved in coronary arteries and peripheral blood vessels, leading to endothelial dysfunction, arterial stiffness and chronic low-grade inflammation consequently to ROS production.

Furthermore, recent studies have reported the association between eNOS polymorphisms and an increased incidence in cardiovascular disease. Specifically, the NOS3 678T> C has been addressed to cause a reduction in eNOS production, leading to a decrease in NO level.

Consequently, individuals carrying this polymorphism face a higher risk of developing PH and other diseases, such as preeclampsia, diabetes, retinopathy, and migraine[33,40–43]. Another study conducted by Nassereddine suggests that the eNOS-894 G> T polymorphism may play a role in the onset of essential PH[44].

Isoform's name	**neuronal NOS** (nNOS, NOS1)	**inducible NOS** (iNOS, NOS2)	**endothelial NOS** (eNOS, NOS3)
Localisation	chromosome 12	chromosome 17	chromosome 7
Cell type/tissue	neuronal, skeletal	macrophages, cardiovascular system	endothelial cells, cardiac myocytes, platelets
Is it dependent on intracellular calcium level?	yes	no	yes
(COOH) reductase domain	NADPH, FAD, FMN		
(NH2) oxidative domain	BH4, heme group, L-arginine site		

Table 2I. **Summary of Nitric Oxide Synthase isoforms**.
In the table are reported the gene localisation, the type of cells in which isoforms are more abundant, their dependence on intracellular calcium level, the cofactors present in the reductase domain along with those in the oxidative domain. BH_4= (6R)5,6,7,8-tetrahydro-L-biopterin ; FAD = flavin adenine dinucleotide; FMN = flavin mononucleotide; NADPH= nicotinamide adenine-dinucleotide phosphate.

eNOS regulation: a molecular overview

The expression and activity of eNOS are intricately regulated across multiple tires, encompassing transcriptional, post-transcriptional, and post-translational levels. In the eNOS promoter region there is the presence of several *cis*-regulatory elements encompassing AP-1 and AP-2 sites, p53 binding region, NF-1 elements, CCAT box, GATA motifs, shear stress response element and Specific Protein 1 (Sp1). Moreover, it is reported the lack of TATA box[45]. At transcription level, eNOS gene is controlled by the transcription factor Sp1 , a protein which is involved in various biological processes, namely cell differentiation, cell growth, apoptosis, immune response, response to DNA damage and chromatin remodelling[46]. Additionally, post-translational modifications (phosphorylation, acetylation, O-GlcNAcylation, as well as proteolytic processing) on Sp1 protein can enhance its role as activator or repressor protein. Beyond Sp1 protein, the promoter region of eNOS can be bound by other transcription factors (Sp3, Ets-1, YY1 and MYC-associated zinc finger protein) determining the methylation of DNA, which is the main phenomenon for eNOS transcriptional regulation[45]. Indeed, DNA

methylation is responsible for histone modifications resulting in chromatin remodelling that makes the eNOS promoter region inaccessible to the transcription factors. Additionally, it has been reported that one polymorphism consisting of 27-nt repeats in eNOS intron 4, may generate a microRNA able to reduce the expression of eNOS at either transcriptional or post-translational level via β-actin[47,48].

At post-transcriptional level, eNOS is modulated via numerous processes including some modifications on the primary RNA structures, nucleocytoplasmic transport, subcellular localisation, mRNA stability and translation efficiency. In the eNOS 3'-UTR the AUUUA motif (generally associated with labile transcripts) is frequently identified, however, it does not seem to modulate the half-life of eNOS mRNA . eNOS RNA stability could be granted by the presence of 158-nt length of a CU-motif in the 3'UTR, along with other *cis*-regolatory elements suggesting the possible interaction RNA-proteins[45]. At the post-transcriptional level, eNOS may undergo acetylation of fatty acid, phosphorylation, and protein-protein interactions. Additionally, eNOS activity may be influenced by the availability of both the substrate and co-factors that are essential for the NO production. Moreover, the activation of eNOS depends on the phosphorylation on various sites, including tyrosine, serine and threonine residues. Furthermore, direct binding or interaction with caveolin-1 may determine eNOS inactivation[49].

endothelial NOS, nitric oxide, and the complex landscape of pulmonary arterial hypertension

Once produced in endothelial cells, NO exerts positive cardiovascular effects such as S-nitrosylation and the nitrite formation, leading to post-translational modification of proteins. Additionally, NO inhibits PASMC apoptosis, platelet thrombosis, vascular smooth cell proliferation, as well as collagen production [3,50,51].

Moreover, NO has a local vasodilatory effect. It diffuses across the cell membrane and exerts its functions acting on PASMC by causing the activation of the soluble guanylate cyclase that consequently leads to the increase of cyclic guanosine monophosphate (cGMP) production[24,52,53]. On a molecular level, in PASMC, NO determines the conversion of cyclic guanosine-5'-triphosphate (GTP) into cyclic guanosine monophosphate (cGMP), initiating a phosphorylation cascade that culminates in the activation of the cGMP-dependant protein kinase. This activation, in turn, leads to the activation of the myosin phosphate and subsequent release of calcium from intracellular storage, allowing vasculature relaxation. Additionally, cGMP influences gene expression in PASMC via the activation of transcription factors, mediates other responses to NO, or alters the response to other stimuli[54]. The effect of NO in PASMC is terminated by the phosphodiesterase enzymes regulated by the cGMP[3,37,55].

The loss of NO produced by the endothelium is considered one of the main causes in endothelial dysfunction, as often observed in PAH and atherosclerosis. In PAH, several studies reported a NO reduction secondary to defects in BH4 synthesis, leading to a decrease in eNOS activity and subsequent NO release[3,55]. Data retrieved from lung vessels of PAH patients display various phenotypes characterised by differences in eNOS expression level. Some studies reported an increase in eNOS expression[3,56], while others exhibit no changes or a notable reduction in eNOS production. Notably, in plexiform lesions, a sensitive reduction in eNOS expression has been described[3,57].

A study performed on an ovine model demonstrated that the reduction in eNOS production is followed by an altered mitochondrial biogenesis, affecting redox signalling and oxygen sensing [58]. As a main consequence, this alteration activates transcription factors that are generally associated with hypoxia condition, such as HIF-1α, contributing to PASMC proliferation and vascular remodelling[54].

Non-coding RNAs

High throughput techniques, such as the next generation sequencing technique, have allowed scientists to discover that only a small fraction of the DNA encodes for protein, while almost 79% is constituted by genes that do not encode for proteins. For this reason, the class of RNA deriving from these genes is known as non-coding RNA.

The non-coding RNA classification takes into consideration the role played by the non-coding RNA inside the cells. For this reason, non-coding RNA can be divided in RNA constitutively expressed by cells and essential for their homeostasis (transfer RNA (or tRNA), ribosomal RNA (rRNA), small nuclear RNA (snRNA)), and non-coding RNA with regulatory function (micro RNA (miRNA), long non-coding RNA (lncRNA), pico RNA (piRNA))[59,60]. The non-coding RNA class has a wide spectrum of action, however only for few components have been reported relevant information about their specific role and mechanism of action in health and disease. Despite this, a growing body of evidence suggests their involvement in different pathologies, including PAH.

miRNA and lncRNA in PAH

miRNAs and lncRNA biogenesis and features

PAH is marked by a complex pathogenesis in which endothelial and smooth muscle cell dysfunctions (cell proliferation, migration, apoptosis and endothelial to mesenchymal transition (EndMT)) take part. Although several pathways have been highlighted to be involved in PAH pathogenesis, more needs to be done to characterise this pathology well. To date, numerous studies focussed on miRNAs and lncRNAs have shown how these molecules can contribute to PAH onset and development being able to interact with various pathways and cellular processes.

miRNAs are endogenous molecules composed, approximately, by a single strand of 22-nucleotides. Two different pathways are involved in miRNA biogenesis, namely the canonical and non-canonical pathways. In the first case, miRNA are transcribed in the nucleus by the RNA polymerase II which reads the miRNA genes and creates a hairpin-like structure of about 1,000 nucleotides. This structure is processed both in the nucleus and cytoplasm to produce the final miRNA structure[59,61,62]. The first step of the maturation process occurs in the nucleus and sees the involvement of several enzymes. Indeed, the primary immature miRNA is cleaved by the microprocessor complex composed by an RNA-binding protein DiGeorge Syndrome Critical Region 8 and a ribonuclease enzyme (Drosha) to form a shorter hairpin of

70 nucleotides long. This precursor is then translocated by exportin-5 from the nucleus to cytoplasm. In the cytoplasm, the miRNA precursor is further cleaved by the ribonuclease Dicer into a short double-stranded immature miRNA which is then separated to form the mature miRNA. At the end of the maturation process, the miRNA is incorporated into a specific site in Argonaut proteins. This step is essential to allow the miRNA to interact and form the silencing complex by binding its target. the term non-canonical pathway is referred to all the processes in which the immature miRNAs are processed by different enzymes, generally used in the canonical pathway[63,64]. To date, studies have reported that miRNAs have the potentiality to regulate about 50-60% of all the protein coding messengers by binding the complementary sequence in the 3' untranslated region (UTR). Following the interaction between the miRNA and the specific binding site on mRNAs, the mRNA stability is altered determining the downregulation of protein expression. This regulation can occur on several levels, indeed a specific mRNA can be targeted by different miRNAs due to the presence of several binding sites in its structure. Additionally, miRNAs can act on different levels in a specific pathway determining their role in both cellular homeostasis and disease[59,65,66].

As miRNAs, the lncRNA class is not involved in protein synthesis but can be part of a regulatory process that can occur either in the nucleus or in the cytoplasm. However, differently from the miRNA, lncRNAs are characterised by a tissue-specific expression which is in turn strictly regulated by the activation of their promoter region[67]. The process that leads to lncRNA production shares some part with the miRNA and mRNA formation process. Indeed, in the same way of miRNAs and mRNAs, lncRNAs are transcribed by the polymerase II. On the contrary of miRNAs, lncRNA stability is reached analogously via post-transcriptional modifications that occur in mRNA maturation process as well, namely, the 5'-cap and poly-A tail. Splicing and alternative splicing are post-translational modifications occurring on lncRNA transcripts thanks to the presence of AG and GU nucleotides bordering the intron extremities and guiding the spliceosome to cleave the transcript in those sites. In spite of the splicing and alternative splicing, lncRNAs are characterised by the presence of longer introns and a few number of exons. Consequently to the few numbers of exons in the sequence and the splicing mechanism, the lncRNA has a length of 200 nucleotides[68]. Regulation of lncRNAs involves post-transcriptional modifications of which the N6-methyl-Adenosine (m6A) is the pivotal modifications executed by several enzymes. Thus, this modification may determine either the lncRNA structure alteration or the recruitment of specific m6A protein[60,69]. Similar to mRNA, lncRNAs undergo degradation via interaction of several enzymes. Specifically, the initial step of degradation is dependent on the 5' decapping mediated by Dpc2. Subsequently, the degradation proceeds in the nucleus with RAT1, an exonuclease enzyme with a 5' to 3' activity[60,70,71]. Furthermore, RNA binding proteins (RPs) can selectively recognize specific

nucleotide sequences on lncRNAs, modulating both the enhancement and reduction of degradative processes acting on lncRNAs. Notably, the investigation into the role of miRNAs in lncRNA regulation has only recently gained attention. Nowadays, a limited number of miRNAs (miR-let-b, miR-9, miR-34s, miR-547-5p and miR-124) have been identified as contributors to the modulation of lncRNA stability[61]. The lncRNA position within the cells determines the non-coding activity. Indeed, regulatory processes on gene expression level occur when the lncRNA elicits its function in the nucleus. In this way, the lncRNA can elicit function such as epigenetic control by acting on chromatin, regulation of specific gene's promoter region, activation or inhibition of transcripts, X-chromosome inactivation, epigenetic regulation, and maintenance of nuclear architecture. In the cytoplasm, lncRNAs are mainly involved in post-transcriptional regulation processes by influencing either mRNA stability or signal transduction pathway, and regulating miRNA interaction with the mRNA. Moreover, considering that lncRNA are characterised by a single strand of nucleotides with multiple (and complementary) binding sites, lncRNAs can act as competing endogenous RNA (ceRNA) by acting as miRNA sponge[59].

Considering that both miRNAs and lncRNAs act on different levels and influence various aspects of spacing from gene expression to protein regulation, the deregulation of these mechanisms may lead to PAH onset. Indeed, alterations on gene and protein expression secondary to lncRNA and miRNA dysregulation have been reported to be part of the pathological process leading to pulmonary vascular remodelling as well as NO deficiency in PAH.

Non-coding RNA in nitric oxide deficiency

With a specific focus on the endothelial cells alteration observable in PAH, several studies have reported miRNAs and lncRNA contribution in both the endothelial cells dysfunction and NO production. A summary of the main miRNA and lncRNA involved in endothelial cells dysfunction and NO deficiency is reported in **Table 3l** and **Table 4l**, respectively. As it was already detailed in the previous paragraphs, endothelial cells are constantly exposed to hemodynamic forces generated by the blood circulation. Thus, shear stress and stretch are perceived and integrated by endothelial cells via some mechano-miRNA which are responsible for endothelial cells function, proliferation, as well as dysfunction[72,73]. In PAH the most relevant mechano-miRNAs involved in endothelial cell dysfunction are miR-9, miR-21, miR-126, and miR-143/145.

Specifically, miR-9 and miR-216 were found to be differentially expressed in patients with essential PH and directly associated with endothelial dysfunction. In detail, miR-126

deregulation is involved in endothelial cell dysfunction and reduces endothelial cell angiogenesis in PAH [74]. While a study reported that miR-143/145 produced by endothelial cells can be transferred to smooth muscle cells via either extracellular vesicles or microparticles, determining PASMC de-differentiation. On contrary, miR-143/145 once produced in PASMC and transferred to endothelial cells can block the proliferation and modulate the angiogenic process[75,76].

Moreover, the alteration in NO production in PAH may be influenced by miRNA expression namely miR-24, miR-27b, miR-122, miR-155, miR-182, miR-221/222.

In detail, miR-24 inhibits eNOS expression by targeting one of the nuclear transcription factors involved in eNOS expression, namely the Sp1 protein by recognizing specific binding sites[77].

The aberrant expression of miR-27b seems to be involved in NO deficiency as well. It's possible involvement in this process was investigated either on an *in vivo* model (Monocrotaline rat model) or *in vitro* by using human PAEC cells. In both models miR-27b was demonstrated to interact with and downregulate the peroxisome proliferator-activated receptor (PPAR)-γ. Despite PPAR-γ downregulation, eNOS expression is not affected directly. Indeed, miR-27b seems to obliterate the Hsp90-eNOS complex, determining, as a result, the impairment in NO production[78].

A different mechanism of action was described for the NO impairment in PAH operated by miR-122. This is achieved by the downregulation of L-Arginine and NO metabolism, specifically by targeting the 3'UTR of the Solute Carrier Family 7 Member A 1 (SLC7A1). Additionally, the possible interaction with SLC7A1 polymorphism may determine NO reduction and promote endothelial dysfunction[79,80].

miR-155 and miR-182 were demonstrated to regulate eNOS and NO production. Precisely, miR-155 via interacting with eNOS transcript can reduce its stability, determining a reduction in eNOS expression. However, the exact mechanism is not known yet. Conversely, miR-188 can impair NO metabolism via inducing the AKT/mTORK pathway[81]. Finally, a study demonstrated that miR-221 and miR-222 are indirectly responsible for eNOS regulation. Indeed, it was demonstrated by means of bioinformatics algorithms the lack of interaction with the 3'-UTR eNOS region. Thus, eNOS regulation and NO production may be affected on gene level via either translational or post-translational mechanism[82] .

	Name	Function	Outcome
microRNA	**miR-24**	• eNOS inhibition • ↑ endothelial cells proliferation	• ↓ NO production • ↑ thickness
	miR-27b	• PPAR-γ inhibition	• ↓ NO secondary to the block of Hsp90-eNOS complex
	miR-122	• inhibition of SLC7A1	• ↓ NO production • endothelial dysfunction
	miR-155	• activation AKT/mTORC pathway	• ↓ NO production
	miR-182	• ↓ eNOS stability	
	miR-221/222	• unknown	

Table 3I. Summary of the main microRNA involved in endothelial cell dysfunction and nitric oxide deficiency in PAH. In the table are reported the name, indicated as miR followed by a number. In the function column is reported the miR target while in Outcome the results observed endothelial cells. ↑ = increase, ↓= decrease, NO = nitric oxide, PPAR-γ= peroxisome proliferator-activated receptor γ; SLC7A1 =Solute Carrier Family 7 Member A 1

Among lncRNAs the lncRNA GATA binding Protein 6-AS (GATA6-AS), H19, Host Gene MIR22 (MIR22HG), MIR210HG, Maternally Expressed 9 (MEG9), Metastasis-Associated Lung Adenocarcinoma Transcript a (MALAT1), MANTIS are involved in endothelial cells dysregulation and endothelial to mesenchymal transition (EndMT). However, the exact role of MIR22HG, MIR210HG and MEG9 in PAH remain still unknown.

Nowadays, it has not been reported the possible involvement of lncRNAs in eNOS pathway and NO production, even though for many of them their role has not been established yet.

Currently, the most relevant lncRNAs reported in endothelial dysfunction are: GATA6-AS, MALAT1, and MANTIS. However, the exact mechanism of action of MANTIS remains still unknown, despite its expression was found to be downregulated in patients with iPAH and MCT-rat[83].

Endothelial gene expression is epigenetically regulated by GATA6-AS via inhibiting the deaminase function of lysyl oxidase-like 2 (LOXL2) and suppressing two genes namely, the angiogenesis-related gene Prostaglandin-Endoperoxide Synthase 2 (PTGS2) and Periostin (POSTN). For this reason, GATA6-AS is a relevant key player in the endothelial to mesenchymal transition by controlling endothelial cell function[84].

MALAT1 has different functions strictly dependent on the type of cells, namely PAEC and PASMC. In detail, in endothelial cells, it is physiologically involved in migration and cell cycle regulation. Additionally, the increase in the oxidised-LDL (ox-LDL) leads to MALAT1 overexpression which in turn is responsible for beta-catenin upregulation. Thus via the activation of the Wnt/beta-catenin pathway, MALAT1 is responsible for the endothelial to mesenchymal transition. Indeed, knocking-down MALAT1, endothelial to mesenchymal transition is prevented[85] and EndMT[86].

Another study suggested that MALAT1 may act as a miRNA sponge. In this study, following the TGF-beta treatment, MALAT1 underwent to an upregulation and sponged off miR-145 leading to the release of TGF-beta receptor type 2 and SMAD3[87].

	Name	Function	Outcome
lncRNA	GATA6-AS	● inhibition of LOXL2	● suppression of PTGS2 and POSTN ● endothelial to mesenchymal transition
	MALAT1	● ↑ beta-catenin (activation of Wnt/B-catenin) (PAEC) ● sponge-off miR-145 (PASMC)	● endothelial to mesenchymal transition (PAEC) ● release TGF-beta receptor type 2 and SMAD3 (PASMC)
	MANTIS	● unknown	● endothelial cells dysregulation ● endothelial to mesenchymal transition

Table 4l. Summary of the main long non-coding RNA (lncRNA) reported to be involved in endothelial cells dysfunction and endothelial to mesenchymal transition.
↑ = increase, LOXL2 = lysyl oxidase-like 2; PAEC =pulmonary artery endothelial cells, PASMC= pulmonary artery smooth muscle cells, POSTN = Periostin , PTGS2 = Prostaglandin-Endoperoxide Synthase 2

Material and Methods

Commercial human Pulmonary Artery Endothelial Cells

Commercial female human primary PAEC (hPAEC) (PCS-100-022) were purchased from American Type Culture Collection (ATCC, PCS-100-022; Rockville, MD). hPAECs were seeded either in six-wells microtiter plates or in p60 dishes, and cultured with the Vascular Growth Basal medium (PCS-100-030; Rockville, MD) with the addition of Endothelial Cell Growth Kit-BBE (PCS-100-040; Rockville, MD). hPAECs were used from passage 5 to passage 8 to perform the experiments.

Treatment: 24 hours of high-pressure exposure

hPAECs were seeded with a density of 5,000 cells/ cm^2. Once reached the 70% of confluency, hPAECs were incubated for 24 hours in a control condition or at 40mmHg pressure condition higher than the atmospheric one in a dedicated chamber

The table below summarises the experiments performed with commercial hPAECs after the treatment exposure. These experiments will be discussed in other paragraphs of the material and methods section.

Treatment	simulation of PAH *in vitro*	Commercially available hPAECs were seeded and exposed to 40mmHg pressure higher than the atmospheric one in a dedicated chamber for 24 hours
Analysis	NO production	Flow Cytometry (DAF-FM)
	eNOS pathway	Western Blot
	Transcriptome Analysis	RNA collection, RNA sequencing (Next Generation Sequencing technique)
	Transcriptome data validation	RNA collection and RT-qPCR

Table 1M. Summarises key details regarding the treatment and the analytical methods employed in the investigation of nitric oxide (NO) deficiency in commercial primary human pulmonary artery endothelial cells (hPAECs) exposed to high-pressure conditions (40mmHg) for 24 hours alongside the control group.

Measurement of nitric oxide production by means of flow-cytometry

hPAECs from control and high-pressure conditions were washed twice with Dulbecco's Phosphate Buffered Saline 1X (D-PBS) (Euroclone, ECB4004L; Milan, Italy), stained with diamino-fluorescein (DAF-FM) fluorescent probe (1μM) purchased from Sigma-Aldrich (D1946 - DAF-FM DA; St Louis, MO) in serum-free condition for 30 minutes. Subsequently, hPAECs underwent two additional washes with D-PBS 1X before being incubated in the complete medium for additional 30 minutes. Commercial hPAECs were then washed with D-PBS, trypsinized using Trypsin-EDTA 1X in PBS (Euroclone, ECB3052D; Milan, Italy), spun and resuspended in complete medium. A population of at least 10,000 cells were gated based on their relative fluorescence intensity at ex/em 495/515 by using a Coulter NAVIOS or a Cytoflex flow cytometer (Beckman Coulter, USA).

Western blot for eNOS pathway

Commercial hPAEC were lysed with lysis buffer (20 mmol/L Tris HCl [PH 7.5] 150 mmol/L NaCl, 1 mmol/L Na2-EDTA, 1 mmol/L EGTA, 1% NP 40, 2.5 mmol/L Na2P2O7, and 1 mmol/L b-glycerophosphate) supplemented with 1 mmol/L phenylmethylsulfonyl fluoride, 1 mmol/L Na3VO4, and a protease inhibitor cocktail (Thermo Fisher Scientific, C10491; Waltham, MA). To study eNOS pathway in the commercial hPAEC, the following primary antibody were used: anti–phosphorylated AKT (Ser473; 4060; Cell Signalling Technology; Danvers, MA), anti-AKT (sc-5298; Santa Cruz Biotechnology Inc.; Dallas, TX), anti–phosphorylated eNOS (Ser1177; sc-12972; Santa Cruz Biotechnology Inc.; Dallas, TX), anti–eNOS (5080; Cell Signalling Technology; Danvers, MA), HRP-conjugated anti-β-actin (sc-47778; Santa Cruz Biotechnology Inc.; Dallas, TX). Moreover, the primary CamK2b antibody (Invitrogen, Cat#13-9800) and anti-phosphorylated CamK2b were used (Cell Signaling Technology, Cat#12716. After 1 hour of incubation with proper horseradish peroxidase-conjugated secondary antibody (Santa Cruz Biotechnology Inc.; Dallas, TX), bands were visualised with Clarity Western ECL Substrate (Bio-Rad) and quantified by densitometry by means of an image analysis system (UVItec). The reference protein used for protein normalisation was β-actin. The amount of the phosphorylated proteins was adjusted on the respective non-phosphorylated form.

RNA sequencing

Three independent biological replicates, each with technical replicates, were used for transcriptome analysis. Cells were initially seeded in p60 dishes and exposed to either control or high pressure. Subsequently, cells were washed twice with D-PBS 1X, and total RNA was collected using peqGOLD TriFast™ reagent (Peqlab, Cat#30-2030). The extracted total RNA was then sent to the Translational and Integrative Genomics Laboratory (Genova, Italy) for the RNA sequencing (RNAseq). Preceding library preparation, total RNA was reverse transcribed using SuperScript™ IV VILO™ Master Mix. The Ion AmpliSeq™ Transcriptome Human Gene Expression Panel kit (Thermo Fisher, A26325) was employed to generate cDNA libraries using the Ion Chef™ Instrument System (Thermo Fisher, 4484177). After assessing the quality of the generated cDNA library, the RNA-sequencing protocol for Next Generation Sequencing technique (NGS) was applied to conduct the study.

Transcriptome data analysis

Transcriptomic data analysis was performed to discern differentially expressed genes (DEGs) between the control and the experimental conditions. A total of 11,486 DEGs were identified. Subsequent, Functional Enrichment analysis on the top 10% of DEGs. This selection was based on the 90th centile obtained by calculating the absolute logFold Change (logFC) and applying a p.value cut-off set at 0.05. The bioinformatics tool ShyniGO v6.0 (ShinyGO v0.61: Gene Ontology Enrichment Analysis + more) was employed for both data analysis and result visualisation.

Transcriptomic data validation with RT-qPCR

For total RNA collection, commercial hPAECs were washed with PBS1X and lysed using TriFast™ . According to manufacturer instruction, Quick-RNATM MiniPrep (Zymo Research, Cat#R1050) was used to extract the RNA from the samples, and SparkControl software (Tecan Italia S.r.l.) was used to assess RNA concentration. From 500 ng to 1,000 ng of total RNA was used as input to generate cDNA using iSCRIPT™ Reverse Transcription Supermix for RT-qPCR (Bio-Rad, Cat#1708841) according to manufacturer instructions. Real Time quantitative PCR (RT-qPCR) was performed with EagleTaq Universal Master Mix (ROX) (Roche, Cat#07249926190) and gene-specific probes purchased from Integrated DNA Technologies (IDT) were used for transcriptomic data validation. The following genes were

tested: R spondin 3 (RSPO3) (Cat.No. 232651485), Calcium-Calmodulin Dependent Kinase 2B (CAMK2B) (Cat#.231138528), and NOS3 (Cat#231138524), were purchased from IDT. Beta-Actin (ACTB) was used for gene expression normalisation.

Bioinformatics characterization of a lncRNA target

The bioinformatic characterisation of the lncRNA DSCR9 involved the utilisation of various bioinformatics tools, software, and databases. The DSCR9's RNA sequence was retrieved from NCBI database (ncbi.nlm.nih.gov) by using as an input the following accession number NR_026719.2.

To evaluate the localisation and potential function of DSCR9, LncATLAS database (lncatlas.crg.eu) was consulted[88]. Additionally, LncBookK 2.0[89] (https://ndgc.cncb.ac.cn/lncbook) provided insight into DSCR9's conservation among species, and single nucleotide polymorphisms (SNPs) associated with pathological condition in the lungs. To identify the presence of repetitive elements within the DSCR9 sequence, the DFam database[90] (dfam.org/home) was consulted. The mFOLD[91] web server (mfold.org) was employed to predict the DSCR9 possible structure, and a custom script was generated to highlight the most probable structure. This script considered the relative ΔG value, the base pair in common in each sequence. The potential interaction between the lncRNA DSCR9 and CAMK2B as well as NOS3 RNA sequences was investigated with the LncRRIsearch[92] (http://www.rtools.cbrc.jp/LnvRRIsearch/).

GEO Dataset and GEO dataset analysis

The Gene Expression Omnibus (GEO) Database was consulted to retrieve information about the enrichment of the lncRNA DSCR9 in PAH. Datasets with accession number GSE90943, GSE15197, and GSE117261 were used. Raw data were downloaded and DSCR9 expression level was analysed to assess its enrichment in PAH.

Primary Pulmonary Artery Endothelial Cells

Primary hPAECs were obtained from both female patients with iPAH and donors. The cells were isolated from the lung artery and cultivated in a 0.1% gelatine-coated p60 dish in endothelial cell growth medium (ECM, -Science Cells Research Laboratory Cat#1001)

supplemented with Endothelial Cell Growth kit (ECGS, Cat#1052) and 5% Foetal Bovine Serum (FBS) (Cat#0025)). To ensure high purity, a selection based on VE-Cadherin (CD144+) surface marker was carried out using CD144+ MicroBeads human (Miltenyi Biotec, Cat#130-097-857). Primary hPAECs were used from passage 4 to passage 6 to perform the experiments.

The table below shows experiments performed with primary hPAECs.

Analysis	Data validation of results obtained in commercial hPAEC	RT-qPCR
	lentiviral overexpression	RT-qPCR, immunofluorescence staining,
	Analysis of eNOS pathway	Western Blot, RT-qPCR

Table 2M. Summarises pivotal experiments conducted on both PAH-hPAEC and contr-hPAEC to validate the findings with commercial hPAEC

Lentiviral overexpression in primary PAH-PAEC

DSCR9 plasmid (Origene,Cat# RC209011L4), containing the human DSCR9 sequence fused with the green fluorescence protein (DSCR9-GFP), as well as chloramphenicol and puromycin antibiotic resistances for bacterial and mammalian selection, was reconstitute according to manufacturer's instruction.

E.Coli STBL3 cells (Invitrogen™, Cat#C737303) served for plasmid amplification, and were cultured with Terrific Medium supplemented with chloramphenicol (25 µg/ml) to enable bacterial selection. A negative control was generated to verify the success of bacterial selection and to exclude any potential bacterial contamination.

Lentiviral particles were produced in HECK-293T cells cultured in DMEM medium containing L-Glutamine and Sodium Pyruvate (Life Technologies, Cat#11995073) supplemented with 10% FBS, 0.1mM MEM non-essential Amino Acid, and 1% P/S. Cell confluence was maintained between 40% and 70% to ensure a proper lentiviral particle production.

Lentiviruses carrying the DSCR9-GFP construct were tested on primary hPAECs derived from donors. The selection process involved the use of cECM medium containing puromycin. Then, DSRC9 overexpression was performed on PAH-PAEC. The percentage of cells expressing the DSCR9-GFP construct was assessed with immunofluorescence staining for GFP, and the efficiency of DSCR9 overexpression and the effects on eNOS pathway were evaluated with RT-qPCR with the expression of DSCR9, eNOS and CaMK2B being normalised against the one in cells infected with lentiviruses containing a construct without the DSCR9 sequence (plkO control).

RT-qPCR on primary PAH-PAEC before and after DSCR9 overexpression

Total RNA samples from primary PAH-PAECs and contr-PAECs were collected and extracted using the RNeasy® Mini Kit (Quiagen, Cat#74104). Similarly, total RNA samples from PAH-PAEC were collected after DSCR9 overexpression and RNA concentration and purity was assessed with Nanodrop. 500 ng to 1000 ng of total RNA were used as input for cDNA generation. Thus, the iSCRIPT™ Reverse Transcription Supermix for RT-qPCR (Cat#1708841) was used. DSCR9, CAMK2B and NOS3 expressions were analysed with RT-qPCR. RT-qPCR was performed with iQ™ SYBR® Green Master MIX (Biorad, Cat#1708886), 30 ng of cDNA per reaction was used as input. Specific forward and reverse primers for DSCR9, CAMK2B and NOS3 were designed and validated. The BACT gene was used for gene expression normalisation. The table below shows the list of primers used.

GENES	Down Syndrome Critical Region 9	DSCR9	FW:TGCATCTGGCTTTATCTCTG	RV:CTGTGACCTCCCATGTATTGT
	Calcium-Calmodulin protein kinase 2B	CAMK2B	FW:GAATTTCTCAGCCCGGAAGCA	RV:TGGGTCACAGATTTTCGCGT
	eNOS synthase	NOS3	FW:TTTAAAGAAGTGGCCAACGCC	RV:GCCATACAGGATTGTCGCCT
Housekeeping gene	Beta Actin	BACT	FW:AGTCATTCCAAATATGAGATGCGTT	RV:GCTATCACCTCCCCTGTGTG

Table 3M. List of forward (FW) and reverse (RV) primers used for DSCR9, CAMK2B and NOS3 expression evaluation.

Western blot on PAH-PAEC after lentiviral overexpression

Primary hPAEC were rinsed with PBS1X and lysed with commercial Cell Lysis Buffer (Cell Signaling, Cat#CST9803). To study the perturbation in the eNOS pathway after DSCR9 overexpression, identical primary and secondary antibodies, experimental protocols, and detection system detailed in the previous section were applied. B-actin served as the reference protein for protein normalisation. Similarly, in the analysis, the amount of the phosphorylated proteins was adjusted on the respective non-phosphorylated form.

Induced Pluripotent Stem Cells (iPSC) lines used

To conduct the experiments, three distinct hiPSC lines were used: iPHCTL04, iBMPR01, and iso01BMPR01.
The iPHCTRL04 line, derived from a female donor, was used to set up the iPSC-ECs differentiation protocol. Consequently, iPHCTRL04 was used to assess gene expression through the differentiation stages (MI, VS, EC, and the iPSC-ECs p2).

Immunofluorescence staining against VE-Cadherin, SOX17, von Willebrand Factor (vWF) was performed to confirm endothelial differentiation and level of maturity. Immunofluorescence staining for αSMA to assess the presence of any unwanted differentiated cell subpopulations that can occur during the differentiation process.
Conversely, female iPSC carrying a PAH-causing mutation in gene encoding bone morphogenetic Protein receptor 2 (BMPR2) (iBMPR01 line) and their isogenic counterpart (iso01BMPR01) were used to investigate DSCR9, CAMK2B and eNOS expression . In the iBMPR01 line mutated BMPR2 was replaced with a non-mutated gene via CRISPR-Cas9 technique. Consequently, the iso01BMPR01 line functioned as baseline control for DSCR9 expression.

hiPSC lines (p2)	iPHCTRL04	iPs-ECs characterisation	RT-qPCR, immunofluorescence staining
	iBMPR01, iso01BMPR01	DSCR9's expression	RT-qPCR

Table 3M. Summary of the iPSC lines employed in the study, along with the corresponding experiments and analysis performed with each line.

Induced Pluripotent Stem Cell culture and maintenance

The hiPSC carrying the BMPR2 mutation (iBMPR01 line) and the isogenic counterpart (iso01BMPR01), were maintained in mTeSR™ Plus (StemCell ™ technologies, Cat# 100-0276) on vitronectin-coated plate (Vitronectin XF™, StemCell technologies, Cat#100-0763). Colony splitting was performed at 80-90% of confluence using PBS-EDTA (0.5mM). During the splitting procedure the Rock Inhibitor (RI) (Y-27632 2HCl (Dihydrochloride) orb154626 100mg) was added 1:1000 ratio to mTeSR™ Plus to facilitate cell attachment and growth. The

day after splitting, iPSCs were washed with D-PBS and the medium was replaced with mTeSR™ Plus. Cells from passage 20 up to passage 40 were used for endothelial cells differentiation.

Endothelial Cells derived from iPSC (iPSC-EC) differentiation and purification

To induce differentiation of hiPSCs into endothelial cells (EC)s within a 10 day timeframe, Orlova's protocol[93] was applied. The hiPSCs were dissociated using PBS-EDTA (0.5 mM), seeded onto a vitronectin-coated 6-well plate at a 1:10 ratio when reaching 70-80% of confluency, and cultured for 24 hours in mTeSR™ Plus with RI (1:1000). On day 0, the RI was removed and the Mesodermal Induction was induced by supplementing the B(P)EL medium with 8µM CHIR (Bio-techne, Cat#4423/10). Vascular specification (VS) was induced on day 3 by adding SB431542 (10 µM) and the recombinant human vascular endothelial growth factor (rhVEGF) (50 ng/ml) to the B(P)EL medium. Endothelial cell expansion maintained the same composition of the VS medium. EC expansion was applied on day 6 and 9 from the beginning of the differentiation. On day 10, the differentiated cells were purified by selecting for the VE-Cadherin expression marker.

Figure 1M shows the different steps and time points needed for the differentiation and **Table 4M** indicates the B(P)EL medium composition.

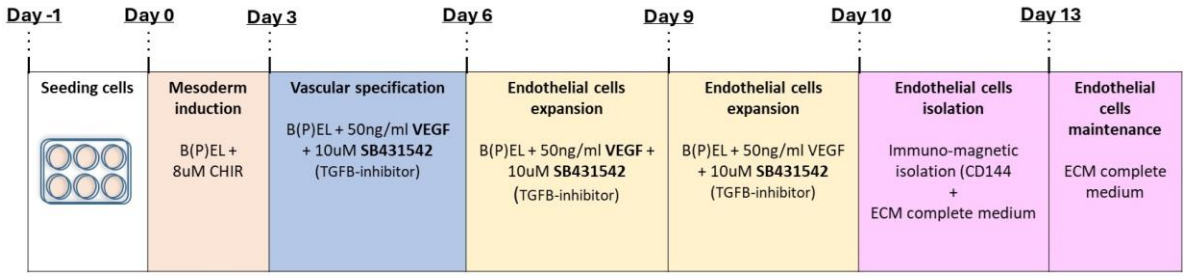

Figure 1M. Schema of iPSC-ECs differentiation.

iPSC-ECs purification and culture

Prior to start the purification process, the FACS (1.25 g of Bovine Serum Albumin (BSA) resuspended in 250 ml of sterile D-PBS) and FACS-10 (FACS buffer supplemented with 10% FBS) buffers were prepared and filtered to maintain the sterility. Subsequently, the hiPSC-ECs were washed with D-PBS and detached using Trypsin/EDTA 0.05% (Lonza, BE17-160E) for 30-35 seconds at room temperature. The enzymatic reaction was neutralised with FACSB-10 and the resulting cell suspension was filtered to remove any clumps. The detached hiPSC-ECs were centrifuged for 10 minutes at 300 x g.

Following this passage, the cells were resuspended in Anti-VE-Cadherin (CD144+) MicroBeads (Miltenyi Biotec, Cat#130-097-857) prepared accordingly with manufacturer instructions and diluted in FACS-10 buffer, and spin for 15 minutes at 4 degrees. The hiPSC-ECs were washed with 1ml of cold FACS buffer and centrifuged for another 10 minutes at 4°C. The immunoselection of differentiated hiPSC-EC expressing the CD144+ marker was conducted using magnetic columns. Following the manufacturer's instructions, cells binding the CD144+ beads were passed through a column. The cells not expressing the CD144+ marker were not retained in the column and were discarded, leaving only the CD144+ fraction for further culture. Subsequently, the CD144+ hiPSC-ECs were seeded on a gelatine 0.1%-coated T25 flask and cultured with cECM medium supplemented with 1% Penicillin/Streptomycin (P/S).

hiPSC-ECs expansion

The day after the purification, the culture medium was replenished with cECM supplemented with 1% P/S and then refreshed every two days. hiPSC-ECs passage 0 were expanded until reaching passage 2. The splitting procedure involved the use of Trypsin/EDTA 0.05% , followed by the neutralisation with a Washing Medium, composed of Dulbecco's Modified Eagle Medium (DMEM), 10% Foetal Bovine Serum (FBS) and 1% P/S. At passage 2 hiPSC-ECs were used for both gene expression analysis and the assessment of DSCR9 expression along with CAMK2B and NOS3 expression.

RT-qPCR for gene expression evaluation after iPSC-EC differentiation

Total RNA samples from the iPHCTRL04 line were collected during the differentiation steps (MI, VS, EC, iPSC-ECsp2) to follow the gene expression through the differentiation in ECs. RNA pool from primary contr-PAEC was used to compare the gene expression. Rt-qPCR data were normalised on the RPLP0 gene. Total RNA samples from iBMPR01 and iso01BMPR01 lines were collected and analysed for DSCR9, CAK2B and NOS3 expressions, gene expression normalisation was performed on the BACT gene. As described in the previous section, the iSCRIPT^{TM} Reverse Transcription Supermix for RT-qPCR (Cat#1708841) was used to obtain cDNA at the final concentration of 50 ng/µl. Subsequently, 2.5 ng per reaction was loaded to assess gene expression during the differentiation in ECs (list of FW and RV primers in **Table 5M**), while 15ng per reactions were used to establish any differences in DSCR9, CAMK2B, and NOS3 expression in iBMPR01 and iso01BMPR01 lines (FW and RV primers are listed in **table 3**M). Relative RNA expression levels were measured using SYBR Green Supermix (BioRad) with CFX96 Touch Real-Time PCR Detection System.

GENES	Pluripotency markers	NANOG	FW:TTTGTGGGCCTGAAGAAAACT	RV:AGGGCTGTCCTGAATAAGCAG
		SOX2	FW:TGGACAGTTACGCGCACAT	RV:CGAGTAGGACATGCTGTAGGT
	Endothelial cells markers	CD144	FW:CTGCATCCTCACCATCACAG	RV:ACCGACACATCGTAGCTGGT
		CD31	FW:TGGAGCACAGTGGCAACTACAC	RV:CCACGATGCTGCTGACCTT
		NOS3	FW:TTTAAAGAAGTGGCCAACGCC	RV:GCCATACAGGATTGTCGCCT
	Maturity marker	vWF	FW:AGCCACCCCTCAGTGAAATG	RV:TTCACATTCACCTCCCCGTC
	Arterial markers	SOX17	FW:TTCGTGTGCAAGCCTGAGAT	RV:TAATATACCGCGGAGCTGGC
		JAG1	FW:TTTGGAGCGACCTGTGTGGATGAGA	RV:TGGTGATGCAAGGTCTCCCTGAAACT
	Venous marker	NRP2	FW:CGGCTTTTGCAGTGGACATC	RV:TTTCTTTGTCGGTCGAGGGG
	Smooth muscle cells marker	ACTA2	FW:AAAAGACAGCTACGTGGGTGA	RV:GCCATGTTCTATCGGGTACTTC
Housekeeping gene	Ribosomal protein lateral stalk subunit P0	RPLP0	FW:TCGACAATGGCAGCATCTAC	RV:ATCCGTCTCCACAGACAAGG

Table 5M. Summary of the primers used for assessing induced pluripotent stem cells (iPSC) differentiation in endothelial cells (ECs).

Immunofluorescence staining

Primary hPAECs, hiPSC-ECs were fixed with 4% paraformaldehyde, washed three times with D-PBS and stored at 4 degrees with D-PBS supplemented with sodium azide until stained. The permeabilization was performed with 0.2% Triton 100X for 5 minutes, washed three times with D-PBS and blocked with BSA 1% for 1 hour at RT. Primary antibodies were incubated in BSA 0.1% overnight at 4 degrees. The day after secondary antibodies were incubated with 1:200 dilution for 1 hour in the darkness at RT, and Hoechst was added with 1:1000 dilution for nuclei visualisation at the end of the procedure. iBiDi mounting reagent was used, and Nikon AXR LC confocal microscope was used to observe stained samples. ImageJ Software was used to determine the percentage of cells expressing the markers of interest.

Statistical analysis

Statistical analysis was performed using Student's T test. All the results were represented as mean ± standard deviation. A p-value <0.05 was considered significant. Each experiment was performed at least three times (unless otherwise specified) with technical replicates.

Previous Results

Previous experiments were performed on commercial hPAEC, purchased from ATCC. Commercially available hPAEC were exposed to two distinct pressure conditions: the atmospheric and high-pressure conditions. Under high-pressure conditions cells experienced a pressure elevation of 40mmHg above the atmospheric one by means of a specific chamber. After either 2 or 24 hours of high-pressure exposure, hPAEC were tested for viability (MTS assay), NO and Reactive oxygen species production. Additionally, the effect of high-pressure exposure on the eNOS pathway was studied via Western Blot.

The MTS assay results demonstrated consistent cell viability across varying seeding densities, indicating that high-pressure conditions did not impair the cell viability at both 2 and 24 hours of high-pressure exposure.

Preliminary results on NO production were evaluated via Diaminofluorescein (DAF-FM) assay, and showed a significant reduction in NO production after 2 and 24 hours of high-pressure conditions. The evaluation of the ROS production via Cell-ROX depicted an increase in ROS production only after 24 hours of high-pressure exposure, while no differences were detected after 2 hours. The initial investigation on the effect of high-pressure exposure on the eNOS pathway was assessed by western blot. After 2 hours of 40mmHg pressure treatment, data showed no differences in eNOS expression, while the phosphorylation on the eNOS ser1177 showed a significant rise. However, after 24 hours of treatment, it was possible to observe a two-fold augmentation in eNOS synthesis while eNOS phosphorylation on ser 1177 decreased more than half (p-value $< 0,05$).

Objective

Building upon this data, we have chosen to extend our investigation in NO impairment after 24 hours of high-pressure condition. This decision is due to the identification of the most promising results observed at this specific time point.

The primary aim of this study is to unravel the possible mechanism responsible for the decrease in NO production, in the pathology of PAH.

To achieve this, our analysis encompasses three different cell models: commercially available human PAEC, primary PAEC sourced from patients with idiopathic PAH, and endothelial cells derived from induced pluripotent stem cells carrying the mutation in the BMPR2 gene.

Results

Commercial human Pulmonary Artery Endothelial Cells

Evaluation of Nitric Oxide production after 24 hours of high-pressure exposure

Commercial hPAEC incubated for 24 hours at high-pressure conditions displayed a reduction in NO production (**Figure 1R**). The relative reduction of NO observed in the high-pressure condition was 14.78% ± 2.32% (p-value ≤ 0.001).

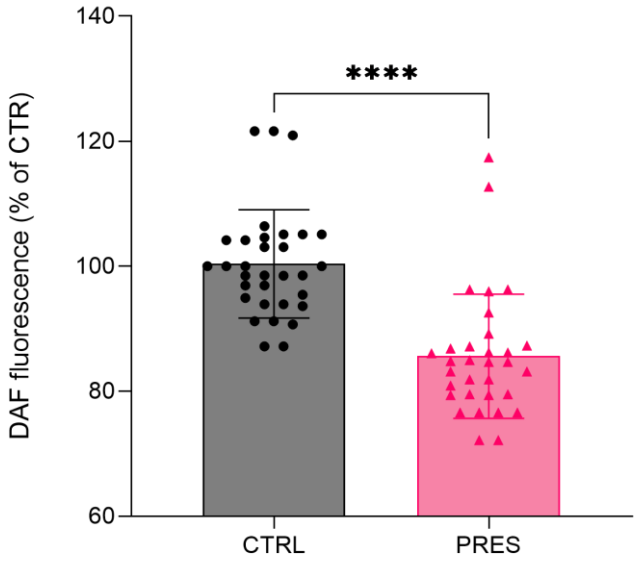

Figure 1R. Analysis Nitric Oxide production after 24 hours of high-pressure exposure.
CTRL= control, PRES = High-pressure (40mmHg)

Investigation of the eNOS pathway alteration after 24 hours of high-pressure exposure

After 24 hours of high-pressure exposure, commercial hPAEC samples were collected, as reported in the materials and methods section, from both the experimental and control conditions. Western Blot analysis of the eNOS pathways alteration was performed to assess the abundance of CamK2B, AKT and eNOS proteins and their phosphorylated counterparts. High-pressure conditions did not impair total Camk2B and AKT protein levels (**Figure 2R**). Additionally, no differences were highlighted in the active form for these two proteins (**Figure 3R**). On the contrary, a significant increase was assessed for total eNOS (relative increase 26.81% ± 15.5%, p-value ≤ 0.001) in the experimental conditions. Moreover, high-pressure conditions determined a reduction in the phosphorylation of Serine 1177 of p-eNOS (relative reduction 24.8% ± 19.55%, p-value ≤ 0.0067) (**Figure 4R**).

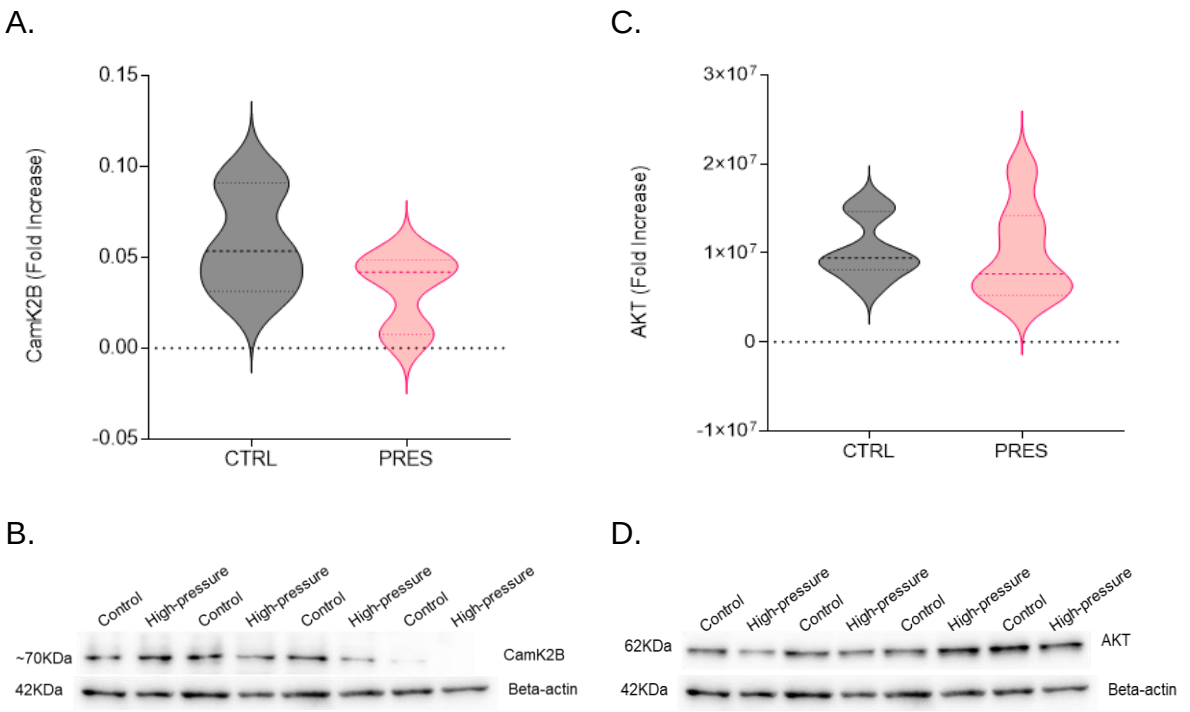

Figure 2R. Analysis of total CamK2B and AKT after 24 hours of high-pressure exposure.
(A)High-pressure conditions did not impair total Camk2b and (C) AKT expression level in commercial hPAEC.
B. Band densitometry for total CamK2B,
D. Band densitometry for total AKT

CTRL= control, PRES = High-pressure (40mmHg)

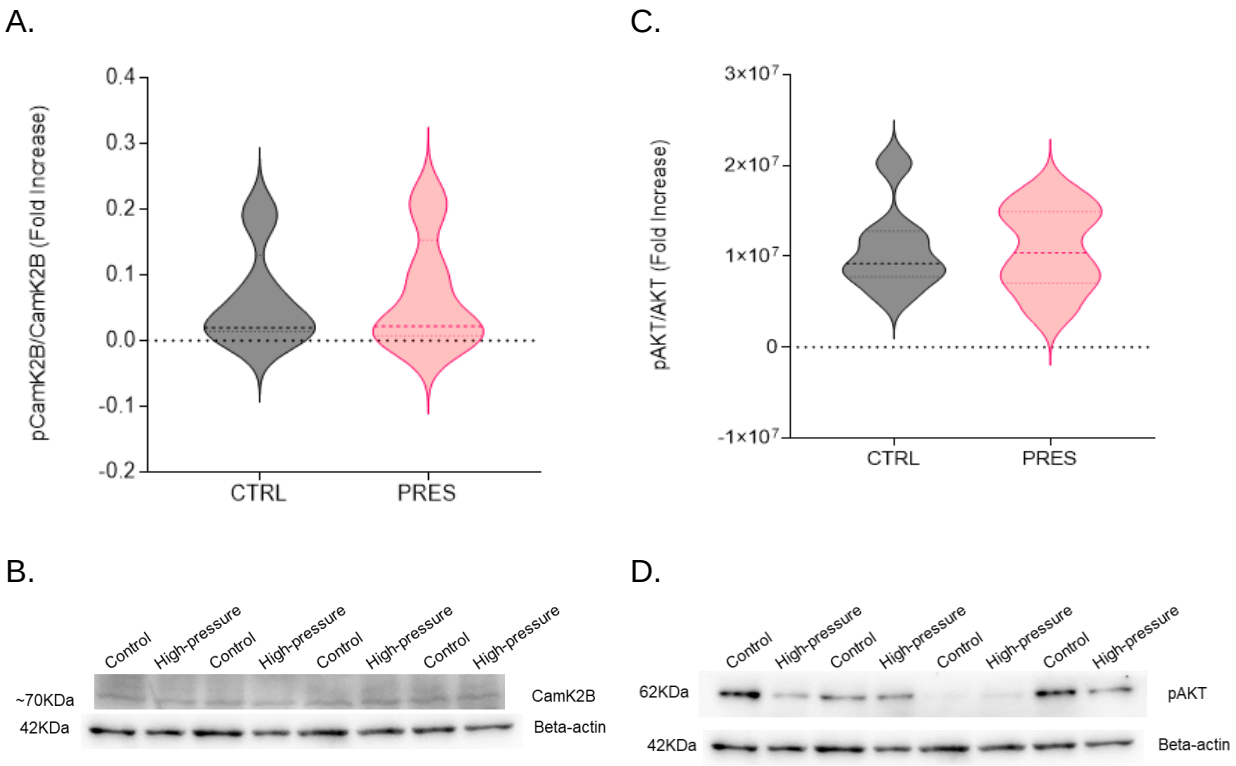

Figure 3R. **Analysis of phosphorylated CamK2B (pCamk2B) and AKT after 24 hours of high-pressure exposure.**
A.high-pressure exposure caused no differences in the activation of Camk2B (expressed as ratio between pCamK2B/CamK2B)
B. Band densitometry of CamK2b
C. high-pressure exposure caused no differences in the activation of AKT (expressed as ratio between pAKT/AKT)
D. Band densitometry of AKT

CTRL= control, PRES = High-pressure (40mmHg)

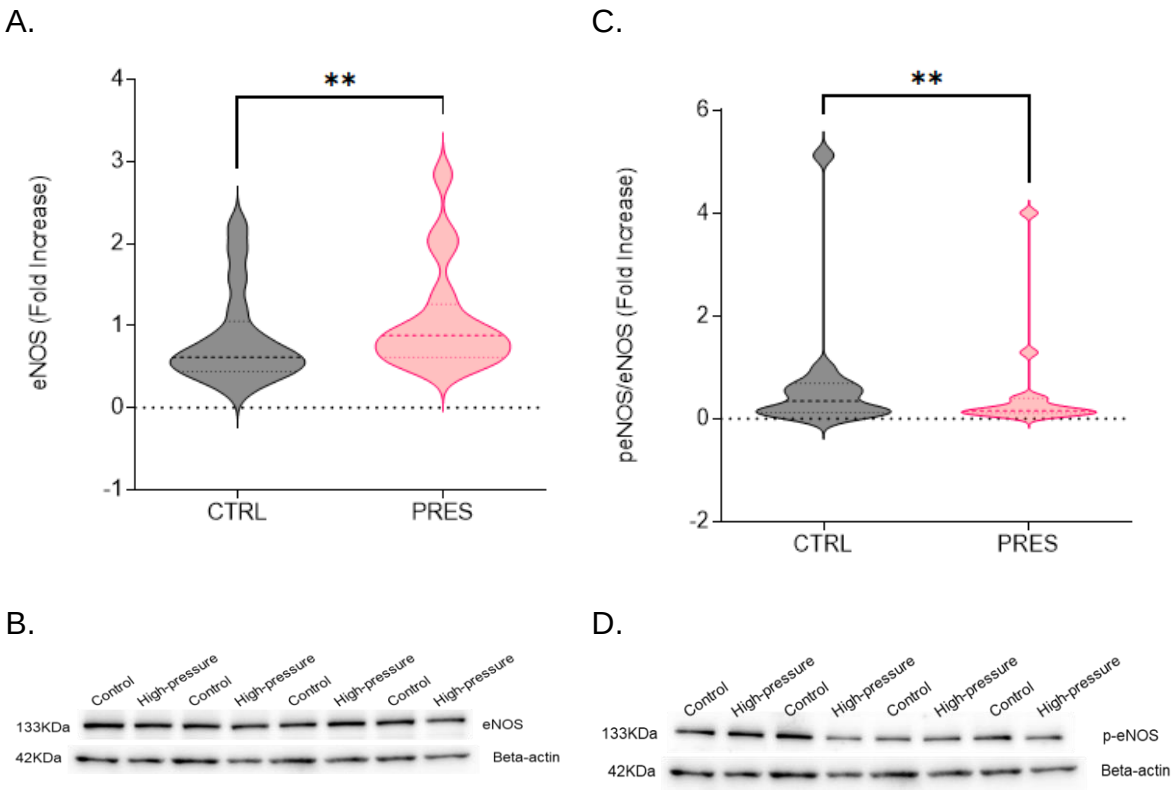

Figure 4R. **Analysis of total eNOS level and eNOS phosphorylation after 24 hours of high-pressure exposure**.
A. High-pressure exposure caused a rise in total eNOS level. B. Band densitometry of total eNOS.
C. 24 hours of high-pressure exposure determined a decrease in eNOS active form (expressed as a ratio peNOS/eNOS).
D. Band densitometry of phosphorylated eNOS.

CTRL= control, PRES = High-pressure (40mmHg)

Transcriptome differential expression analysis

Transcriptomic data analysis was performed to assess differences between the control and experimental conditions. The comprehensive transcriptome sequencing (RNA-seq) yielded 11,486 differentially expressed genes (DEGs) comprising 4,963 down-regulated (DW) and 6,219 up-regulated (UP). The distribution of the DEGs is illustrated in the volcano plot in **Figure 5R** , where the sorting criteria include the Log(Fold Change) and -Log(p-value) adjusted for the False Discovery Rate (FDR). Notably, the plot highlights relevant genes associated with the eNOS pathway in blue, with each corresponding dot annotated with the gene's name. Additionally, a significance threshold line, set at p-value of 0.05, facilitates the differentiation between DEGs with statistical significance from those without. In the upper left corner are represented the down-regulated genes, while in the upper right corner the up-regulated genes.

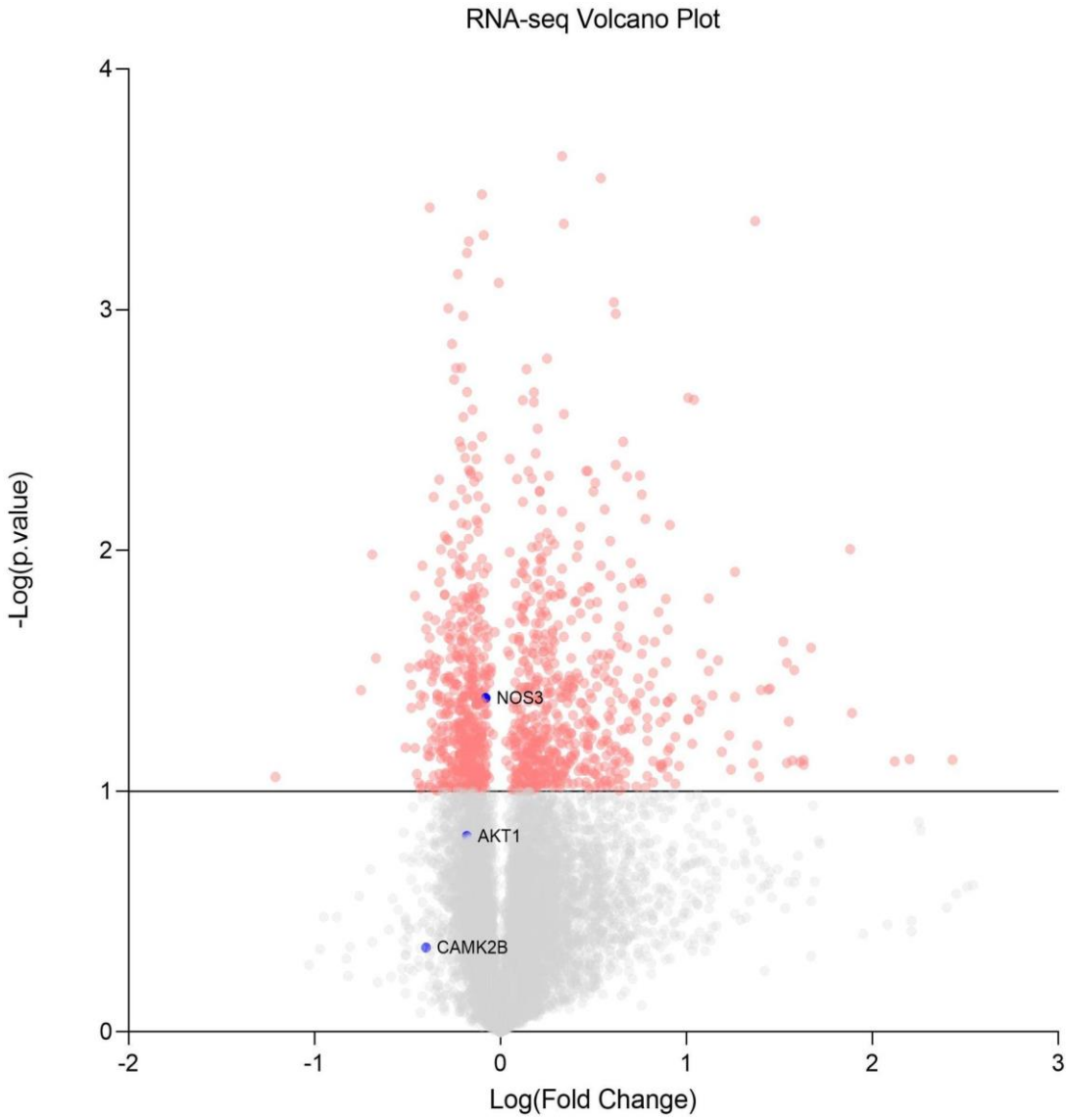

Figure 5R. Volcano Plot Differentially Expressed Genes.
In the volcano plot are highlighted the principal genes involved in the eNOS pathway.

From the transcriptomic data, CAMK2B and AKT1, two genes involved in eNOS pathways do not display a significant p-value and fold change between the two conditions analysed. On the contrary, NOS3, the gene encoding for eNOS, is slightly down-regulated with a fold change of -0.08 and a significant p-value.

For the subsequent transcriptome analysis, DEGs were analysed by using stringent criteria based on the selection of DEGs falling in the 90th centile. Thus, the final amount of DEGs analysed was 141 of which 21 down-regulated and 119 up-regulated. However, only DEGs

presenting a significant p-value and a fold change > 1.5 were considered for the analysis in order to reduce the odds of false-positive results. The volcano plot in **Figure 6R** shows the new visual distribution of the DEGs. Two threshold lines were established for data analysis- one corresponding to the fold change and the second for the p-value. Data displaying values major that a fold change of 1.5 and a significant p-value were further analysed for the possible involvement in the eNOS pathway. In the plot were highlighted the top 10 up- and down-regulated genes in red and green, respectively.

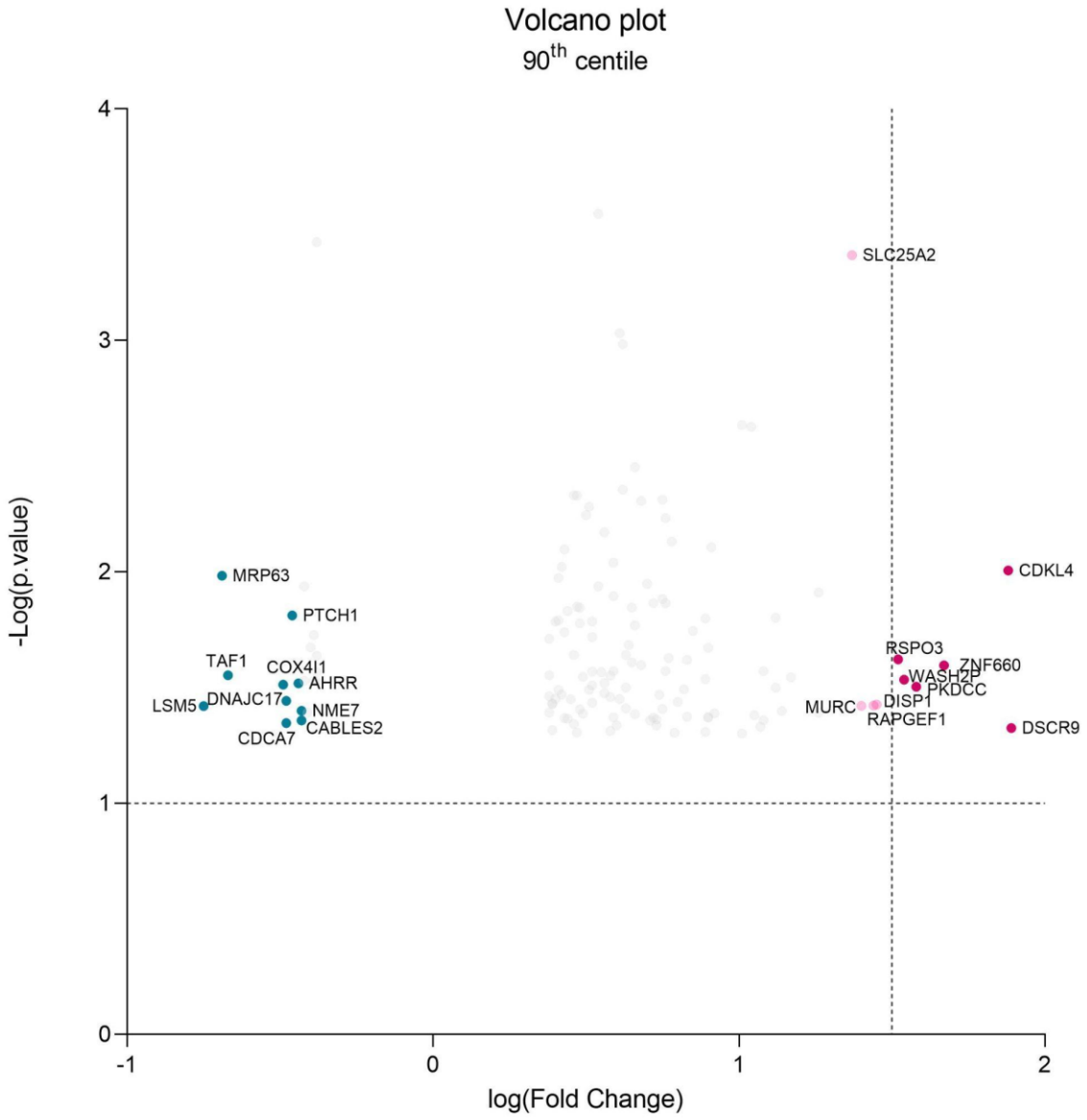

Figure 6R. **Volcano Plot of the differential expressed genes falling within the 90th centile.** Two threshold lines, aligned with the fold change and p-value, were established. DEGs exhibiting a significant p-value and a fold change greater than 1.5 were considered in the analysis. The top up-regulated DEGs are in red, while the top 10 down-regulated DEGs are depicted in green.

Transcriptome analysis: Functional Characterisation

The 140 DEGs falling within the 90th centile underwent analysis using the bioinformatics tool ShinyGO v0.61. The initial analysis consisted of an enrichment analysis utilising an hypergeometric distribution, with subsequent false discovery rate correction set at 0.05. This initial analysis was performed without dividing up and down regulated genes and focused on the selection of the Gene Ontology (GO) Biological Process. The **Table 1R**, presented below, illustrates the primary functional category in which DEGs falling in the 90th centile are mainly involved. From this analysis, two distinct groups emerge prominently namely, inflammation and gene silencing. The first group encompasses functions such as response to type I interferon, the type one I interferon signalling pathway and the cellular response to type I Interferon. The second group is composed of the following categories: negative regulation of gene silencing by miRNA, negative regulation of posttranscriptional gene silencing and negative regulation of gene silencing by RNA.

Enrichment FDR	Functional Category	Genes
0.033654145	Response to type I interferon	TRIM6, TYK2, IFIT3, XAF1 MX1, ISG20
0.033654145	Negative regulation of viral genome replication	IFIT5, MX1, ZC3H12A, TRIM6, ISG20
0.033654145	Type I interferon signalling pathway	TRIM6, TYK2, IFIT3, XAF1, MX1, ISG20
0.033654145	Cellular response to type I interferon	TRIM6, TYK2, IFIT3, XAF1, MX1, ISG20
0.033654145	Nuclear protein quality control by the ubiquitin-proteasome system	ANKZF1, KLHL15
0.038627146	Negative regulation of gene silencing by miRNA	BCDIN3D, DND1, ZC3H12A
0.038796789	Negative regulation of posttranscriptional gene silencing	BCDIN3D, DND1, ZC3H12A
0.038796789	Negative regulation of gene silencing by RNA	BCDIN3D, DND1, ZC3H12A
0.04472832	Regulation of viral genome replication	IFIT5, MX1, ZC3H12A, TRIM6, ISG20

Table 1R. ***Enrichment***. Main functional categories. In the *Enrichment section* of ShinyGO v0.61, it is shown the genes present in our list connected to the functional category.

Additional pieces of information were retrieved via the Network plot shown in **Figure 7R**. Possible interactions among the various categories are highlighted by means of connecting lines. Additionally, the size of the nodes is indicative of the number of genes involved in the processes. This network plot allows a better visualisation of the functional categories involved in the process. From this network plot it is possible to observe that the functional categories related to inflammation and gene silencing display the biggest nodes and the darker colour meaning that these groups display a larger and enriched gene set.

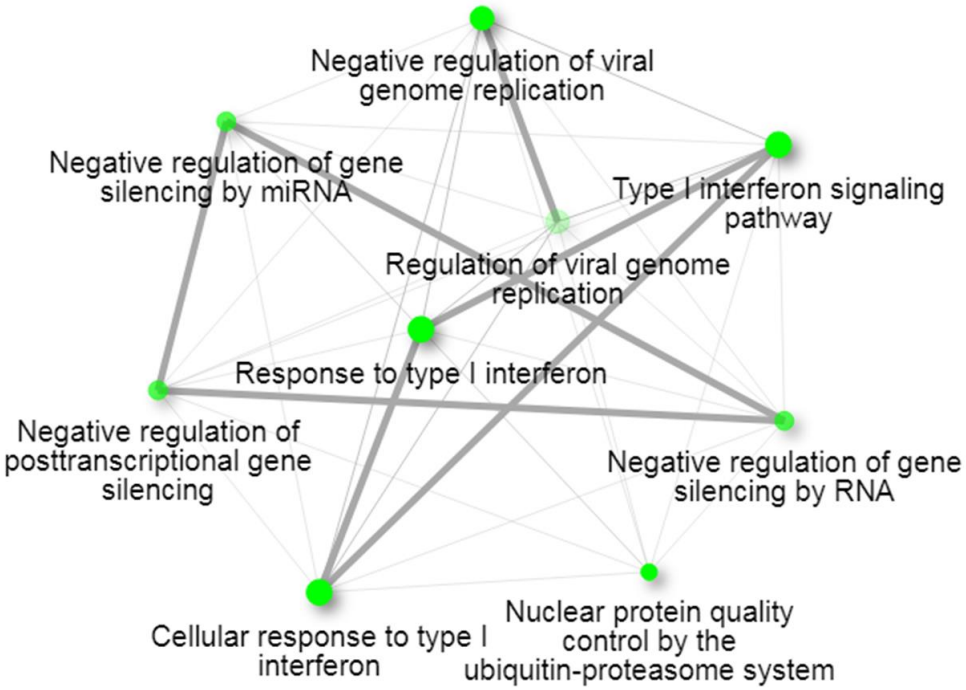

Figure 7R. ***Network plot***. Up and down Differential Expressed Genes (DEGs). Nodes represent pathways. Two pathways are connected if they share 20% or more genes. Moreover, bigger is the node larger is the gene set present in that pathway. The darker nodes indicate a more significant enriched gene set. Grey lines represent gene sets connection, thicker lines indicate more overlapped genes.

Transcriptome analysis: Genes and Gene Groups

Among the 140 genes falling in the 90th centile, 0.7% encodes for small nuclear RNA (snoRNA), 2.14% encodes for transcribed processed pseudogenes and processed-pseudogenes, 2.86% encodes for lncRNA, and 92% detain the information to encode for proteins. **Table 2R** summarises the genes encoding for snoRNA, lncRNA, transcribed processed pseudogenes and processed-pseudogenes as well as proteins.

Gene Type	Gene Names
snoRNA	SNORA58
lncRNA	FOXD2-AS1, PVT1, DSCR9, ZNF674-AS1
processed pseudogenes	RPL13AP6, NDUFAF4P1, FOXO3B,
transcribed processed pseudogenes	CAMTA1, PER3, DDI2,
protein coding	ZC3H12A, SPATA6, BTBD8, ATXN7L2, GABPB2, SH2D2A, NME7, DISP1, TMEM63A, WNT9A, TTC32, TTC27, CDKL4, PKDCC, PAIP2B, TCF7L1, TGOLN2, ANKRD23, IL1RL1, DBI, CDCA7, CYP27A1, ANKZF1, IRAK2, ZNF660, DNAH1, FAM3D, MYH15, NEK11, ZIC1, KCNAB1, FGF12, MSX1, ANKRD37, AHRR, CCDC152, MCTP1, SLC22A5, DND1, PCDHB10, SLC25A2, KIF4B, TMEM217, RSPO3, PC, MT1, RAET1L, LSM5, CROT, OR4F21, LETM2, JPH1, MTBP, PTPRD, SH3GL2, TMEM8B, SHB, PTCH1, LHX6, RPL35, RAPGEF1, AKR1E2, IFIT3, IFIT5, ACSL5, PSTK, TRIM6, OR2D2, NA, V2, DGAT2, CD163L1, TAS2R20, BICD1, BCDIN3D, BRCA2, NALCN, GNG2, DNAJC17, SPTBN5, FAM227B, ISG20, TM2D3, ZNF263, PDXDC1, COX4I1, XAF1, ACAP1, EFCAB13, MRPL27, ARHGAP28, GRIN3B, ATP8B3, TYK2, ZNF491, ZNF626, HSPB6, ZNF420, ZNF180, BLOC1S3, PTGIR, KPTN, VSIG10L, ZNF667, ZNF547, ZNF324, GDF5, CABLES2, TCFL5, SLC17A9, SETD4, MX1, GAS2L1, APOBEC3B, DENND6B, XG, KLHL15, DDR1, MRM1, TAF1, TAF7L, BEX1, CLIC2

Table 2R. Summary of gene types present in the DEGs falling in the 90th centile.

Considering the GO biological processes, up and down regulated DEGs were grouped in functional categories defined by the high level of GO terms. The analysis displayed the Regulation of response to stimulus as the most enriched category with a total of 30 DEGs of which 27 up-regulated and 3 down-regulated. Other relevant categories emerging from the

analysis included regulation of signalling, response to stress, response to external stimulus, immune system process, immune response, regulation of immune system process, and response to endogenous stimulus.

Transcriptome analysis: Up-regulated and Down-regulated Differential Expressed Genes

In order to assess the main pathway involved in each category separately, DEGs belonging to the 90th centile were divided into up and down-regulated. This analysis identified the two principal clusters related to inflammation and gene silencing within the up-regulated group **Figure 8R**. Conversely, the down-regulated group displayed interconnections among the metabolism pathways related to purine and pyrimidine synthesis (75%), carbohydrate synthesis and enzymes involved in carbohydrates and lipids metabolism (25%) **Figure 9R**.

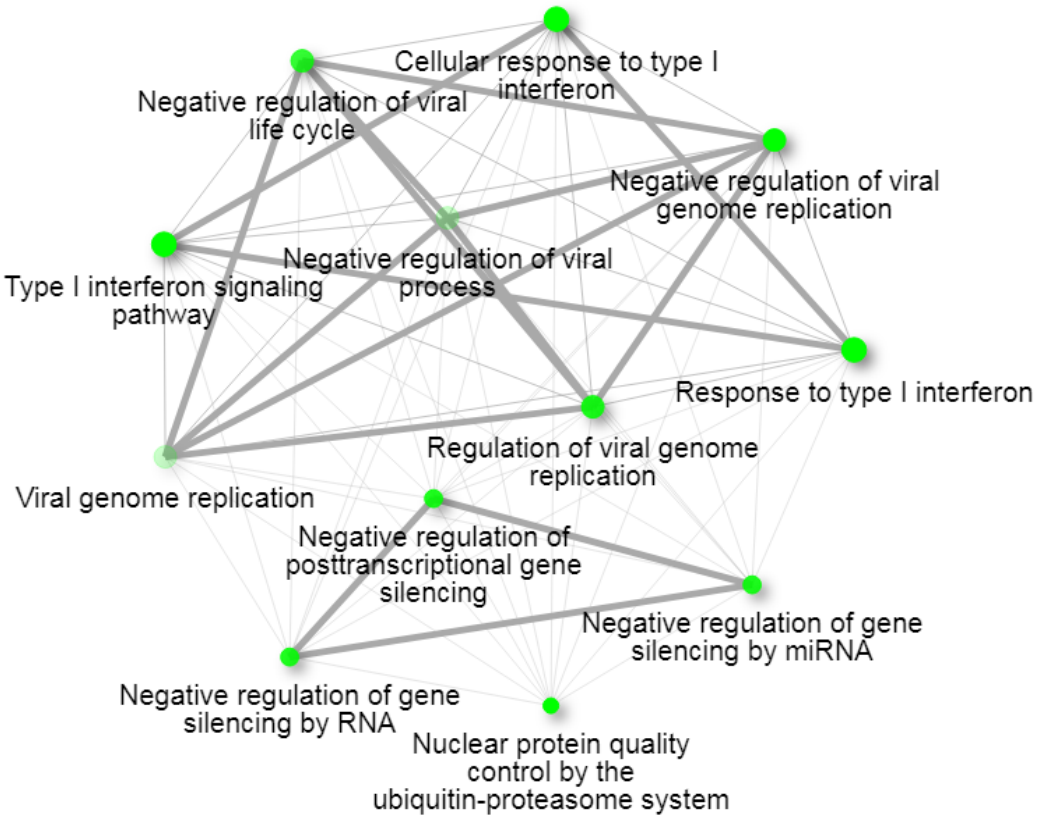

Figure 8R. Up-regulated DEGs. The Up-regulated genes analysis showed two main interconnected pathway groups.

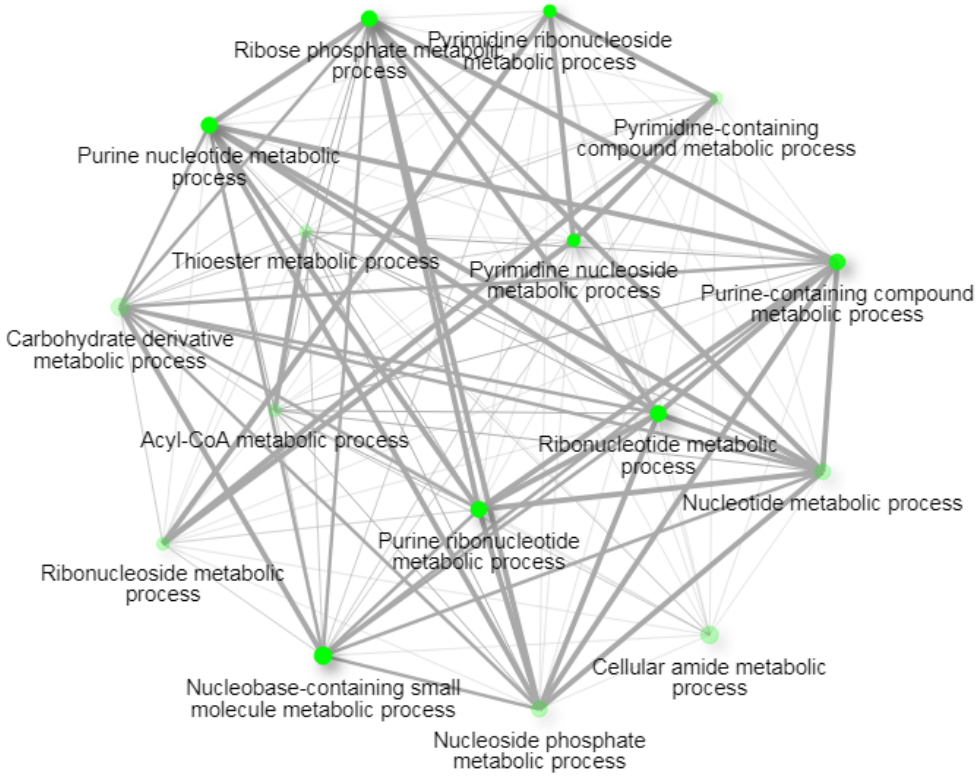

Figure 9R. Down-regulated DEGs. The down-regulated genes analysis showed no main interconnected pathway group easily detectable.

Subsequently, 23 DEGs were isolated from the 90th centile by setting a significant p-value cut-off and an absolute log(fold change) > 1. The DEGs highlighted by this approach are summarised in **Table 3R**.

Genes	NCBI name	log(Fold Change)	p-value
DSCR9	Down syndrome critical region gene 9 non-protein coding	1.89	0.047387
CDKL4	cyclin-dependent kinase-like 4	1.88	0.009867
ZNF660	zinc finger protein 660	1.67	0.025354
PKDCC	protein kinase domain containing cytoplasmic	1.58	0.031414
WASH2P	WAS protein family homolog 2 pseudogene	1.54	0.029258
RSPO3	R-spondin 3	1.52	0.02388
DISP1	dispatched homolog 1 Drosophila	1.45	0.037505
RAPGEF1	Rap guanine nucleotide exchange factor GEF 1	1.44	0.037827
MURC	muscle-related coiled-coil protein	1.4	0.037992
SLC25A2	solute carrier family 25 mitochondrial carrier ornithine transporter member 2	1.37	0.000428
MX1	myxovirus influenza virus resistance 1 interferon-inducible protein p78 mouse	1.26	0.012274
NDUFA 4P1	NADH dehydrogenase ubiquinone complex I assembly factor 4 pseudogene 1	1.26	0.040624
ZIC1	Zic family member 1	1.17	0.028595
FAM3D	family with sequence similarity 3 member D	1.14	0.039924
BLOC1S3	biogenesis of lysosomal organelles complex-1 subunit 3	1.12	0.01582
GRIN3B	glutamate receptor ionotropic N-methyl-D-aspartate 3B	1.12	0.03164

Table 3R (continue). Top 23 DEGs falling in the 90th centile

Genes	NCBI name	log(Fold Change)	p-value
DDI2	DNA-damage inducible 1 homolog 2 S. cerevisiae	1.08	0.026821
ATP8B3	ATPase amino phospholipid transporter class I type 8B member_3	1.08	0.043787
VSIG10L	V-set and immunoglobulin domain containing 10 like	1.07	0.046739
BEX1	brain expressed X-linked 1	1.05	0.041687
IFIT3	interferon-induced protein with tetratricopeptide repeats 3	1.04	0.002362
DND1	DND microRNA-mediated repression inhibitor 1	1.01	0.002322
PTPRD	protein tyrosine phosphatase receptor type D	1.01	0.049927

Table 3R (continue). Top 23 DEGs falling in the 90th centile

Transcriptome analysis: Co-expression gene network analysis

The lncRNA Down Syndrome Critical Region 9 (DSCR9) was the DEGs with the highest Fold change value e significant p-value. To establish how DSCR9 might contribute to the PAH development, a co-expression gene network analysis based on DSCR9 role on neurological disorders was taken into consideration[94] given the substantial number of neurological genes present in our transcriptomic data. Using the information retrieve from this study was possible to point out five different DEGs from our transcriptomic data namely, prostaglandin I2 prostacyclin receptor IP (PTGIR); pannexin 2 (PANX2); myosin light chain kinase (MYLK); calcium-calmodulin dependent protein kinase II beta (CAMK2b); 5-hydroxytryptamine serotonin receptor 1B G protein-coupled (**Table 4R**).

Gene	Name	Fold Change	p-value
CAMK2B	calcium-calmodulin dependent protein kinase 2 beta	-0.4	0.44667
HTR1B	5-hydroxytryptamine serotonin receptor 1B G protein-coupled	0.13	0.51694
MYLK	myosin light chain kinase	1.59	0.22294
PANX2	pannexin 2	0.88	0.12904
PTGIR	prostaglandin I2 prostacyclin receptor IP	0.9	0.02131

Table 4R. Differential Expressed Genes in common between the Hum Genomics. 2018 study and our transcriptome data. In the table are reported the Fold Change and p-value present in the transcriptome data.

The possible interactions with genes involved in the eNOS pathway were analysed via the bioinformatics tool UCSC genome browser. HTR1B, PANX2 and PTGIR do not display interactions with relevant genes involved in the eNOS pathway and for this reason were not taken into consideration to carry on the analysis. The MYLK gene shows an interaction with CAMK2B but not relevant interaction with other genes involved in the eNOS pathway. Thus, of these genes only CAMK2B was reported[95,96] to be involved in the pathway of interest. To establish at which level CAMK2B interacts with genes involved in the eNOS pathway, the initial analysis considered the top 30 interactions (**Figure 10R**) with supporting information derived

from text-mining, database and pathway database support. On these bases, the CAMK2B interactions with AKT1 and NOS3 were highlighted.

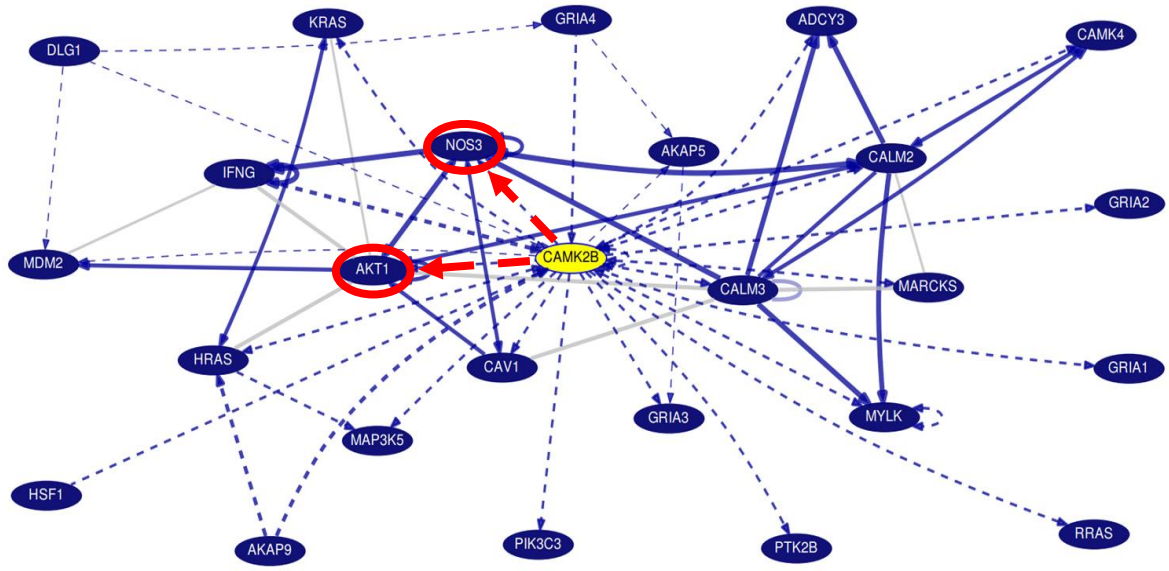

Figure 10R. **Top 30 gene's interactions**.
CAMK2B (in yellow) is the gene of interest. The map shows the predicted interaction with AKT1 and NOS3.
Lines interconnecting genes have different meanings. Solid grey lines indicate the interaction supported only by text-mining support and the thickness indicates the number of articles supporting it. Dashed blue lines show information derived from one curated database. Dark blue lines describe the information derived from papers describing fewer than 10 interactions. Light blue lines indicate information derived from a high-throughput paper describing more than 10 interactions. Solid blue lines show information derived from both curated database and text-mining interaction. The arrows show the directionality of interaction that is determined by majority support. In red is shown the interaction of CAMK2B with AKT1 and eNOS.

In order to understand the mechanism of action by which CAMK2B may interact with the eNOS pathway, the top 3 interactions were analysed (**Figure 11R**). According to the interaction map, the first three interactions are essential to determine the activation of both CamK2B and AKT. Specifically, HSF1 interacts directly on CAMK2B determining the following autophosphorylation event on CAMK2B. Notably CAMK2B exhibits the capability to undergo a self-activation via the phosphorylation on Threonine-287. Subsequent to this event, CAMK2B assumes an activated state facilitating the interaction with AKT (**Figure 12R**). Notably, it is with the 26th interactions that CAMK2B can interact and activate NOS3 through the phosphorylation on serine-1177 (**Figure 12R**).

Figure 11R. Top 3 interactions.
HSF1 interacts with CAMK2B determining CAMK2B self-autophosphorylation on threonine 287. Following this event, active CAMK2B can interact and activate AKT1.

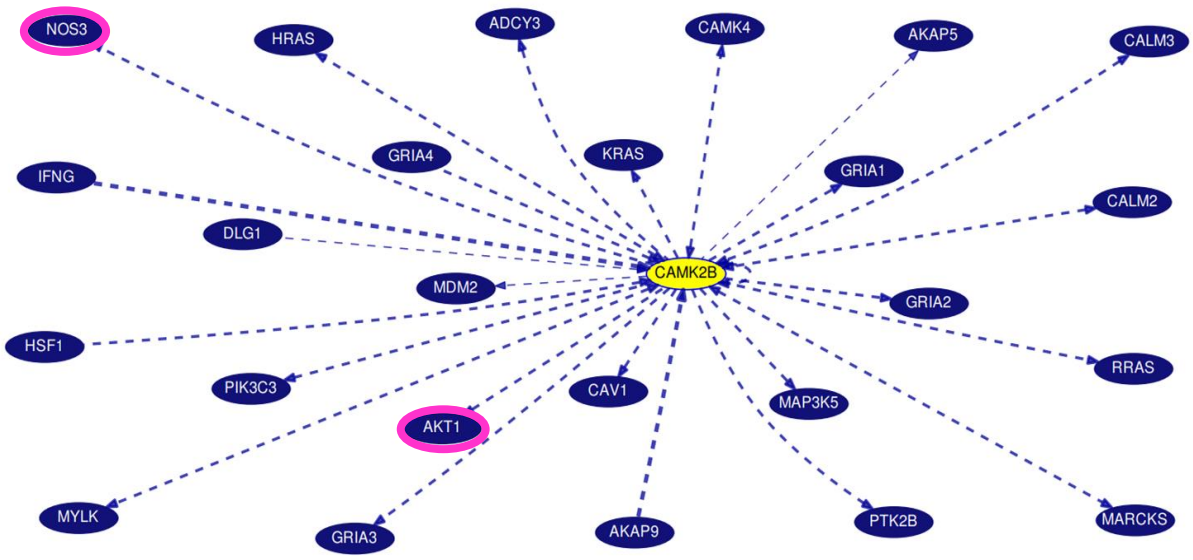

Figure 12R. **Top 26 interactions**.
The graph shows the top 26 interactions. CAMK2B can interact directly with AKT1 and NOS3.

Transcriptome data validation

RT-qPCR was employed to validate the transcriptome data utilising three independent biological replicates exposed either to the control or high-pressure conditions for 24 hours. In conjunction with the top upregulated DEGs identified in our transcriptomic data, namely DSCR9 and RSPO3 chosen for their substantial fold change and significative p-value, we take into consideration other genes implied in the eNOS pathway, specifically NOS3 and CAMK2B. Data normalisation was achieved using the ACTB gene, as the most stable housekeeping gene present in our sample.

In contrast with the transcriptomic data, RT-qPCR did not reveal any differences in NOS3 expression (**Figure A 13R**). Conversely, RT-qPCR substantiated the transcriptome data for CAMK2B, DSCR9 and RSPO3 (**Figure B 13R, C 13R, D 13R**). Specifically, as seen in transcriptomic data, 24 hours of high-pressure condition did not induce any changes in CAMK2B expression. However, it can significantly increase DSCR9 and RSPO3 expression, demonstrating a fold change of 2.0, and 1.53, respectively. It is essential to note that RT-qPCR, being a less sensitive technique, may not detect subtle fluctuation in gene expression like that observed for NOS3 (fold change of -0.08, p-value= 0.041) in transcriptomic data. Nevertheless, the validation via this method of the two most upregulated genes along with the expression of CAMK2B contributed to validate transcriptomic data, affirming the reliability of our findings. (**Table 3R** and **Table 4R** for Fold Change and p-value of DSCR9, RSPO3, and CAMK2B, respectively)

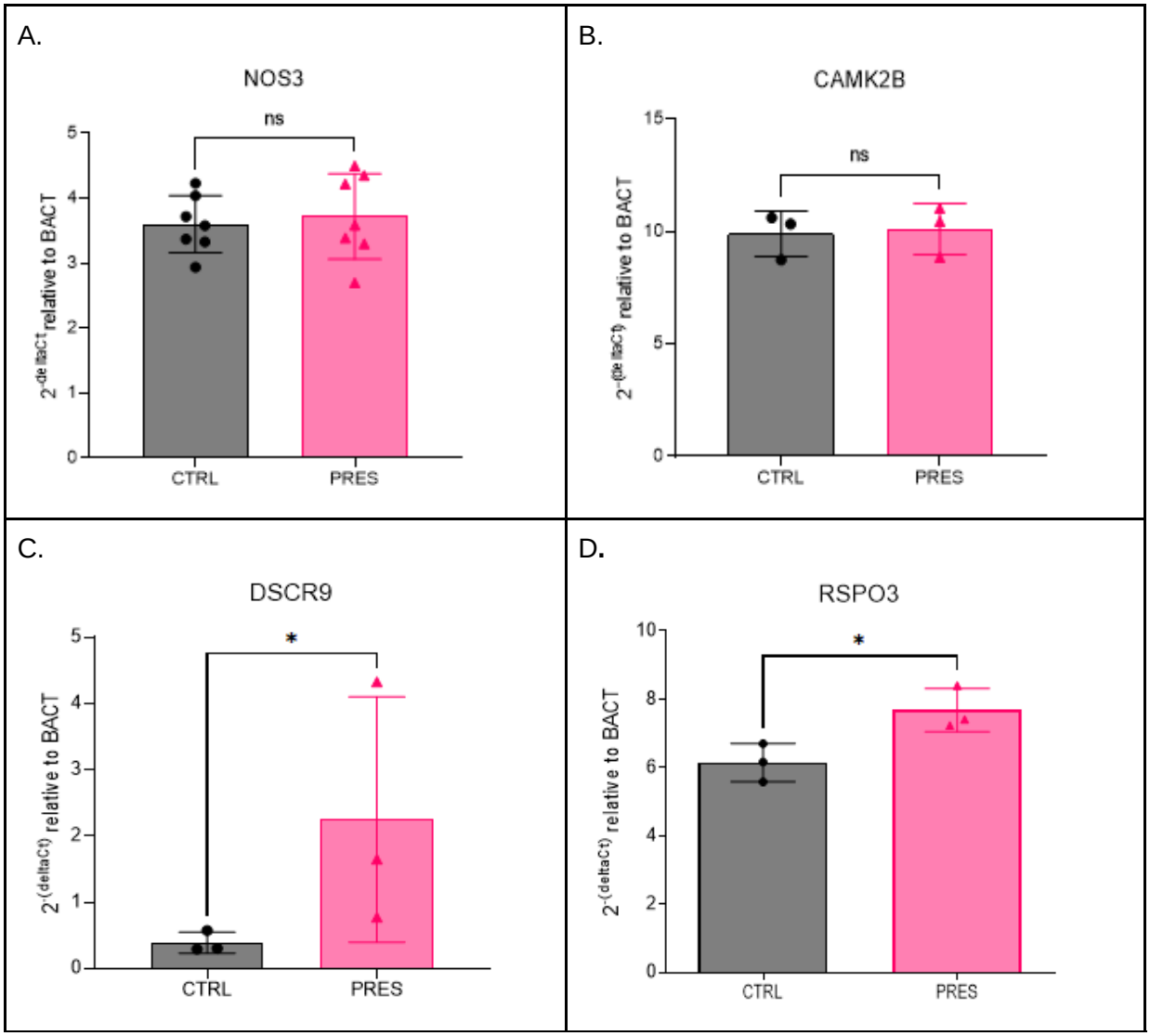

Figure 13R. RT-qPCR for transcriptome data validation. Changes in gene expression are indicated as $2^{-(\Delta Ct)}$ relative to ACTB expression. Differences were evaluated by comparing control to pressure samples and applying unpaired t-student tests. Asterisks indicate significant differences between samples with a p-value < 0.05. In **A** and **B.** is reported in the NOS3 and CAMK2B expression. Their expression did not change after 24 hours of high-pressure exposure. **C.** and **D.** DSCR9 and RSPO3 gene expression in samples exposed to control and high-pressure conditions. DSCR9 and RSPO3 displayed a significant increase in their expression after 24 hours of high-pressure exposure.

CTRL= Control, PRES = High-pressure (40mmHg)

DSCR9: Bioinformatics Characterisation

Cellular and Subcellular Localisation: lncATLAS Database

The lncRNA DSCR9 is situated on chromosome 21 at q22.13 position on the positive strand. DSCR9 is composed of 1681 nucleotides, and it is organised in three exons and two introns. Notably, there exist five different isoforms of DSCR9, all sharing a common sequence in the first two exons and the initial intron. DSCR9 is regulated by SPI1 (PU.1) and TCF4 transcription factors and presents oestrogen responsive elements in correspondence of DSCR9's enhancer region. Additionally, a recent study[97] performed in MCF7 cells highlighted the colocalization of SET and oestrogen receptor α proteins on DSCR9's enhancer region, determining the formation of an active chromatin.

To elucidate the cellular localisation of DSCR9, data from lncAtlas database were employed. In this database, the concentration of DSCR9 (ENSG00000230366) in the cell is quantified using the Relative Concentration Index (RCI) which gives the concentration of a gene per unit mass of RNA between two cellular compartments, namely the nucleus and the cytoplasm.

For this analysis, two well-established lncRNAs, MALAT1 (ENSG00000251562) and DANCR (ENSG00000226950), were chosen as reference genes due to their distinct localisation inside the cell. Specifically, MALAT1 is predominantly localised within the nuclear region, while DANCR is in the cytoplasm. Caring on a comparative approach among these three lncRNAs enhances our understanding about DSCR9's subcellular localisation and potential function.

Figure 14R is a bar plot representing the summary of DSCR9 localisation inside various cell lines (x axes). In the graph, the RCI value (on y axes) and the individual Fragments per kilobase per million mapped (FPKM), a value used to calculate the RCI index, are reported (on the top and bottom of the bars). As it is possible to observe, DSCR9 displays the same behaviour of the reference lncRNA MALAT1, even though it was not possible to determine the abundance of DSCR9 in all the cell types. This result suggests a possible action inside the nucleus of the cells. Additionally, DSCR9 expression is not reported in all the cell types mentioned in the graph, this is due to the fact that if the FPKM in one of the two compartments is not detectable, the corresponding cytoplasmic/nuclear (NC) RCI cannot be calculated. Negative values along the y axes indicate a nuclear localization. On the contrary, positive values indicate a cytoplasmic localisation.

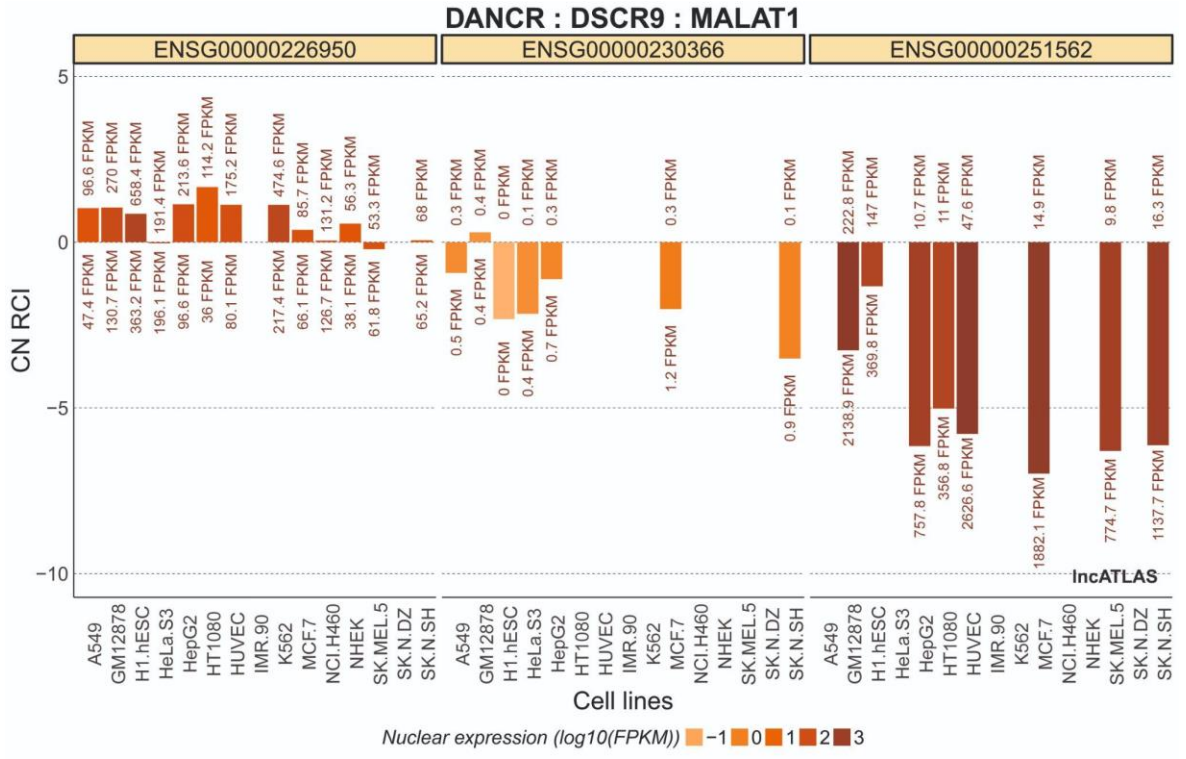

Figure 14R. **DSCR9 localisation in different cell lines**.
In the bar chart DSCR9 and the two reference genes, DANCR and MALAT1, are reported in various cell types. The colour of the bars indicates their absolute nuclear expression. Positive CN RCI value indicates cytoplasmic localisation, while the negative values of CN RCI indicate nuclear localisation. Bars represent the CN-RCI value for DSCR9, DANCR and MALAT1 across all the cell lines. The expression value (FPKM) is indicated for either the nuclear or the cytoplasmic compartment, on bottom and top for each compartment, respectively.

To compare the distribution of DSCR9 within a specific cell type with those of other genes, the cell line MCF7 was selected due to the high level of DSCR9 expression. Once again, the same two reference genes (MALAT1 and DANCR) were taken in the analysis to perform a clear comparison. The contour plot in **Figure 15R**, displays the lncRNA DSCR9 and reference gene DANCR as the ratio between the RCI value and the whole cell expression. As for the previous graph, negative Cn RCI values are representative of a nuclear localisation while the positive ones indicate a cytoplasmic localisation. Thus, due to the fact that DSCR9 has a negative RCI value as the reference gene MALAT1, it is possible to say that DSCR9 might exploit its function inside the nucleus.

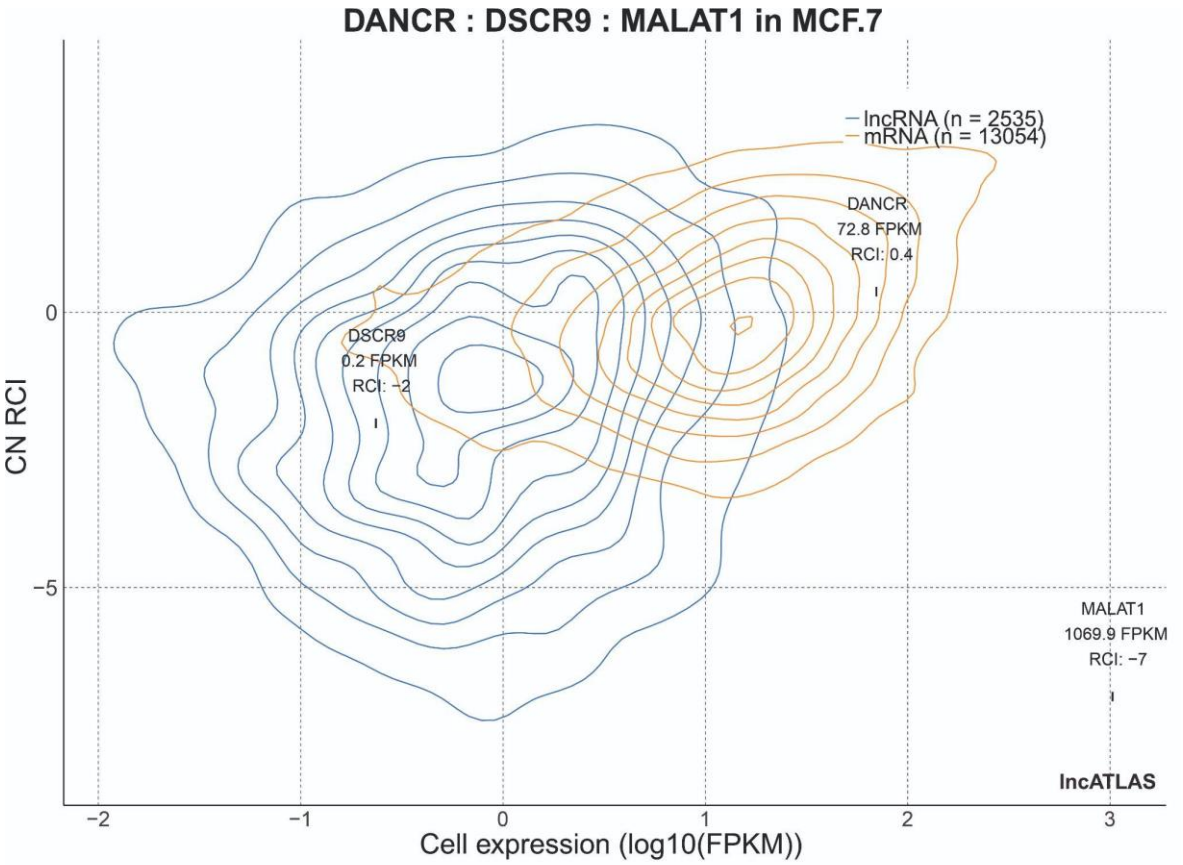

Figure 15R. **Contour plot of DSCR9 localisation within MCF7 cells**.
MALAT1 and DANCR are used as reference genes for nuclear and cytoplasmic localisation, respectively. In this graph, lncRNAs and mRNAs are displayed as functions of CN RCI (y axes) and whole cell expression [Log(FPKMs)] (x axes). DSCR9, MALAT1 and DANCR are displayed together with their whole cell expression and RCI value. In orange is shown the total mRNAs population, while in blue is displayed the population of lncRNAs. The number (*n*) reported is referring to the total numbers of mRNAs and lncRNAs. Dots in the graph with the RCI value indicate the position of the lncRNA of interest. For convenience, MALAT1 is not reported inside the graph to facilitate the reading and avoid overlaps with DSCR9.

Considering these data, differences of DSCR9 and DANCR localisation across various cell types and within a specific one (MCF7) is quite clear from **Figure 14R** and **Figure 15R**. Additionally, the cytoplasmic-nuclear localisation of DSCR9 is closer to MALAT1 localisation and consistent across the various cell types (**Figure 14R)**, supporting the possibility of a DSCR9 action inside the nucleus of the cells.

Data on DSCR9 sub-compartmental localisation is shown in **Figure 16R** along with the two reference genes used. The percentile rank of DSCR9, DANCR and MALAT1 is reported for each subcellular compartment. MALAT1 displays the highest percentile rank for the insoluble fraction (86.7%) and cell membrane (81.8%), when compared to DANCR and DSCR9 which

are showing the same value for both the insoluble fraction (21.5%) and cell membrane localisation (51.5%). Additionally, DSCR9 has been found enriched in the nuclear compartment, namely the nucleolus (96.5%), nucleoplasm (94%) and on chromatin level (93.2%). Notably, DSCR9 has a stronger affinity with the nuclear compartment when compared to the two reference genes. The highest percentage of DSCR9 enrichment that is found at the nuclear level suggests that DSCR9 may exert its function by regulating the chromatin access (chromatin level) and nuclear transports (nucleoplasm) or modulating stress response, enzymatic activity, nucleolar structure (nucleolus).

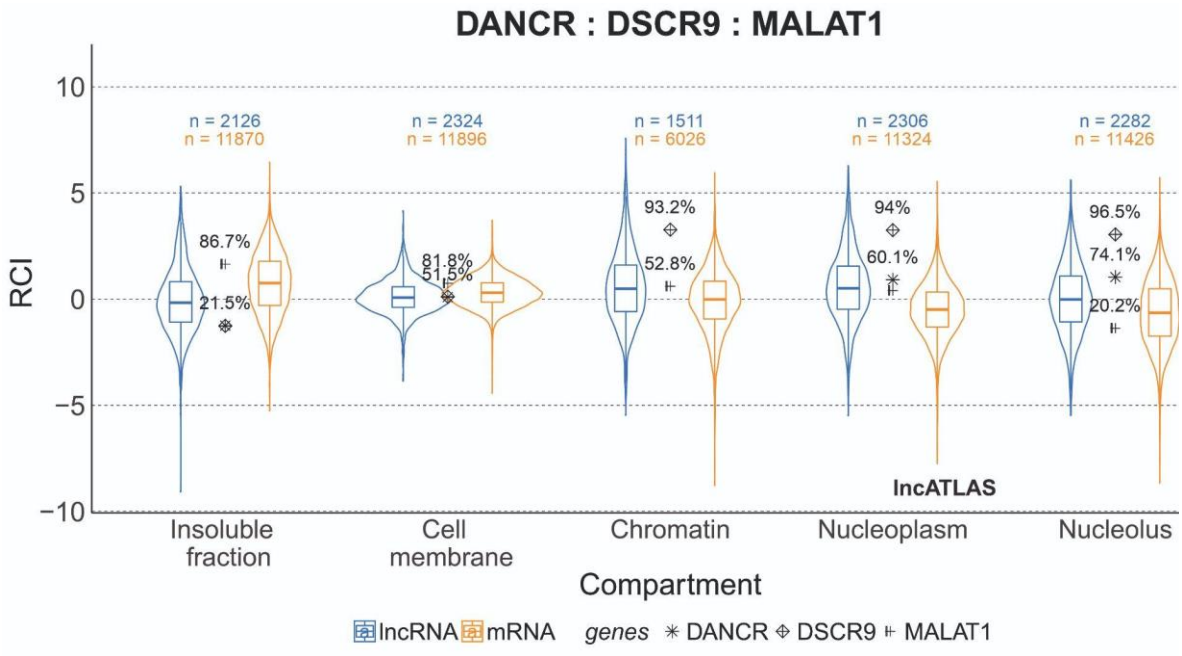

Figure 16R. **DSCR9 Subcellular localisation.**
The box plot indicates the relative concentration index (RCI) for both lncRNA and mRNA and their distribution across the various cytoplasmic or nuclear sub compartment. *n* indicate the total number of genes in each distribution. In orange is displayed mRNA, in blue lncRNA. The percentile rank of the DSCR9, DANCR, and MALAT1 is reported for each compartments to give an idea about their overall distribution within a cell.

DSCR9 structure prediction: mFOLD 2.3

mFOLD 2.3 web server was employed to predict the possible three-dimensional structure of DSCR9, a crucial step in gaining insight into the likely role and function of this lncRNA. Employing mFOLD 2.3 the energy matrices were computed in order to provide both the optimal and suboptimal secondary structure of DSCR9. Thus, DSCR9 FASTA sequence was submitted to the mFOLD2.3 web server, and the analysis was conducted with default parameters, including enthalpies and temperature set at 37°C for RNA folding. These parameters were retained unchanged, given the assumption that they remain constant within temperature range occurring *in vivo* and in the laboratory[91]. mFOLD 2.3 generated 36 different possible DSCR9 structures according to all the possible base-base interactions and the ΔG values. A summary of the all possible structures of DSCR9 is reported in **Figure 17R**.

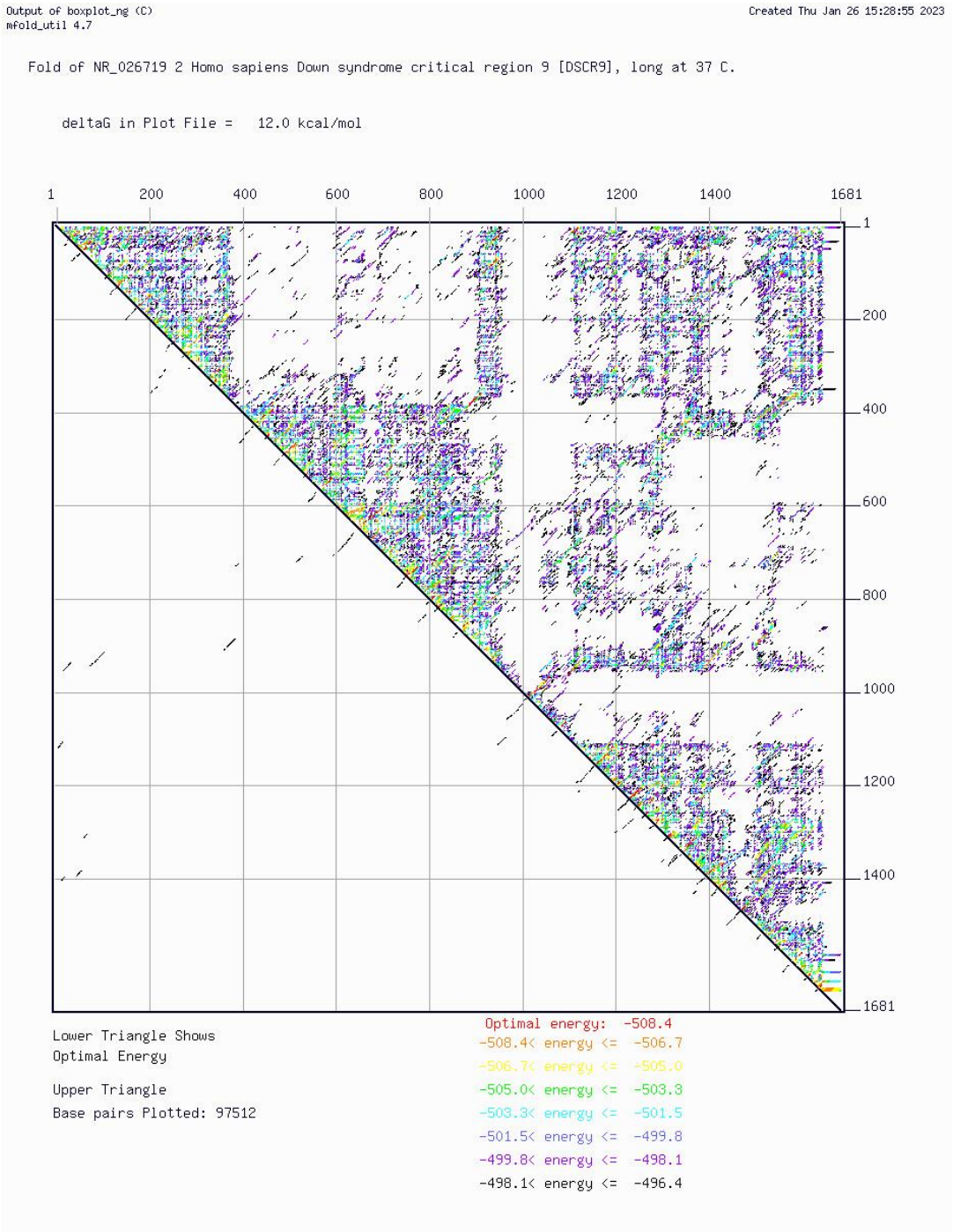

Figure 17R. Energy dot plot of all the possible DSCR9 3D structures.
In the matrix the numbers indicate the bases and the dots correspond to the possible interaction that can occur. the colour of the dots correspond to the ΔG value of each interaction. In the upper part of the graph is reported all the possible base pairs, while in the lowest triangle is illustrating the base pairing with the optimal energy. Base pairs occurring in all the structures are coloured in black, while those occurring in two or more structures but not in all are displayed in grey.

Considering mFOLD 2.3 instructions, to determine which of these structures was the most reliable, a new script was generated. This script considered the relative ΔG value and the base-base pair interaction shared among the structures was generated. According to this analysis, the structure 22 (**Figure 18R**) was chosen since it displayed the highest score in terms of ΔG value and base-base pair interaction.

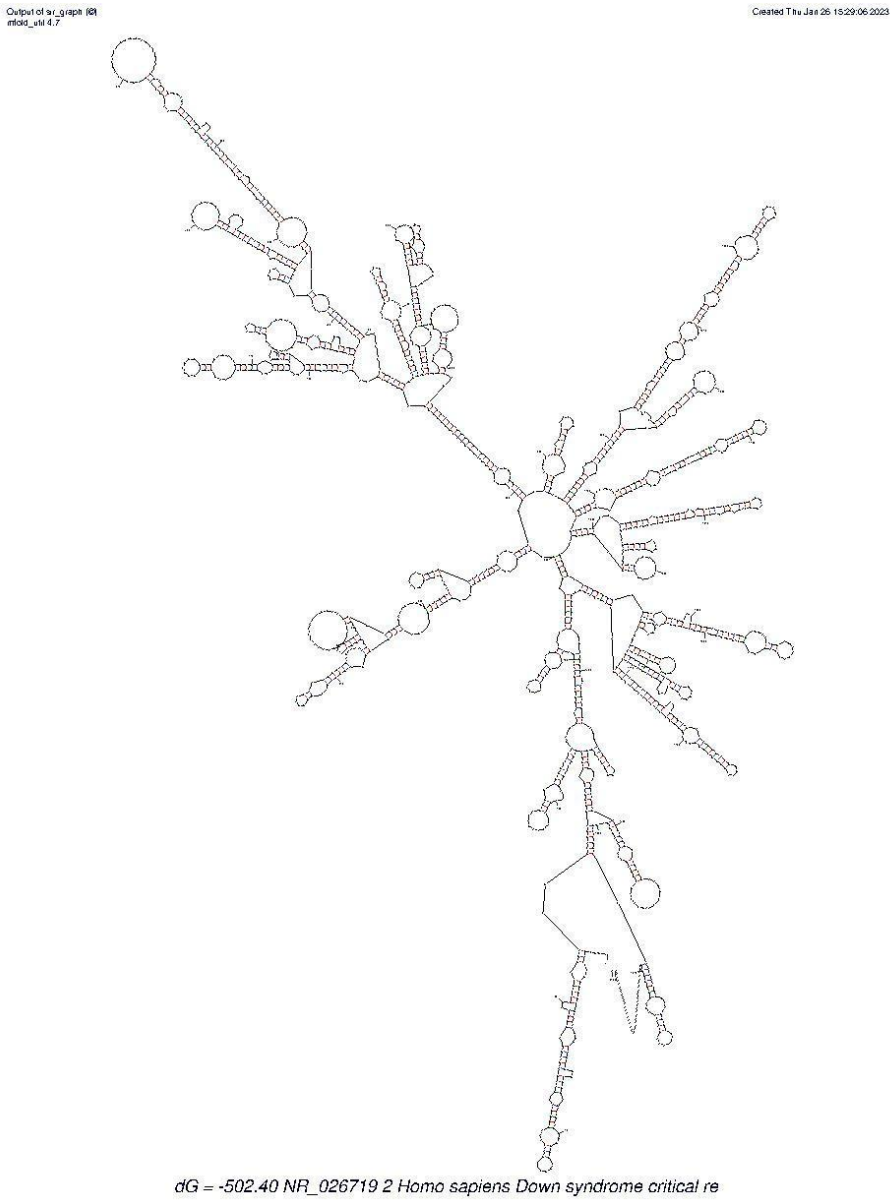

Figure 18R. **DSCR9 three-dimensional structure**

DSCR9 conservation and single nucleotide polymorphisms: lncBook 2.0

The examination of DSCR9 conservation across species was conducted by employing the lncBOOK 2.0 (https://ngdc.cncb.ac.cn/lncbook). Data revealed notable conservation of DSCR9 among twelve species. About the coding potentiality, in Pongo Abelii, the DSCR9 sequence does not encode for protein. However, in Pan paniscus, Pan troglodytes, Callithrix jacchus, it is reported to encode for a protein. For Homo sapiens no annotations are available, leaving the question about the DSCR9's role still unanswered. A summary of DSCR9 conservation among species is reported in **Figure 19R**.

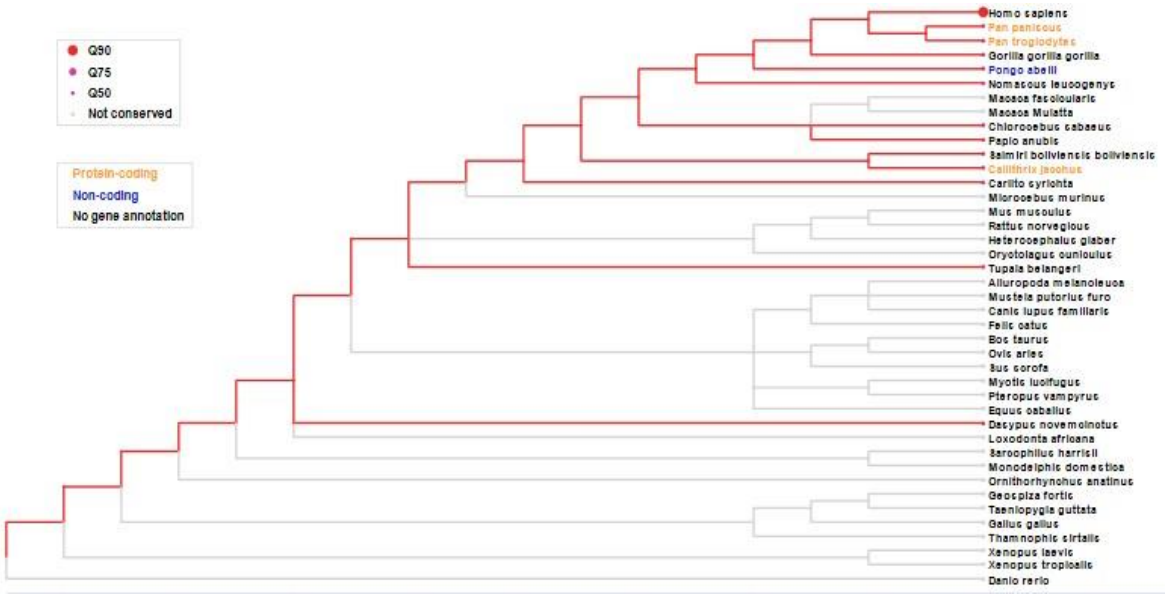

Figure 19R. **DSCR9 conservation among species.**
The phylogenetic tree represents the conservation of the lncRNA DSCR9 among species. Red line indicates conservation, while the grey one indicates in which species the DSCR9 sequence is not conserved. Species' names are reported in specific colours. Yellow name is for those sequences which encode for protein, Blue names for non-coding sequence. The name of the species is in black when there is no gene annotation. Dots dimension indicates how the sequence is conserved among species. For a specific species, the homologous sequences/genes are determined if the alignment performance (measured by alignment length and identity) of lncRNAs exceeds the introns' Q50 threshold, which represents the intermediate level of intron alignments.

Seven distinct single nucleotide polymorphisms (SNP), encompassing both transition and transversion types, have been reported within the DSCR9 sequence. **Table 5R** presents a summary of the SNPs observed in lung tissue. Notably, even though the SNPs observed have been reported to be related to a pathogenic outcome, the exact impact of this variation is still unknown.

variation name	dbSNP ID	Mutation ID	Effect
NC_000021.9:g.37221308C>T	rs2835677	COSV55706525	**Pathogenic**
NC_000021.9:g.37221444A>G	-	COSV99898758	
NC_000021.9:g.37221446C>T	-	COSV55704783	
NC_000021.9:g.37227709C>A	-	COSV55706280	
NC_000021.9:g.37228361G>A	rs1569230715	COSV99898743	
NC_000021.9:g.37228369G>A	rs748554450	COSV55708184	
NC_000021.9:g.37232391G>T	-	COSV55706709	

Table 5R. Single Nucleotide Polymorphisms in DSCR9 sequence.
The table shows only the modifications reported to be related with pathological conditions in lungs.

DSCR9 analysis of repetitive elements: DFam

The analysis of repetitive elements within the Homo sapiens DSCR9 sequence revealed distinctive structural features, including a tandem repeat and a simple repeat segment. This part is constituted by a polyadenylated sequence starting from the 1644th nucleotide to 1681st nucleotide. Furthermore, a Short Interspersed Nuclear Element (SINE) was identified, encompassing a nucleotide position 124 to 236 (**Figure 20R)** with a length of 262 base pairs. This is indicative of a non-autonomous transposable element. Additionally, the internal region of the DSCR9 sequence seems to originate from a tRNA, exhibiting a pronounced conservation in the 5' region.

At the 3' terminal region, DSCR9 sequence aligned with the CRE1 class - a cis regulatory element known for its enhancer functionality within the genomic landscape.

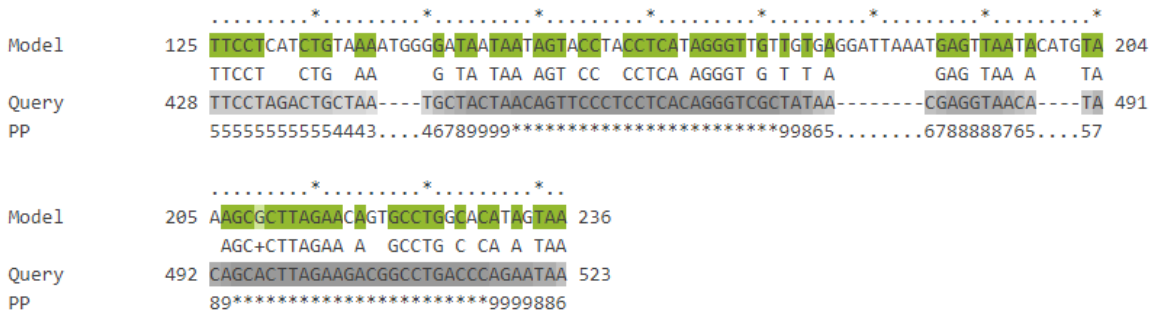

Figure 20R. Short Interspersed Nuclear Element (SINE) of DSCR9 sequence.
In the alignment presented in the figure, the model line shows the internal region of the consensus sequence, with colours corresponding to the match line. The PP value is indicative of the posterior probability and represents the degree of confidence in each aligned residue. Asterisk symbols present on top of the sequence (*) are indicative of the highest confidence, while the low number shows lower confidence. The Query is colourized in a grey scale corresponding to the confidence level. Darker is the colour higher is the confidence.

DSCR9 interactions: LncRRIsearch

The investigation into the interaction between DSCR9 and CAMK2B, as well as NOS3 mRNAs, was conducted by employing LncRRIsearch. The analytical framework involved the application of an energy threshold of -12 Kcal/mol to delineate base-pairing interactions between DSCR9 and specific targets. The analysis encompassed a comprehensive exploration of potential interaction sites on CAMK2B and NOS3 mRNAs.

The outcome of the analysis revealed putative interactions with the 5'-untranslated region (UTR) of CAMK2B and the 3'-UTR of NOS3. Furthermore, other interaction sites were identified in the coding sequence of both transcripts. **Table 6R** illustrates the interactions predicted by LncRRIsearch between DSCR9 and CAMK2B. Notably, four distinct interaction points within the 5' UTR were identified, independently of DSCR9 isoforms chosen for the analysis. Similarly, this analysis showed three possible interaction points in the CAMK2B coding sequence.

In **Table 7R** are listed the interactions between DSCR9 and NOS3, with the analysis maintaining the threshold energy at -12 Kcal/mol. In contrast to the interaction profile observed for CAMK2B, DSCR9 exhibited the capacity to engage with NOS3 transcript at limited points.

Specifically, DSCR9 demonstrated a singular binding point within the 3'-UTR region of NOS3, and only three interaction points within the coding sequence.

predicted DSCR9 interaction sites on CAMK2B					
energy (Kcal/mol)	**DSCR9 interaction starting point (left)**	**DSCR9 interaction ending point (right)**	**CAMK2B starting binding point (left)**	**CAMK2B starting binding point (right)**	**region**
1. -155,077 2. -155.084 3. -15.508 4. -155.077	1. 365 2. 423 3. 454 4. 512	1. 386 2. 444 3. 475 4. 533	1211	1238	5'-UTR
1. -14.752 2. -147.538 3. -14.753 4. -147.526	1. 366 2. 424 3. 455 4. 513	1. 407 2. 465 3. 496 4. 554	2651	2689	CDS
1. -140.357 2. -140.405 3. -140.383 4. -134.695	1. 366 2. 424 3. 455 4. 513	1. 382 2. 440 3. 471 4. 529	1660	1677	5'-UTR
1. -134.692 2. -134.696 3. -134.695 4. -134.695	1. 366 2. 424 3. 455 4. 513	1. 385 2. 443 3. 474 4. 532	1661	1677	5'-UTR
1. -127.218 2. -127.266 3. -127.244 4. -127.254	1. 366 2. 424 3. 455 4. 513	1. 382 2. 440 3. 471 4. 529	1402	1419	5'-UTR
1. -121.901 2. -121.904 3. -121.901 4. -121.898	1. 383 2. 441 3. 472 4. 530	1. 399 2. 457 3. 488 4. 546	2398	2414	CDS
1. -120.194 2. -120.11 3. -121.083 4. -120.228	1. 10 2. 10 3. 10 4. 10	1. 28 2. 28 3. 28 4. 28	3033	3052	CDS

Table 6R. predicted DSCR9 interaction sites on CAMK2B transcript. The first column of the table is displaying the energy value predicted for the interaction between DSCR9 and CAMK2B, expressed in Kcal/mol. The second and the third columns indicate the starting and ending point by which DSCR9 can interact with the target mRNA. The fourth and fifth columns indicate the starting and ending site in which DSCR9 interacts. The last column clarifies the nature of the region on the target mRNA. Numbers (1. , 2. , 3., 4.,) present in the first three columns indicate DSCR9 isoforms. The number corresponds to the number of DSCR9 isoforms.

UTR = untranslated region, CDS= coding sequence

predicted DSCR9 interaction sites on NOS3					
energy (Kcal/mol)	**DSCR9 interaction starting point (left)**	**DSCR9 interaction ending point (right)**	**NOS3 starting binding point (left)**	**NOS3 starting binding point (right)**	**region**
1. -138.848 2. -138.867 3. -138.858 4. -143.017	1. 376 2. 434 3. 465 4. 523	1. 387 2. 445 3. 476 4. 534	2952	2963	CDS
1. -125.861 2. -125.882 3. -125.873 4. -125.868	1. 366 2. 424 3. 455 4. 513	1. 396 2. 454 3. 485 4. 543	3112	2134	CDS
1. -133.851 2. -13.388 3. -133.867 4. -133.869	1. 367 2. 425 3. 456 4. 514	1. 388 2. 446 3. 477 4. 535	4065	4084	3'-UTR

Table 7R. predicted DSCR9 interaction sites on NOS3 transcript. The first column of the table is displaying the energy value predicted for the interaction between DSCR9 and NOS3, expressed in Kcal/mol. The second and the third columns indicate the starting and ending point by which DSCR9 can interact with the target. The fourth and fifth columns indicate the starting and ending site in which DSCR9 interacts. The last column clarifies the nature of the region on the target mRNA. Numbers (1. , 2. , 3., 4.,) present in the first three columns indicate DSCR9 isoforms. The number corresponds to the number of DSCR9 isoforms.

UTR = untranslated region, CDS= coding sequence

Gene Expression Omnibus datasets analysis

Analysis of three Gene Expression Omnibus (GEO) datasets gave further information about the possible involvement of DSCR9 in PAH.

In GSE90943, DSCR9 expression level significantly increased in hPASMCs after ET-1 exposure. Treatment with BQ123 - the antagonist of ET-1- did not prevent DSCR9 induction.

In the GSE15197, the microarray information about DSCR9 showed a p-value falling between 0.0001 and 0.05 in 25% of patients with either pulmonary idiopathic hypertension or secondary pulmonary hypertension.

GEO microarray from all lung tissues (GSE117261) from PAH patients and controls, give more information about DSCR9's expression in different subtypes of PAH and between sex. This microarray dataset was analysed by dividing patients into the respective PAH category, namely heritable PAH (HPAH), associated PAH (APAH) and idiopathic PAH (IPAH). The analysis showed differences only within the female population with APAH and IPAH, while no differences were retrieved for HPAH. No differences were highlighted in the male population in all the three PAH types. In **Figure 21R**. data are presented after normalisation on ACTB expression for each patient and control.

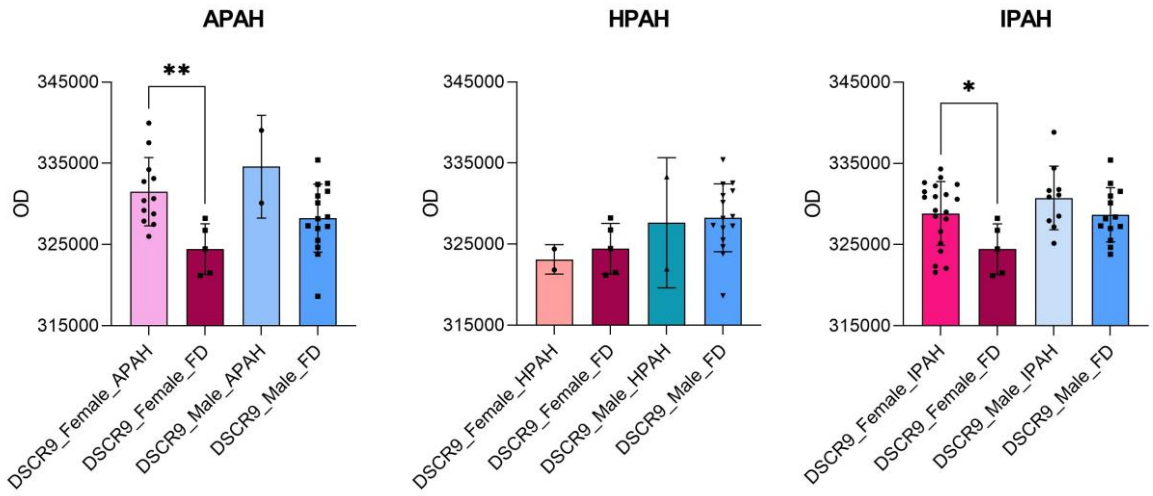

Figure 21R. **DSCR9 expression profile in man and woman in different pulmonary arterial hypertension subtypes.** Microarray data obtained from GSE117261. On the y axis is expressed the Optical density (OD) after the normalisation on the ACTB signal. on x are reported the sex, dived into PAH subtype and control.

APAH= associated pulmonary arterial hypertension, HPAH = heritable pulmonary arterial hypertension, IPAH = idiopathic pulmonary arterial hypertension, OD= optical density, FD =fail donor (control).

Primary human Pulmonary Artery Endothelial Cell

DSCR9 expression in primary human pulmonary artery endothelial cells from PAH patients

Considering the result obtained from the GSE117261 microarray, three female PAH samples and controls were considered for DSCR9 expression evaluation in primary human PAEC cells. DSCR9 expression was considered along with NOS3 and CAMK2B. Data normalisation was performed by using the ACTB gene as the most stable one. In **Figure 22R** is displayed the fold change for DSCR9, CAMK2B and NOS3 in female patients. DSCR9 is induced 93-fold, along with CAMK2B (60-fold) while NOS3 is minimally induced (5-fold).

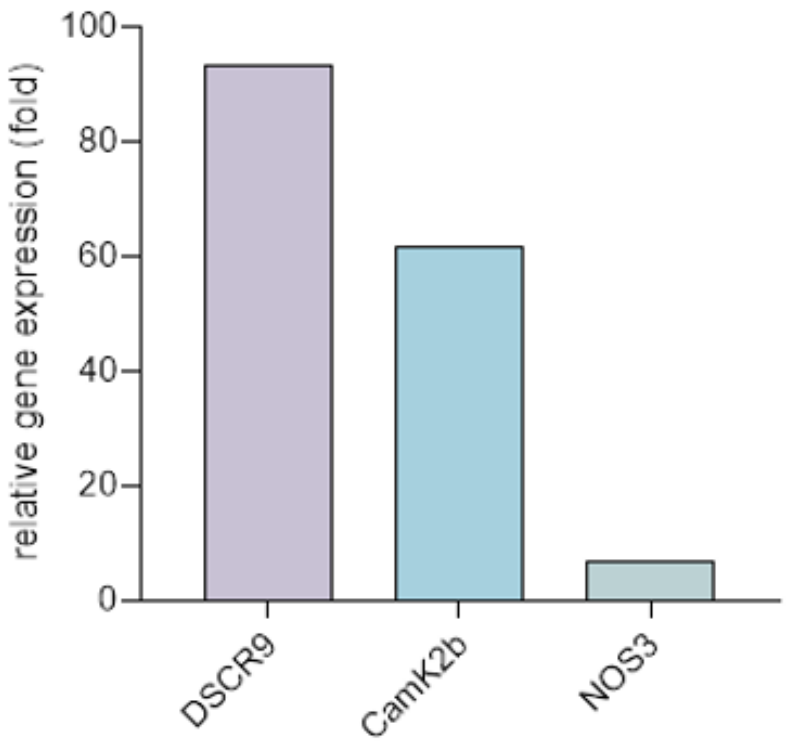

Figure 22R. RT-PCR for DSCR9, CAMK2B and NOS3. In the graph is shown the fold-change of the relative abundance for DSCR9, CAMK2B, NOS3. Data represent three biological replicates for PAH patient and control. y axis relative gene expression (fold), x axis genes.

DSCR9 overexpression dynamic: lentiviral vector construction and validation test

The amplification of the plasmid carrying DSCR9 sequence fused with the green fluorescence protein (DSCR9-GFP) along with the two antibiotic resistances (Chloramphenicol and Puromycin) was conducted successfully in E.Coli STBL3 cells as detailed in the materials and methods section.

In the first stage of the amplification, colony selection was performed by using the Chloramphenicol antibiotics and a negative control was taken to exclude any potential bacterial contamination.

Lentiviral particles were built in HECK-293T cells, and the virus was tested on control samples to assess the quality of the vector as well as the dynamic of DSCR9 overexpression. For this purpose, three different time points were selected: 24 hours, 48 hours and 7 days after the Puromycin selection. The analysis was performed by exposing primary control PAEC cells to the plKO vector. The latter time point was chosen to carry on the analysis since the RT-qPCR analysis displays the most significant difference for DSCR9 expression (**Figure 23R**).

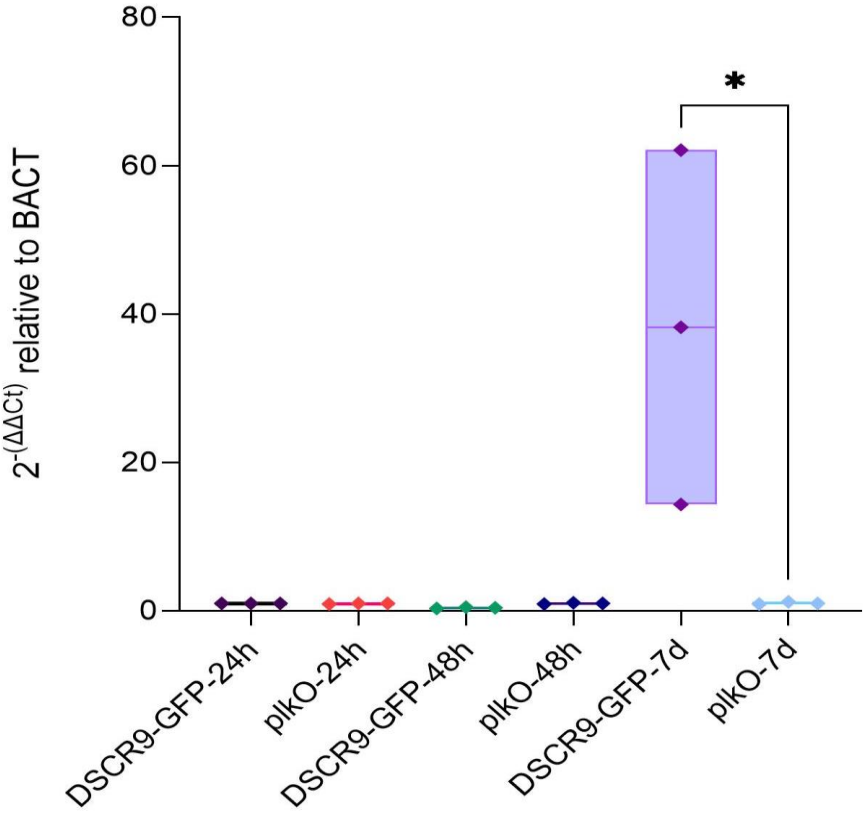

Figure 23R. DSCR9 dynamic of overexpression in control primary PAEC.
DSCR9 overexpression was tested after 24, and 48 hours as well as 7 days from lentivirus exposure. DSCR9-GFP corresponds to the vector carrying the DSCR9 sequence fused with the GFP, while plKO corresponds to the empty vector.

Effect of DSCR9 overexpression on transcript and protein levels.

Primary female PAEC from iPAH patients were subjected to a 16-hours exposure period to either DSCR9-GFP or plkO lentiviral vectors. Puromycin was employed to select the cells that successfully underwent the transduction and immunofluorescence staining against the GFP protein was used to assess the percentage of cells expressing DSCR9 (from 70 to 90%) (representative picture in **Figure 24R**).

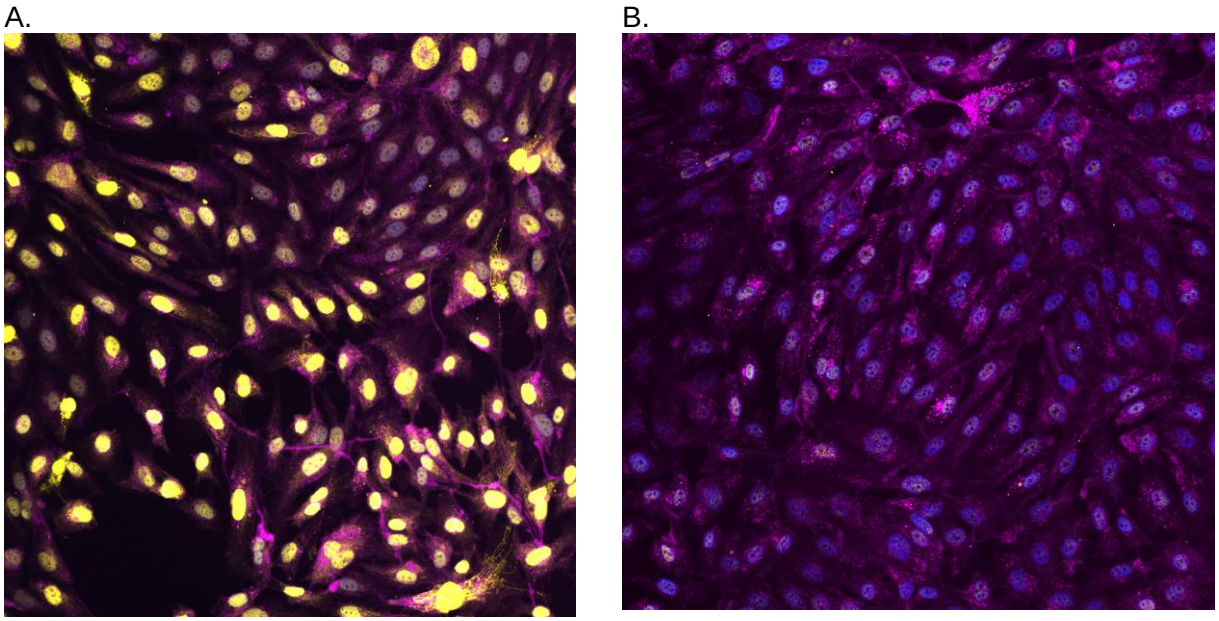

Figure 24R. DSCR9 overexpression in iPAH-PAEC. In A, a representative image of iPAH-PAEC transduced with the DSCR9-GFP vector. In B, a representative image of iPAH-PAEC transduced with the plKO vector.

Results retrieved from the immunofluorescence staining supported the initial bioinformatics analysis which localised DSCR9 inside the nucleus of the cells. To confirm the proper DSCR9 localisation inside the nuclei of the cells, a bioinformatics analysis on the GFP sequence contained in the plasmid was performed.

Thus, the GFP sequence retrieved from the plasmid structure was blasted in BLASTN to identify the kind of GFP employed. Subsequently, the corresponding amino acid sequence was built with BLASTX, and the corresponding protein was selected by considering the percentage of identity (99.15%). The corresponding FASTA sequence was analysed with MULocDeep a protein localisation prediction tool at subcellular and suborganellar level. This analysis showed the GFP protein as localised inside the cytoplasm (**Figure 25R**).

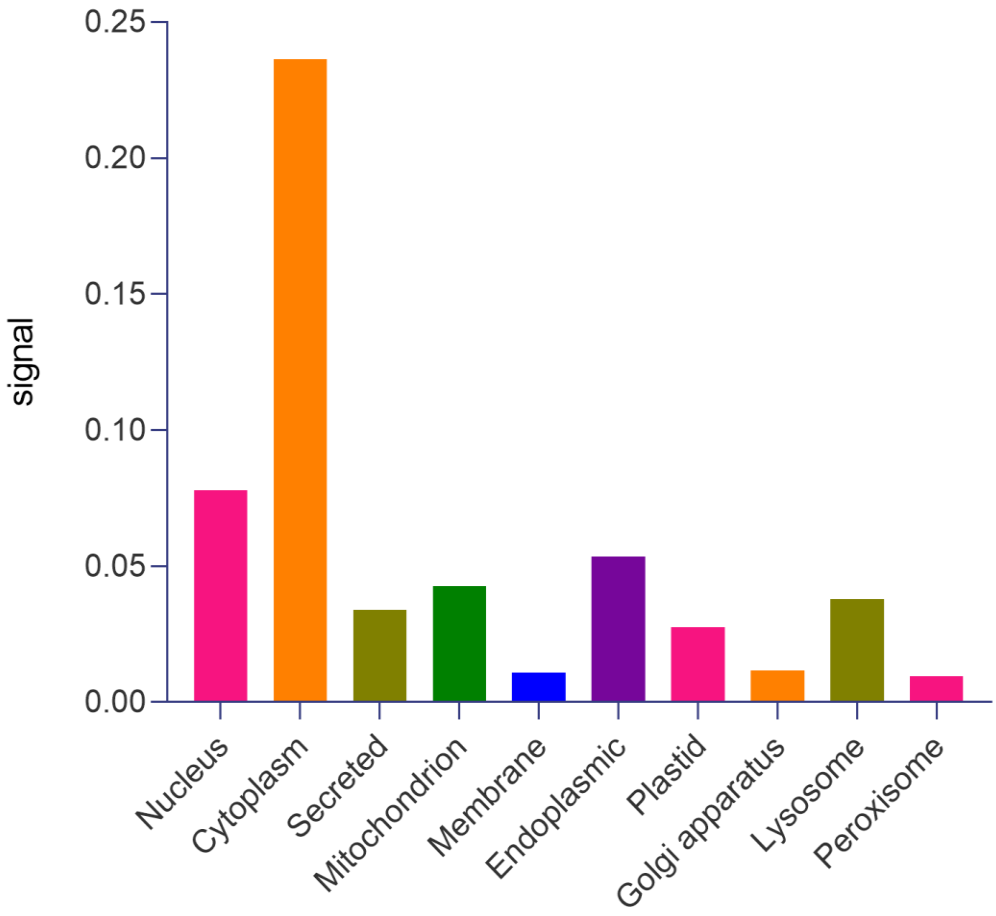

Figure 25R. Green Fluorescence Protein Localisation prediction.

Upon the conclusion of a 7-day period since lentivirus and antibiotics exposure, samples including RNA, protein were collected to gain insight into the possible involvement of DSCR9 in the eNOS pathway. RNAs and protein samples were collected as reported in the materials and methods section.

RT-qPCR was performed to assess DSCR9 overexpression along with CAMK2B and NOS3. DSCR9 overexpression was responsible for a significant reduction of CAMK2B expression of 15-fold, while no differences were detected for NOS3 (**Figure 26R**).

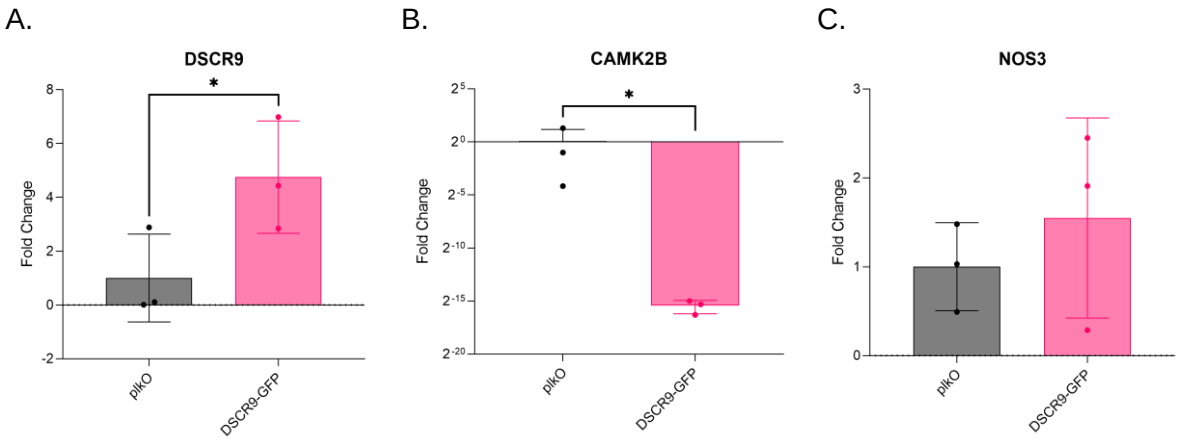

Figure 26R. **DSCR9 overexpression effect in iPAH-PAEC**.
RT-qPCR was performed for DSCR9, CAMK2B and NOS3. Significant differences were highlighted in DSCR9 (A) and CAMK2B (B) expressions, while no differences were pointed out for NOS3 (C). Seven days of DSCR9 overexpression caused a reduction of 15 fold in CAMK2B expression.

Protein samples collected after 7-days of DSCR9 overexpression were analysed in order to assess whether DSCR9 overexpression could affect Camk2B, AKT protein expression. Thus, total CamK2B, AKT and eNOS levels as well as their phosphorylated counterparts were analysed. Normalisation for total protein fraction was performed on Beta-actin signal. The active form is shown as the ratio between total protein and phosphorylated signal.

Even though DSCR9 overexpression determined a decrease in CAMK2B RNA expression level, on a protein level no statistical differences were highlighted in total CamK2B and its active form as shown in **Figure 27R**. Additionally, DSCR9 overexpression did not impair AKT and pAKT level (**Figure 28R**).

On the contrary, DSCR9 overexpression determines a significant increase in total eNOS (60,85% ± 35.10%, p-value= 0.047) and a significant decrease(-406.1% ± 192.9%, p-value=0.0338) in peNOS (**Figure 29R**).

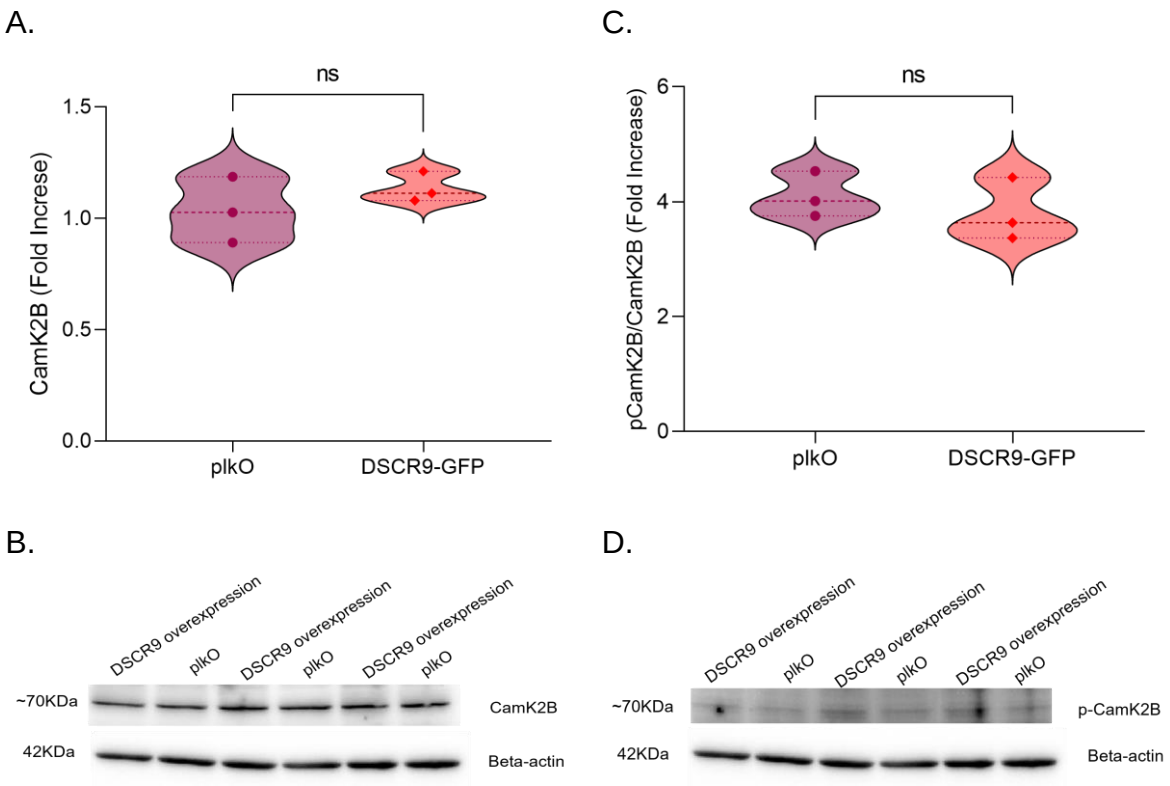

Figure 27R. Analysis of CamK2B and phosphorylated CamK2B expression after DSCR9 overexpression.
No differences were highlighted in total CamK2B (A) and the phosphorylated counterpart (C) after DSCR9 overexpression.
B, Band densitometry of total CamK2B
D, Band densitometry of pCamK2B

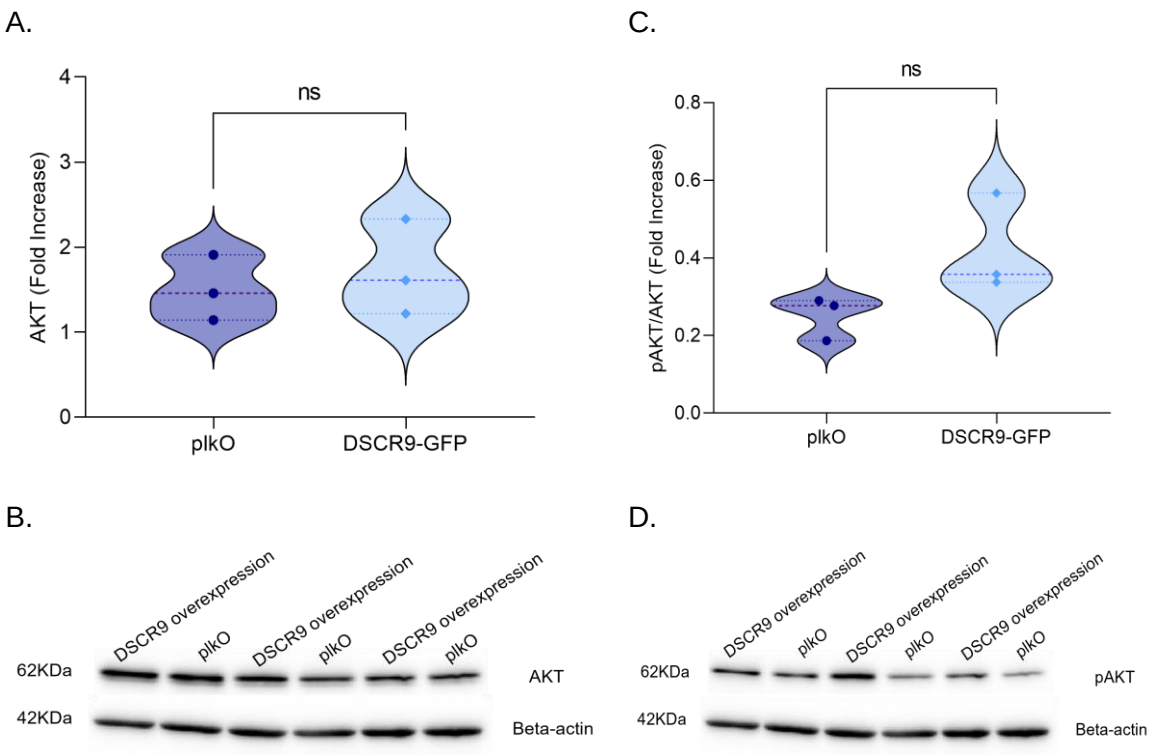

Figure 28R. Analysis of AKT and phosphorylated AKT expression after DSCR9 overexpression.
No differences were highlighted in total AKT (A) and the phosphorylated counterpart (C) after DSCR9 overexpression.
B, Band densitometry of total CamK2B
D, Band densitometry of pCamK2B

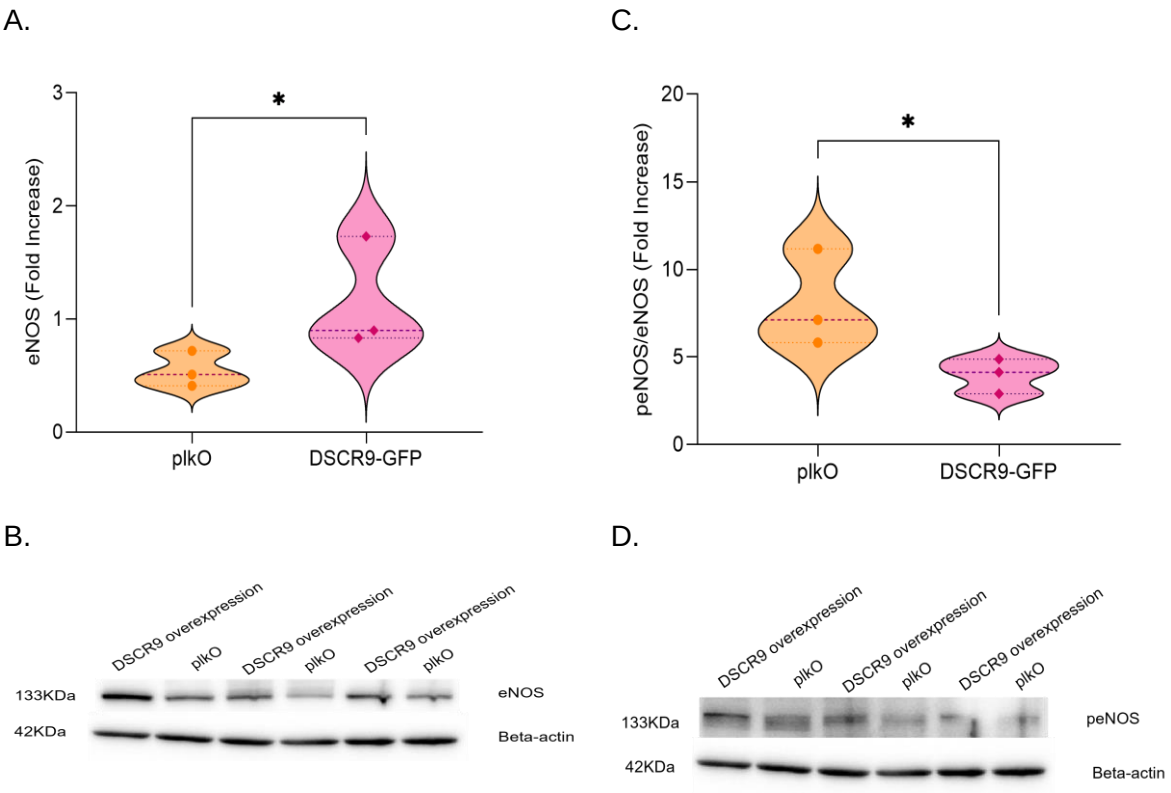

Figure 29R. **Analysis of eNOS and phosphorylated eNOS after DSCR9 overexpression.** Significant differences were highlighted in total eNOS(A) and the phosphorylated counterpart (C) after DSCR9 overexpression.
B, Band densitometry of total eNOS
D, Band densitometry of peNOS

Induced Pluripotent Stem Cell-derived Endothelial Cells

iPHCTRL04 line was used to establish the endothelial lineage cells, while DSCR9 expression was investigated on endothelial cells derived either from induced pluripotent stem cells (iPSC-ECs) carrying the Bone Morphogenetic Protein Receptor 2 (BMPR2) mutation or the isogenic line (iso01BMPR01) in which the mutation was replaced with CRISPR-Cas9 genome editing technique. As detailed in the materials and methods section, iPSC-ECs were obtained by applying Orlova's protocol. Human primary PAECs were used as control for the differentiation.

Validation of a model: RT-qPCR

Healthy female iPHCTRL04 iPSCs line was used to obtain endothelial lineage cells by applying Orlova's protocol. To assess the type of cells obtained the following genes were considered: NANOG and SOX as markers of pluripotency, VE-Cadherin (CD144), platelet endothelial cell adhesion molecule (PECAM1 or CD31), NOS3, as generic endothelial cell markers, and von Willebrand Factor (vWF) as a marker of maturity, SOX17, JAG1 as arterial marker, NRP2 as a venous marker, α-SMA as smooth muscle marker. RNA pool of primary pulmonary artery endothelial cells (PAEC) from donors was used to compare the gene expression level in all the differentiation steps. Thus, RNA samples were collected during the various time points of the differentiation process, namely the mesodermal induction (MI), vascular specification (VS), endothelial cells expansion (ECs) and after the purification (iPSC-EC). RT-qPCR was employed to assess the proper differentiation into endothelial cells, data were normalised on RPL27, as the most stable gene expressed during the differentiation.

The RT-qPCR confirmed that undifferentiated markers (NANOG and SOX2) decrease during the differentiation process suggesting a proper commitment of these cells into the differentiation process. Additionally, RT-qPCR showed an increase in endothelial cells marker, namely VE-Cadherin and PECAM1 during the VS and EC expansion time points. VE-cadherine and PECAM1 reach the expression peak at the final time point of the differentiation. NOS3 expression is related to PECAM1 and VE-Cadherin expression, and NOS3 is more induced during the vascular specification and endothelial cell expansion due to the activation of PI3K pathways[98]. RT-qPCR showed an increase of NOS3 expression level during the vascular specification and endothelial cells expansion, however NOS3 has a lower expression in iPSC-ECs. Generally, NOS3 is mainly induced during the first stages of the differentiation process (the vascular specification and the endothelial cells expansion), allowing the expression of VE-Cadherin and PECAM1 in the latter phase of the differentiation[99]. The marker of maturity (vWF) remains at low level during all the steps of the differentiation process suggesting that iPSC-ECs are not fully mature at the end of the differentiation[100]. SOX17 is a transcription factor and a well-known arterial marker. The increase of SOX17 and JAG1 during the differentiation process suggests the arterial nature of iPSC-ECs[100,101].

NRP2 is a venous marker and its expression is higher in comparison to the level present in PAEC cells. Despite this, the iPSC-ECs obtained more closely resemble arterial rather than venous ECs, as documented by the immunostaining. α-SMA expression increases during the

VS and ECs expansion. However, α-SMA expression is lower after the purification process. A summary of gene expression through the differentiation stages is shown in **Figure 30R**.

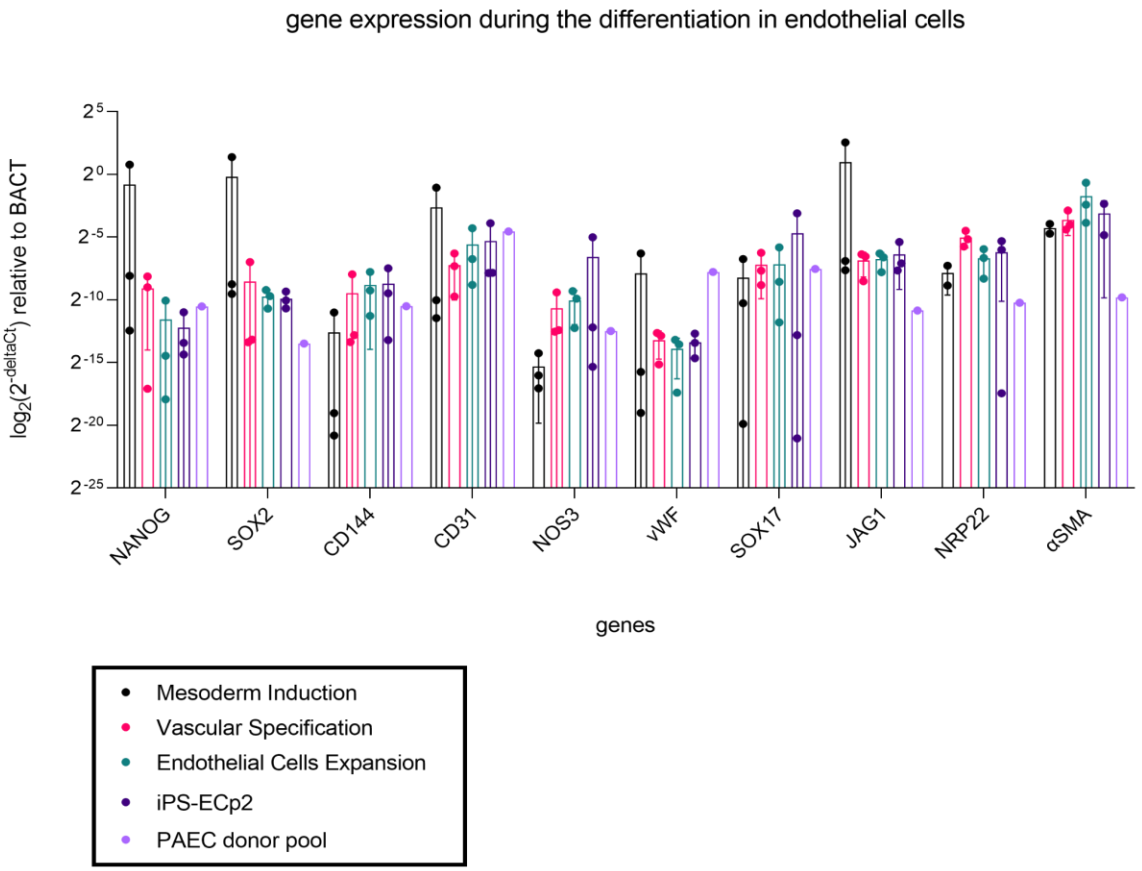

Figure 30R. Gene expression during the differentiation in endothelial cells. Different time points were considered (Mesodermal Induction, Vascular Specification, Endothelial Cells expansion, iPSC-EC at passage 2). A pool of three human primary PAEC donors was used as positive control to compare the gene expression during the differentiation.

Validation of a model: immunostaining

Immunofluorescence staining was performed to determine the effective presence of arterial endothelial markers, establish the percentage of iPSC-EC cells obtained, and exclude the presence of smooth muscle cells as a side product of the differentiation[102]. Thus iPSC-EC cells were stained for VE-Cadherin, SOX17, vWF, and αSMA (representative images- **Figure 31R** and **Figure 32R)**. Primary human PAEC cells were stained as well and were used as positive control for the staining.
The images were acquired with confocal microscopy as detailed in the materials and methods sections and analysed with ImageJ Software. According to RT-qPCR data, only a few cells expressed the vWF (4%) indicating that they are not completely mature. The percentage of endothelial cells obtained by calculating the number of cells expressing VE-Cadherin is 88,61% of which 94,5% are expressing SOX17, indicating that the iPSC-EC obtained have an arterial nature. 11.39% of cells are expressing αSMA.

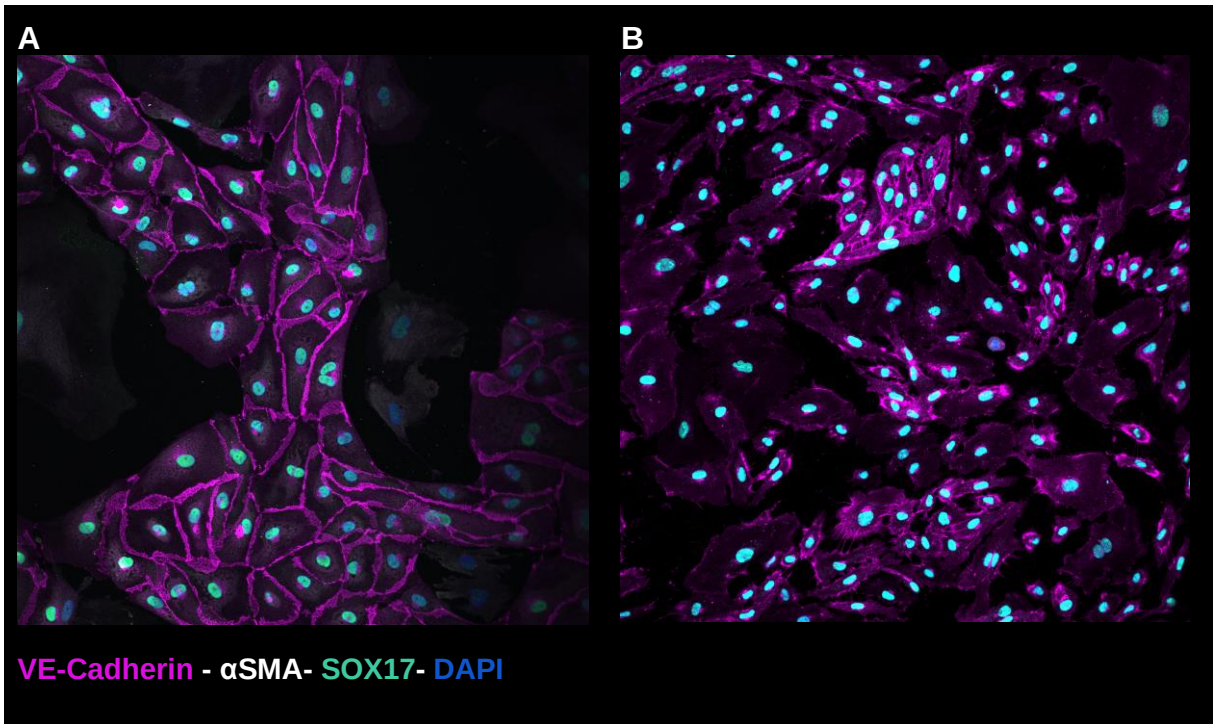

Figure 31R. Immunofluorescence staining on iPSC-ECs and human primary PAEC.
Cells were stained for VE-Cadherin to assess the endothelial nature of the iPSC-EC obtained from the differentiation, αSMA to exclude the presence of smooth muscle cells, and SOX17 in order to establish the arterial nature of these cells.

In **A** iPSC-ECs
In **B** primary human PAEC cells from a healthy donor

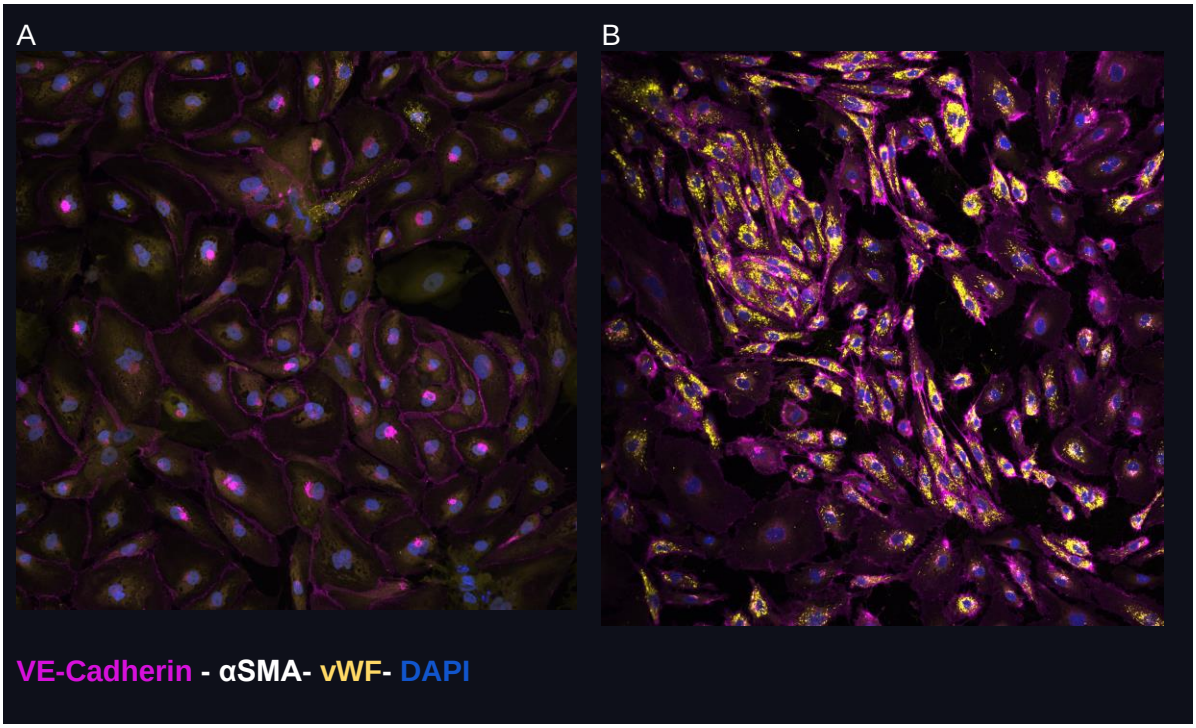

Figure 32R. Immunofluorescence staining on iPSC-ECs and human primary PAEC.
Cells were stained for VE-Cadherin to assess the endothelial nature of the iPSC-EC obtained from the differentiation, αSMA to exclude the presence of smooth muscle cells, and vWF in order to establish the level of cell maturation.

In **A** iPSC-ECs;
In **B** primary human PAEC cells from a healthy donor

RT-qPCR for target genes

DSCR9 expression, along with CAMK2B and NOS3 expression, was investigated in iPSC-ECs derived from the iBMPR01 and iso01BMPR01 lines. Thus, iPSC-ECs were kept in culture to allow the cells to become more mature and then RNA was collected as described in the materials and methods section. RT-qPCR data from iPSC-ECs obtained from the iBMPR01 line showed an increase in DSCR9 expression and in CAMK2B expression of 2-fold and 1.33-fold, respectively. No differences were detected for NOS3 expression (0.14-fold). Despite the augmentation in DSCR9 and CAMK2B expression in the iso01BMPR01 line, no statistical differences were highlighted through the analysis.

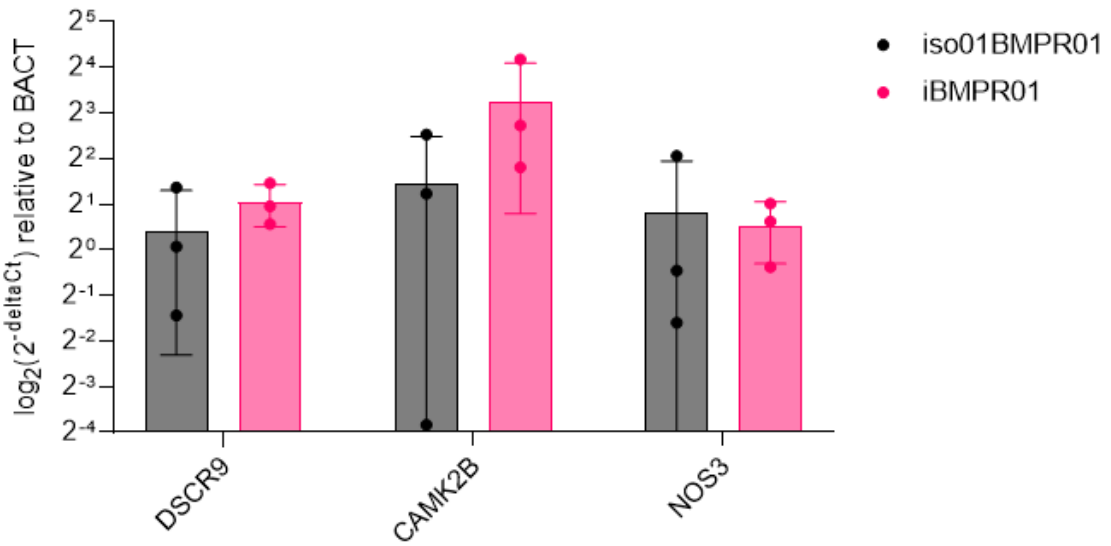

Figure 33R. **Analysis of DSCR9 and relevant gene expression in iPSC-EC.**
In the graph, data from RT-qPCR were presented as $log_2(2^{-\Delta Ct})$ relative to ACTB gene expression. In the analysis are considered DSCR9, CAMK2B and NOS3 expression in iPSC-ECs from iBMPR01 and iso01BMPR01 lines.

Discussion

PAH is a rare and complex disorder, predominantly affecting the female population. Its aetiology is multifactorial and frequently associated with mutation in the BMPR2 gene, although other mutations have been identified. Despite various types of PAH having been described over time, a common pathophysiological feature is evident - a marked vasoconstriction and aberrant vascular remodelling. These pathological modifications are extended all across the three layers of the arterial wall (intima, media and adventitia), involving the types of cell present in that area (PAECs, PASMC, and fibroblast), and contributing to classifying PAH as a vasculopathy.

Remarkable efforts have been dedicated to unveil the primary cause behind the alterations observed in the vasculature of PAH patients in order to improve their prognosis. Consequently, a thorough analysis of alterations in the three layers has been conducted to comprehend the molecular mechanism underlying the histological modifications observed, and revealing potential scenarios contributing to PAH development.

A prominent characteristic in PAH is the lack of NO production, which is recognized as a key driver in the pathology of PAH. Given that NO exerts a local vasodilatory effect, its deficiency can disrupt the vascular homeostasis and exacerbate vascular remodelling.

Several studies have been performed to investigate the reason why endothelial cells of PAH patients reduce their production of NO. Some studies indicate deficiency in BH4 as the main cause of NO deficiency [3,103], others focused on the role of eNOS expression, but the results were sometimes contradictory with both increase and reduction in eNOS expression level being reported[3]. Additionally, an ovine PAH model demonstrated that the reduction in eNOS production was secondary to an altered mitochondrial biogenesis[58]. Additionally, recent studies based on high-throughput techniques have reported the potential role of the non-coding class in the NO deficiency. Currently, only six different miRNA have been identified as involved in NO deficiency, acting on different levels (refer to **Table 3I** in the introduction section). However, no lncRNA have been implicated in NO deficiency. However, despite these studies, exactly how the reduced NO production arises during PAH development remains elusive. Thus, the primary aim of this study is to further investigate the NO impairment observed in PAH. Notably, the most promising results were obtained after 24 hours of high-pressure exposure. For this reason, the initial phase of our investigation comprised transcriptomic data analysis on samples derived from commercial hPAEC exposed for 24 hours at a pressure of 40mmHg higher than the atmospheric pressure. This was followed by transcriptomic data validation, NO production evaluation, western blot analysis of components of the eNOS pathway and an in depth study of the lncRNA DSCR9 in PAH due to its fold change, significant p-value and possible involvement in the eNOS pathway. In this study we

found that the lncRNA DSCR9 is induced by the exposure of hPAEC to high pressure and is up regulated in both PAEC derived from patients with iPAH as well as in endothelial cells isolated from a BMPR2 mutation carrier. Notably, it is interesting to note that in these cellular models, the increased DSCR9 levels either via incubation to high pressure or by lentiviral overexpression, are associated with higher amounts of eNOS protein, which is however hypo-phosphorylated.

To validate the findings obtained in commercially available hPAEC two additional models were employed. First, primary PAEC from patients with idiopathic PAH were employed to investigate DSCR9 expression and secondly the eNOS pathway perturbation was investigated after DSCR9 overexpression. Finally, endothelial cells derived from induced pluripotent stem cells carrying the mutation in the BMPR2 gene and their isogenic counterpart were used to establish whether this is a suitable model to study DSCR9 in another PAH disease model.

Differential gene expression analysis on samples exposed to high pressure and control conditions showed an altered expression of 11,486 genes. A focused examination of the genes involved in eNOS pathways showed that only NOS3 was significantly downregulated, with other eNOS pathway genes (CAMK2B and AKT1) exhibiting no notable differences. Subsequently, the analysis was carried on by considering only the genes falling within the 90th centile, on this basis 141 DEGs were isolated. A deeper analysis about the gene composition revealed that 0.7% of DEGs encompass small nuclear RNA (snoRNA)-encoding, 2.14% are associated with the transcription of processed pseudogenes, 2.86% involve lncRNA transcripts, while the predominant fraction, constituting 92%, is composed of protein-coding genes.

GO biological process analysis of these DEGs revealed the “Regulation of response to stimulus” as the most enriched category. This outcome is coherent with the fact that commercially available hPAEC were exposed for 24 hours at 40mmHg pressure higher than the atmospheric one. Thus, commercial hPAEC exposed to the experimental conditions detecting changes may adjust their response to the environmental stimulus [104].

Functional analysis on the DEGs falling in the 90th centile allowed the identification of two distinct categories related to inflammation (response to type I interferon, type I interferon pathway and cellular response to interferon I) and gene silencing (negative regulation of gene silencing by miRNA, negative regulation of posttranscriptional gene silencing and negative regulation of gene silencing by RNA). This outcome aligns with existing evidence implicating the interferon type I pathway and the non-coding class (miRNA and lncRNA) as possible contributors to the onset of PAH[105–107]. At this stage, an individualized analysis of up-regulated

and down-regulated genes was conducted to discern characteristic gene profiles within the two groups. Notably, the categories related to inflammation and gene silencing appear to be in the up-regulated DEGs. Conversely, analysis of the down-regulated counterpart highlighted interconnected pathways primarily linked to purine and pyrimidine synthesis (75%), carbohydrate synthesis and enzymes involved in carbohydrates and lipids metabolism (25%). The observed alterations align with the pathological features of PAH, where cellular metabolism undergoes perturbations across multiple metabolic pathways including glycolysis, fatty acid metabolism and glutamine metabolism[108]. Furthermore, the down-regulation of genes associated with nucleotides synthesis is in concordance with the expectation, as such down-regulation has been previously linked to genes involved in the glycolytic process. Specifically, under physiological conditions in PAEC cells, an increase in nucleotide synthesis is connected with the increase in glucose consumption[109]. However, in pathological conditions such as PAH, the observed down-regulation of genes associated with purine and pyrimidine synthesis is coherent with the downregulation of genes involved in the glycolytic process.

Among the DEGs, we carried on the analysis by considering the lncRNA DSCR9 as it is the gene having the highest fold change and significant p-value that is within the 90th centile group as well as its possible involvement in the eNOS pathway. Currently, there is no literature about the possible role of DSCR9 in the development of PAH, with two studies describing its involvement in inflammation during pancreatic cancer and rheumatoid arthritis[110,111] . Interestingly, a recent study[94] reported that DSCR9 as co-expressed with one of the main up-stream activators of the eNOS pathway, namely the Calcium-Calmodulin protein kinases 2B (CamK2B). Upon activation, CAMK2B undergoes autophosphorylation on the threonine-287 which induces the phosphorylation of AKT1. Notably, in physiological conditions, both CamK2B or AKT1 have the ability to activate eNOS by phosphorylating the serine-1177[112], thereby facilitating the activation of eNOS for the NO production. Thus, in the perspective of PAH, imbalances in the activation of these proteins could lead to a decrease in NO production[113]. According to data collected in previous experiments, commercial hPAEC exposed for 24 hours to 40mmHg pressure exhibit a significant decrease in NO production which is in accordance with the alteration observed in the eNOS pathway regarding the lower level of phosphorylated eNOS. However, the analysis also indicated that 24 hours of high-pressure did not impair total CamK2B and AKT protein production and activation. These activations were assessed through the phosphorylation on threonine-284 and serine-473, respectively, and it was determined as a ratio between pCamK2B/CamK2B and pAKT/AKT. Conversely, western blot analysis revealed a decrease in the phosphorylation on Serine-1177 of eNOS despite a significant increase in total eNOS production. These results prompt the

hypothesis that other factors may contribute to the alteration observed via a possible interaction between DSCR9 and targets in the eNOS pathway.

Bioinformatics predictions suggest that DSCR9 may exert a role inside the nucleus of the cells by showing a higher affinity with that nuclear compartment by acting on chromatin level (93.2%), nucleoplasm (94%) and nucleolus (96%) (**Figure 16R**). In this context, the highest percentage of DSCR9 enrichment that is found at the nuclear level suggests that DSCR9 may exert its function by regulating the chromatin access (chromatin level) and nuclear transports (nucleoplasm) or modulating stress response, enzymatic activity, nucleolar structure (nucleolus)[59]. Additionally, bioinformatics analysis on possible interaction with CAMK2B transcripts and NOS3 revealed that DSCR9 has putative interaction sites on both CAMK2B and NOS3 transcripts in either the coding sequence or in the 3'UTR region (**Table 7R**), which may prompt the stability of the transcripts and enhancing the translation[114].

Additional evidence of the involvement of DSCR9 in the pathology of PAH is provided by the GEO datasets analysis. The analysis of the GEO dataset GSE117261 performed by separating patients and controls according to their gender, revealed DSCR9 as differentially expressed in the female population with idiopathic PAH, and associated PAH, while no differences were highlighted for heritable PAH (**Figure 21R**). Supporting the result retrieved from the previous microarray analysis, in our study we demonstrated via RT-qPCR performed on primary hPAEC derived from female iPAH patients, that DSCR9 was strongly up-regulated (93-fold). On contrary of what possible to observe in the commercial hPAEC exposed to 40mmHg high pressure, genes like CAMK2B and NOS3 resulted induced. The perturbation of the eNOS pathway analysed after 7 days of DSCR9 overexpression depicted interesting results on both RNA and protein level. In detail, following the significative up-regulation of DSCR9, RT-qPCR depicted a reduction in CAMK2B expression of 15-fold, while no differences where highlighted for NOS3 (**Figure 26R**). Additionally, immunofluorescence staining performed after the overexpression showed DSCR9 presence inside the nuclei of the cells (**Figure 24R**), whose presence is not dependent on the GFP associated with DSCR9 as shown in **Figure 25R**. This result may support the hypothesis of a possible regulation of CAMK2B expression through chromatin remodelling making inaccessible the promoter region of this gene. Despite the alteration in CAMK2B expression on RNA level, western blot analysis after DSCR9 overexpression displayed the same pattern for CamK2B, AKT and eNOS that was observed after 24 hours of high-pressure exposure of commercially available hPAEC (**Figure 27R** and **Figure 2R, Figure 3R, Figure 4R**). Specifically, no notable alterations were highlighted for CamK2B, AKT and their phosphorylated forms. In contrast, following DSCR9 overexpression it was possible to observe upregulation in total eNOS abundance

accompanied by a decrease in its phosphorylated fraction. This observation suggests a potential influence of the lncRNA DSCR9 on the dynamic of eNOS regulation. A plausible explanation for this phenomenon may be linked to the general ability of the lncRNAs to bind the 3'UTR region determining the stabilization of the transcript, protecting it from the degradation and allowing its translation in protein as well as the coding sequence determining an alteration in the final configuration of a protein[59,114]. In this scenario, as supported by the bioinformatics predictions (**Table 7R**), DSCR9 might bind the 3'UTR, leading to transcript stabilization and enhancing translation into a protein. Alternatively, it may mask specific sites crucial for eNOS phosphorylation by binding to specific regions in the coding sequence of the transcript, resulting in a change in its configuration.

Finally, after the differentiation of endothelial cells derived from a female line of induced pluripotent stem cells (iPSC-EC) with the BMPR2 mutation and their isogenic control, we examined the gene expression of the cells obtained and their maturation level using RT-qPCR and immunofluorescence staining, focusing on key genes and proteins. The differentiation protocol employed successfully yielded endothelial cells expressing arterial and endothelial cell markers (**Figure 30B**), such as SOX17 and VE-Cadherin. Immunofluorescence staining supported the results obtained via RT-qPCR by showing the presence of these markers on a protein level. Additionally, maturity assessment was facilitated by the visualization of the vWF, a well-known marker of maturity[100]. Despite displaying arterial and endothelial markers, iPSC-ECs exhibited low expression of vWF both at the RNA and protein level, suggesting these cells need to undergo a maturation process.

To evaluate the suitability of this model to study DSCR9 within the context of another PAH model, we conducted an investigation of DSCR9 expression primarily employing RT-qPCR along with other genes of interest, namely CAMK2B and NOS3. Results revealed a trend towards two-fold increase of DSCR9 and CAMK2B expression within the line carrying the BMPR2 mutation (iBMPR01), which aligns with the up-regulation of DSCR9 highlighted in the other two models. However, because of the heterogeneity between the samples due to the iPSC origin, the data was not statistically significant. Despite this, it is quite interesting to observe that the up-regulation of DSCR9 expression in the presence of BMPR2 mutation accentuates the potential significance of this model to unravel the role of DSCR9 in the context of PAH. Finally, it is quite interesting to note that in line with results obtained in primary cells from iPAH patients, also in this case NOS3 display no differences between the two lines analysed.

Limitation of the study and future perspective

Although the present study has provided valuable insights about the potential contribution of DSCR9 in the pathogenesis of PAH, it is essential to acknowledge the presence of limitations that should be taken into consideration for both a deeper comprehension of the research outcome and to prompt a new research path.

In the first instance, commercially available hPAEC were exposed to high-pressure condition only for 24 hours to simulate the PAH and maybe a longer exposure would be resulted in the same RNA expression pattern observed for CAMK2B and NOS3 in the other two models. Secondly, even though the pressure applied resemble the pressure observed in pathological condition, it would be worthy to evaluate DSCR9 expression and the other relevant target by using a pulsatile pressure instead of the static pressure applied. Additionally, there is no paracrine communication with other cell types as it occurs *in vivo*. For these reasons to enhance this model would be interesting to recreate an in-chip model where a pulsatile pressure will be applied only on the endothelial cells surface in order to recreate an environment as close as possible to the *in vivo* one.

Considering the iPSC-EC model, the cells obtained via the differentiation process did not display a mature phenotype, as depicted by the RNA and protein expression level of the vWF. Thus, despite the two-fold differences in DSCR9 expression in favour of the iBMPR01 line, the statistical test applied did not display any differences. This outcome may be attributed either to the high spread of the data or to DSCR9 involvement during the early stages of embryonic development. Indeed, LncRNA databases indicate that DSCR9 exhibits elevated expression during cell differentiation and organ development, followed by a subsequent decrease over time. Notably, DSCR9 maintains a higher expression only in the testis. Therefore, it may be prudent to enhance the maturation level of iPSC-ECs before conducting further analyses on DSCR9 expression in this model.

Although DSCR9 exhibited up-regulation with significant p-value in both commercial and primary PAEC, variations in CAMK2B expression across the models complicates the establishment of a direct connection with this gene, despite the bioinformatic prediction. Therefore, in the context of PAH, a comprehensive understanding of how DSCR9 expression may influence CAMK2B and delineate the relationship between these two genes would necessitate a time-course experiment spanning the seven-day period assessed for DSCR9 overexpression.

Conclusion

In conclusion, this is the first study in which DSCR9 was pointed out as a possible actor in the PAH scenario. In this study, it has been reported how DSCR9 was induced in three different model of PAH we used, namely commercially available hPAEC, primary hPAEC from female patients with idiopathic PAH, and iPSC-ECs carrying the BMPR2 mutation. Additionally, for the first time, DSCR9 was connected with the eNOS pathways by the demonstration that following its overexpression there is a stable increased level of total eNOS protein and a significant reduction in the phosphorylation on the serine-1177. This observation is in line with the outcome obtained in commercially available PAEC cells exposed to high-pressure condition. Additionally, the same pattern was observed in total CamK2B and total AKT protein, as well as in their active forms. This reinforces the hypothesis of a possible regulation operated by DSCR9 on eNOS either by stabilising its transcript and promoting the translation into protein or masking specific site on eNOS protein preventing its activation.

Publication and Grant

- **Nadia Bernardi** , Eva Bianconi , Andrea Vecchi, Pietro Ameri(2023) *Non-coding RNAs in pulmonary arterial hypertension:current knowledge and translational perspectives.* Heart FailureClinics,2023 Jan;19(1):137-152
- **2023 ESC First Contact Initiative Grant**

Bibliography

1. Southgate, L., Machado, R. D., Gräf, S. & Morrell, N. W. Molecular genetic framework underlying pulmonary arterial hypertension. *Nat Rev Cardiol* **17**, 85–95 (2020).
2. Peacock, A. J., Murphy, N. F., McMurrey, J. J. V., Caballero, L. & Stewart, S. An epidemiological study of pulmonary arterial hypertension. *Eur Respir J* **30**, 104–109 (2007).
3. Shah, A. J., Vorla, M. & Kalra, D. K. Molecular Pathways in Pulmonary Arterial Hypertension. *Int J Mol Sci* **23**, 10001 (2022).
4. Humbert, M. *et al.* 2022 ESC/ERS Guidelines for the diagnosis and treatment of pulmonary hypertension. doi:10.1093/eurheartj/ehac237.
5. Ma, L. *et al.* A Novel Channelopathy in Pulmonary Arterial Hypertension. *New England Journal of Medicine* **369**, 351–361 (2013).
6. Schermuly, R. T., Ghofrani, H. A., Wilkins, M. R. & Grimminger, F. Mechanisms of disease: pulmonary arterial hypertension. *Nat Rev Cardiol* **8**, 443–455 (2011).
7. Bals, R. & Hiemstra, P. S. Innate immunity in the lung: how epithelial cells fight against respiratory pathogens. *Eur Respir J* **23**, 327–333 (2004).
8. Austin, E. D. & Loyd, J. E. Genetics and mediators in pulmonary arterial hypertension. *Clin Chest Med* **28**, 43–57 (2007).
9. Runo, J. R. & Loyd, J. E. Primary pulmonary hypertension. *Lancet* **361**, 1533–1544 (2003).
10. Sztrymf, B. *et al.* Clinical outcomes of pulmonary arterial hypertension in carriers of BMPR2 mutation. *Am J Respir Crit Care Med* **177**, 1377–1383 (2008).
11. McAllister, K. A. *et al.* Endoglin, a TGF-β binding protein of endothelial cells, is the gene for hereditary haemorrhagic telangiectasia type 1. *Nature Genetics 1994 8:4* **8**, 345–351 (1994).
12. Harrison, R. E. *et al.* Molecular and functional analysis identifies ALK-1 as the predominant cause of pulmonary hypertension related to hereditary haemorrhagic telangiectasia. *J Med Genet* **40**, 865–871 (2003).
13. Austin, E. D. *et al.* Whole exome sequencing to identify a novel gene (Caveolin-1) associated with human pulmonary arterial hypertension. *Circ Cardiovasc Genet* **5**, 336–343 (2012).
14. Shintani, M., Yagi, H., Nakayama, T., Saji, T. & Matsuoka, R. A new nonsense mutation of SMAD8 associated with pulmonary arterial hypertension. *J Med Genet* **46**, 331–337 (2009).
15. Nasim, M. T. *et al.* Molecular genetic characterization of SMAD signaling molecules in pulmonary arterial hypertension. *Hum Mutat* **32**, 1385–1389 (2011).
16. Nasim, M. T. *et al.* Molecular genetic characterization of SMAD signaling molecules in pulmonary arterial hypertension. *Hum Mutat* **32**, 1385–1389 (2011).

17. Schermuly, R. T., Ghofrani, H. A., Wilkins, M. R. & Grimminger, F. Mechanisms of disease: pulmonary arterial hypertension. *Nat Rev Cardiol* **8**, 443–455 (2011).
18. Tuder, R. M. *et al.* Relevant issues in the pathology and pathobiology of pulmonary hypertension. *J Am Coll Cardiol* **62**, (2013).
19. Zahid, K. R., Raza, U., Chen, J., Raj, U. J. & Gou, D. Pathobiology of pulmonary artery hypertension: role of long non-coding RNAs. *Cardiovasc Res* **116**, 1937–1947 (2020).
20. Tobal, R. *et al.* Vascular Remodeling in Pulmonary Arterial Hypertension: The Potential Involvement of Innate and Adaptive Immunity. *Front Med (Lausanne)* **8**, (2021).
21. Stacher, E. *et al.* Modern age pathology of pulmonary arterial hypertension. *Am J Respir Crit Care Med* **186**, 261–272 (2012).
22. Wang, A. P. *et al.* Pulmonary Artery Smooth Muscle Cell Senescence Promotes the Proliferation of PASMCs by Paracrine IL-6 in Hypoxia-Induced Pulmonary Hypertension. *Front Physiol* **12**, (2021).
23. Tobal, R. *et al.* Vascular Remodeling in Pulmonary Arterial Hypertension: The Potential Involvement of Innate and Adaptive Immunity. *Front Med (Lausanne)* **8**, (2021).
24. Sitbon, O. & Morrell, N. W. Pathways in pulmonary arterial hypertension: the future is here. doi:10.1183/09059180.00004812.
25. Dupuis, J. Endothelin: setting the scene in PAH. *European Respiratory Review* **16**, 3–7 (2007).
26. Polar secretion of endothelin-1 by cultured endothelial cells - PubMed. https://pubmed.ncbi.nlm.nih.gov/1644793/.
27. Dupuis, J. & Hoeper, M. M. Endothelin receptor antagonists in pulmonary arterial hypertension. *Eur Respir J* **31**, 407–415 (2008).
28. Lang, I. M. & Gaine, S. P. Recent advances in targeting the prostacyclin pathway in pulmonary arterial hypertension. *Eur Respir Rev* **24**, 630–641 (2015).
29. Tamura, Y. & Kimura, M. Treatment of pulmonary arterial hypertension. *N Engl J Med* **351**, 286–294 (2004).
30. Mubarak, K. K. A review of prostaglandin analogs in the management of patients with pulmonary arterial hypertension. *Respir Med* **104**, 9–21 (2010).
31. Ruan, K.-H. Advance in understanding the biosynthesis of prostacyclin and thromboxane A2 in the endoplasmic reticulum membrane via the cyclooxygenase pathway. *Mini Rev Med Chem* **4**, 639–647 (2004).
32. Point mutation in the seventh hydrophobic domain of the human thromboxane A2 receptor allows discrimination between agonist and antagonist binding sites - PubMed. https://pubmed.ncbi.nlm.nih.gov/8246916/.

33. Tran, N., Garcia, T., Aniqa, M., Ali S & Nauli, A. A. Endothelial Nitric Oxide Synthase (eNOS) and the Cardiovascular System: in Physiology and in Disease States. *Am J Biomed Sci & Res* 2022–2037 doi:10.34297/AJBSR.2022.15.002087.
34. Lancaster, J. R. Nitric oxide: a brief overview of chemical and physical properties relevant to therapeutic applications. *Future Sci OA* **1**, (2015).
35. Joannides, R. *et al.* Nitric oxide is responsible for flow-dependent dilatation of human peripheral conduit arteries in vivo. *Circulation* **91**, 1314–1319 (1995).
36. Kolluru, G. K., Siamwala, J. H. & Chatterjee, S. eNOS phosphorylation in health and disease. *Biochimie* **92**, 1186–1198 (2010).
37. Reactome | Metabolism of nitric oxide: NOS3 activation and regulation. https://www.reactome.org/content/detail/R-HSA-202131.
38. Pacher, P., Beckman, J. S. & Liaudet, L. Nitric oxide and peroxynitrite in health and disease. *Physiol Rev* **87**, 315–424 (2007).
39. Gebhart, V., Reiß, K., Kollau, A., Mayer, B. & Gorren, A. C. F. Site and mechanism of uncoupling of nitric-oxide synthase: Uncoupling by monomerization and other misconceptions. *Nitric Oxide* **89**, 14–21 (2019).
40. Niu, W. & Qi, Y. An updated meta-analysis of endothelial nitric oxide synthase gene: three well-characterized polymorphisms with hypertension. *PLoS One* **6**, (2011).
41. Dai, B., Liu, T., Zhang, B., Zhang, X. & Wang, Z. The polymorphism for endothelial nitric oxide synthase gene, the level of nitric oxide and the risk for pre-eclampsia: a meta-analysis. *Gene* **519**, 187–193 (2013).
42. Shoukry, A. *et al.* Endothelial nitric oxide synthase gene polymorphisms and the risk of diabetic nephropathy in type 2 diabetes mellitus. *Genet Test Mol Biomarkers* **16**, 574–579 (2012).
43. Eröz, R., Bahadir, A., Dikici, S. & Tasdemir, S. Association of endothelial nitric oxide synthase gene polymorphisms (894G/T, -786T/C, G10T) and clinical findings in patients with migraine. *Neuromolecular Med* **16**, 587–593 (2014).
44. Nassereddine, S. *et al.* The polymorphism G894 T of endothelial nitric oxide synthase (eNOS) gene is associated with susceptibility to essential hypertension (EH) in Morocco. *BMC Med Genet* **19**, (2018).
45. Searles, C. D. Transcriptional and posttranscriptional regulation of endothelial nitric oxide synthase expression. *Am J Physiol Cell Physiol* **291**, 803–816 (2006).
46. Yang, Y. *et al.* Sp1 modification of human endothelial nitric oxide synthase promoter increases the hypoxia-stimulated activity. *Microvasc Res* **93**, 80–86 (2014).
47. Zhang, M. X. *et al.* Regulation of endothelial nitric oxide synthase by small RNA. *Proc Natl Acad Sci U S A* **102**, 16967–16972 (2005).

48. Ou, H. *et al.* Effect of nuclear actin on endothelial nitric oxide synthase expression. *Arterioscler Thromb Vasc Biol* **25**, 2509–2514 (2005).
49. Ju, H., Zou, R., Venema, V. J. & Venema, R. C. Direct interaction of endothelial nitric-oxide synthase and caveolin-1 inhibits synthase activity. *J Biol Chem* **272**, 18522–18525 (1997).
50. Coggins, M. P. & Bloch, K. D. Nitric oxide in the pulmonary vasculature. *Arterioscler Thromb Vasc Biol* **27**, 1877–1885 (2007).
51. Tonelli, A. R., Haserodt, S., Aytekin, M. & Dweik, R. A. Nitric oxide deficiency in pulmonary hypertension: Pathobiology and implications for therapy. *Pulm Circ* **3**, 20–30 (2013).
52. Ignarro, L. J., Buga, G. M., Wood, K. S., Byrns, R. E. & Chaudhuri, G. Endothelium-derived relaxing factor produced and released from artery and vein is nitric oxide. *Proc Natl Acad Sci U S A* **84**, 9265–9269 (1987).
53. Arnold, W. P., Mittal, C. K., Katsuki, S. & Murad, F. Nitric oxide activates guanylate cyclase and increases guanosine 3':5'-cyclic monophosphate levels in various tissue preparations. *Proc Natl Acad Sci U S A* **74**, 3203–3207 (1977).
54. Chester, A. H., Yacoub, M. H. & Moncada, S. Nitric oxide and pulmonary arterial hypertension. doi:10.21542/gcsp.2017.14.
55. Bin-Nun, A. & Schreiber, M. D. Role of iNO in the modulation of pulmonary vascular resistance. *Journal of Perinatology 2008 28:3* **28**, S84–S92 (2008).
56. Giaid, A. & Saleh, D. Reduced expression of endothelial nitric oxide synthase in the lungs of patients with pulmonary hypertension. *N Engl J Med* **333**, 214–221 (1995).
57. Inducible nitric oxide synthase is present within human atherosclerotic lesions and promotes the formation and activity of peroxynitrite - PubMed. https://pubmed.ncbi.nlm.nih.gov/8683942/.
58. Afolayan, A. J. *et al.* Decreased endothelial nitric oxide synthase expression and function contribute to impaired mitochondrial biogenesis and oxidative stress in fetal lambs with persistent pulmonary hypertension. *Am J Physiol Lung Cell Mol Physiol* **310**, 40–49 (2016).
59. Hombach, S. & Kretz, M. Non-coding RNAs: Classification, Biology and Functioning. *Adv Exp Med Biol* **937**, 3–17 (2016).
60. Long Non-Coding RNA Review and Implications in Lung Diseases - PubMed. https://pubmed.ncbi.nlm.nih.gov/30854513/.
61. Chen, C. *et al.* Long non-coding RNA review and implications in acute lung inflammation. *Life Sci* **269**, (2021).
62. Dueck, A. & Meister, G. Assembly and function of small RNA - argonaute protein complexes. *Biol Chem* **395**, 611–629 (2014).

63. Santos-Ferreira, C. A. *et al.* Micro-RNA Analysis in Pulmonary Arterial Hypertension: Current Knowledge and Challenges. *JACC Basic Transl Sci* **5**, 1149–1162 (2020).
64. O'Brien, J., Hayder, H., Zayed, Y. & Peng, C. Overview of MicroRNA Biogenesis, Mechanisms of Actions, and Circulation. *Front Endocrinol (Lausanne)* **9**, (2018).
65. Condorelli, G., Latronico, M. V. G. & Cavarretta, E. MicroRNAs in cardiovascular diseases: Current knowledge and the road ahead. *J Am Coll Cardiol* **63**, 2177–2187 (2014).
66. Sayed, D. & Abdellatif, M. MicroRNAs in development and disease. *Physiol Rev* **91**, 827–887 (2011).
67. Marchese, F. P., Raimondi, I. & Huarte, M. The multidimensional mechanisms of long noncoding RNA function. *Genome Biol* **18**, (2017).
68. Derrien, T. *et al.* The GENCODE v7 catalog of human long noncoding RNAs: analysis of their gene structure, evolution, and expression. *Genome Res* **22**, 1775–1789 (2012).
69. Pan, T. N6-methyl-adenosine modification in messenger and long non-coding RNA. *Trends Biochem Sci* **38**, 204–209 (2013).
70. Geisler, S., Lojek, L., Khalil, A. M., Baker, K. E. & Coller, J. Decapping of long noncoding RNAs regulates inducible genes. *Mol Cell* **45**, 279–291 (2012).
71. Johnson, A. W. Rat1p and Xrn1p are functionally interchangeable exoribonucleases that are restricted to and required in the nucleus and cytoplasm, respectively. *Mol Cell Biol* **17**, 6122–6130 (1997).
72. Neth, P., Nazari-Jahantigh, M., Schober, A. & Weber, C. MicroRNAs in flow-dependent vascular remodelling. *Cardiovasc Res* **99**, 294–303 (2013).
73. Kumar, S., Kim, C. W., Simmons, R. D. & Jo, H. Role of flow-sensitive microRNAs in endothelial dysfunction and atherosclerosis mechanosensitive athero-miRs. *Arterioscler Thromb Vasc Biol* **34**, 2206–2216 (2014).
74. Kontaraki, J. E., Marketou, M. E., Zacharis, E. A., Parthenakis, F. I. & Vardas, P. E. MicroRNA-9 and microRNA-126 expression levels in patients with essential hypertension: potential markers of target-organ damage. *Journal of the American Society of Hypertension* **8**, 368–375 (2014).
75. Hergenreider, E. *et al.* Atheroprotective communication between endothelial cells and smooth muscle cells through miRNAs. *Nat Cell Biol* **14**, 249–256 (2012).
76. Climent, M. *et al.* TGFβ triggers miR-143/145 transfer from smooth muscle cells to endothelial cells, thereby modulating vessel stabilization. *Circ Res* **116**, 1753–1764 (2015).
77. Zhang, W. *et al.* Roles of miRNA-24 in regulating endothelial nitric oxide synthase expression and vascular endothelial cell proliferation. *Mol Cell Biochem* **405**, 281–289 (2015).

78. Bi, R. *et al.* MicroRNA-27b plays a role in pulmonary arterial hypertension by modulating peroxisome proliferator-activated receptor γ dependent Hsp90-eNOS signaling and nitric oxide production. *Biochem Biophys Res Commun* **460**, 469–475 (2015).
79. Yang, Z. & Kaye, D. M. Mechanistic insights into the link between a polymorphism of the 3'UTR of the SLC7A1 gene and hypertension. *Hum Mutat* **30**, 328–333 (2009).
80. Yang, Z. *et al.* Identification of a novel polymorphism in the 3'UTR of the L-arginine transporter gene SLC7A1: contribution to hypertension and endothelial dysfunction. *Circulation* **115**, 1269–1274 (2007).
81. Sun, H. X. *et al.* Essential role of microRNA-155 in regulating endothelium-dependent vasorelaxation by targeting endothelial nitric oxide synthase. *Hypertension* **60**, 1407–1414 (2012).
82. Suárez, Y., Fernández-Hernando, C., Pober, J. S. & Sessa, W. C. Dicer dependent microRNAs regulate gene expression and functions in human endothelial cells. *Circ Res* **100**, 1164–1173 (2007).
83. Leisegang, M. S. *et al.* Long Noncoding RNA MANTIS Facilitates Endothelial Angiogenic Function. *Circulation* **136**, 65–79 (2017).
84. Neumann, P. *et al.* The lncRNA GATA6-AS epigenetically regulates endothelial gene expression via interaction with LOXL2. *Nat Commun* **9**, 237 (2018).
85. Michalik, K. M. *et al.* Long noncoding RNA MALAT1 regulates endothelial cell function and vessel growth. *Circ Res* **114**, 1389–1397 (2014).
86. Potente, M., Gerhardt, H. & Carmeliet, P. Basic and therapeutic aspects of angiogenesis. *Cell* **146**, 873–887 (2011).
87. Xiang, Y., Zhang, Y., Tang, Y. & Li, Q. MALAT1 Modulates TGF-β1-Induced Endothelial-to-Mesenchymal Transition through Downregulation of miR-145. *Cell Physiol Biochem* **42**, 357–372 (2017).
88. Mas-Ponte, D. *et al.* LncATLAS database for subcellular localization of long noncoding RNAs. (2017) doi:10.1261/rna.060814.
89. Li, Z. *et al.* LncBook 2.0: integrating human long non-coding RNAs with multi-omics annotations. *Nucleic Acids Res* **51**, (2023).
90. Hubley, R. *et al.* The Dfam database of repetitive DNA families. *Nucleic Acids Res* **44**, D81 (2016).
91. Zuker, M. Mfold web server for nucleic acid folding and hybridization prediction. *Nucleic Acids Res* **31**, 3406 (2003).
92. Fukunaga, T., Iwakiri, J., Ono, Y. & Hamada, M. Lncrrisearch: A web server for lncRNA-RNA interaction prediction integrated with tissue-specific expression and subcellular localization data. *Front Genet* **10**, 462 (2019).

93. Orlova, V. V. *et al.* Generation, expansion and functional analysis of endothelial cells and pericytes derived from human pluripotent stem cells. *Nat Protoc* **9**, 1514–1531 (2014).
94. Chen, M. *et al.* Identify Down syndrome transcriptome associations using integrative analysis of microarray database and correlation-interaction network. *Hum Genomics* **12**, (2018).
95. Kobayashi, T. *et al.* Involvement of CaM kinase II in the impairment of endothelial function and eNOS activity in aortas of Type 2 diabetic rats. *Clin Sci (Lond)* **123**, 375–386 (2012).
96. Ebenebe, O. V., Heather, A. & Erickson, J. R. CaMKII in Vascular Signalling: 'Friend or Foe'? *Heart Lung Circ* **27**, 560–567 (2018).
97. Guo, C. *et al.* The SET oncoprotein promotes estrogen-induced transcription by facilitating establishment of active chromatin. *Proc Natl Acad Sci U S A* **120**, (2023).
98. Huang, N. F., Fleissner, F., Sun, J. & Cooke, J. P. Role of nitric oxide signaling in endothelial differentiation of embryonic stem cells. *Stem Cells Dev* **19**, 1617–1625 (2010).
99. Belt, H. *et al.* Temporal Dynamics of Gene Expression During Endothelial Cell Differentiation From Human iPS Cells: A Comparison Study of Signalling Factors and Small Molecules. *Front Cardiovasc Med* **5**, 316594 (2018).
100. Harding, A. *et al.* Highly Efficient Differentiation of Endothelial Cells from Pluripotent Stem Cells Requires the MAPK and the PI3K Pathways. *Stem Cells* **35**, 909–919 (2017).
101. Nakajima-Takagi, Y. *et al.* Role of SOX17 in hematopoietic development from human embryonic stem cells. *Blood* **121**, 447–458 (2013).
102. Lu, X., Dunn, J., Dickinson, A. M., Gillespie, J. I. & Baudouin, S. V. Smooth muscle alpha-actin expression in endothelial cells derived from CD34+ human cord blood cells. *Stem Cells Dev* **13**, 521–527 (2004).
103. Khoo, J. P. *et al.* Pivotal role for endothelial tetrahydrobiopterin in pulmonary hypertension. *Circulation* **111**, 2126–2133 (2005).
104. Vogel, V. & Sheetz, M. Local force and geometry sensing regulate cell functions. *Nat Rev Mol Cell Biol* **7**, 265–275 (2006).
105. Gairhe, S. *et al.* Type I interferon activation and endothelial dysfunction in caveolin-1 insufficiency-associated pulmonary arterial hypertension. *Proc Natl Acad Sci U S A* **118**, (2021).
106. Savai, R. *et al.* Immune and inflammatory cell involvement in the pathology of idiopathic pulmonary arterial hypertension. *Am J Respir Crit Care Med* **186**, 897–908 (2012).

107. Bernardi, N., Bianconi, E., Vecchi, A. & Ameri, P. Noncoding RNAs in Pulmonary Arterial Hypertension: Current Knowledge and Translational Perspectives. *Heart Fail Clin* **19**, (2023).
108. Tura-Ceide, O. *et al. REVIEWED BY Metabolic Reprogramming: A Novel Metabolic Model for Pulmonary Hypertension*.
109. Sharma, S. & Aldred, M. A. DNA Damage and Repair in Pulmonary Arterial Hypertension. doi:10.3390/genes11101224.
110. Zhuang, H. *et al.* A four prognosis-associated lncRNAs (PALnc) based risk score system reflects immune cell infiltration and predicts patient survival in pancreatic cancer. *Cancer Cell Int* **20**, (2020).
111. Wen, J. *et al.* lncRNA expression profiles related to apoptosis and autophagy in peripheral blood mononuclear cells of patients with rheumatoid arthritis. *FEBS Open Bio* **10**, 1642–1654 (2020).
112. Fleming, I., Fisslthaler, B., Dimmeler, S., Kemp, B. E. & Busse, R. Phosphorylation of Thr(495) regulates Ca(2+)/calmodulin-dependent endothelial nitric oxide synthase activity. *Circ Res* **88**, (2001).
113. Kobayashi, T. *et al.* Involvement of CaM kinase II in the impairment of endothelial function and eNOS activity in aortas of Type 2 diabetic rats. *Clin Sci (Lond)* **123**, 375–386 (2012).
114. Sebastian-Delacruz, M., Gonzalez-Moro, I., Olazagoitia-Garmendia, A., Castellanos-Rubio, A. & Santin, I. The Role of lncRNAs in Gene Expression Regulation through mRNA Stabilization. *Noncoding RNA* **7**, 1–13 (2021).